

FLOOD MANAGEMENT AND REMEDIAL MEASURES FOR DIKMEN,
NORTHERN CYPRUS

A THESIS SUBMITTED TO
THE BOARD OF GRADUATE PROGRAMS
OF
MIDDLE EAST TECHNICAL UNIVERSITY, NORTHERN CYPRUS CAMPUS

BY

NOOR AHMAD YAQUBI

IN PARTIAL FULFILLMENT OF THE REQUIREMENTS
FOR
THE DEGREE OF MASTER OF SCIENCE
IN SUSTAINABLE ENVIRONMENT AND ENERGY SYSTEMS PROGRAM

AUGUST 2022

Approval of the Board of Graduate Programs

Prof. Dr. Cumali Sabah

Chairperson

I certify that this thesis satisfies all the requirements as a thesis for the degree of Master of Science

Assoc. Prof. Dr. Ceren Ince Derogar

Program Coordinator

This is to certify that we have read this thesis and that in our opinion it is fully adequate, in scope and quality, as a thesis for the degree of Master of Science.

Assist. Prof. Dr. Bertuğ Akıntuğ

Co-Supervisor

Assist. Prof. Dr. Hasan Zaifoğlu

Supervisor

Examining Committee Members

Assist. Prof. Dr. Hasan Zaifoğlu Civil Engineering
Prog. METU NCC _____

Assist. Prof. Dr. Bertuğ Akıntuğ Civil Engineering
Prog. METU NCC _____

Assist. Prof. Dr. Canraş Batunlu Electrical and
Electronics
Engineering Prog.
METU NCC _____

Assist. Prof. Dr. İbrahim Bay Civil Engineering
Dept. EUL _____

Assist. Prof. Dr. Kemal Maşera Mechanical
Engineering Prog.
METU NCC _____

I hereby declare that all information in this document has been obtained and presented in accordance with academic rules and ethical conduct. I also declare that, as required by these rules and conduct, I have fully cited and referenced all material and results that are not original to this work.

Name, Last name : Noor Ahmad, Yaqubi

Signature :

ABSTRACT

FLOOD MANAGEMENT AND REMEDIAL MEASURES FOR DIKMEN, NORTHERN CYPRUS

Yaqubi, Noor Ahmad

Master of Science, Sustainable Environment and Energy Systems Program

Supervisor: Asst. Prof. Dr. Hasan Zaifoğlu

Co-Supervisor: Asst. Prof. Dr. Bertuğ Akıntuğ

August 2022, 138 pages

This study aims to execute a flood management system and examine the appropriate structural measures to protect Dikmen town against the impacts of flooding. At first, hydrologic models using HEC-HMS tools are developed to simulate the rainfall-runoff processes in each of the three main ungauged sub-basins on the upstream side of the town.

Next, the discharge hydrographs of the 5th December 2018 flood event are defined in the 2D HEC-RAS model, and the flood inundation maps of the study area are generated. The initial model indicates a 78% goodness-of-fit between the observed flood map and the model flood map. However, the model is then calibrated using Manning's roughness coefficients until the goodness-of-fit ratio rises to 84%, and the relative error (RE) between the two maps declines from 4.2% to 1.5%.

Furthermore, a technical impact analysis of the three mitigations measures (i.e., the concrete channel, the reservoirs, and the integration of both the channel and the reservoirs) are performed along with their cost analyses to determine the optimal solution in terms of reducing the risks of flooding with the optimum cost.

The results indicate that the concrete channel with the lowest cost has the potential to protect against up to 100-year floods. However, for more extreme events, such as having a 500-year return period, the channel capacity cannot be sufficient to keep the flood water in the channel. Therefore, additional non-structural measures, such as increasing flood awareness and developing early flood warning systems, also need to be considered.

Keywords: Hydraulic Modeling, Hydrologic Modeling, Flood Inundation Map, Dikmen, Northern Cyprus

ÖZ

DİKMEN, KUZEY KIBRIS İÇİN TAŞKIN YÖNETİMİ VE İYİLEŞTİRİCİ ÖNLEMLER

Yaqubi, Noor Ahmad
Yüksek Lisans, Sürdürülebilir Çevre ve Enerji Sistemleri
Tez Yöneticisi: Dr. Öğr. Üyesi Hasan Zaifoğlu
Ortak Tez Yöneticisi: Dr. Öğr. Üyesi Bertuğ Akıntuğ

Ağustos 2022, 138 sayfa

Bu çalışma, bir taşkın yönetim sistemi yürütmeyi ve Dikmen ilçesini selin etkilerinden korumak için uygun yapısal önlemleri incelemeyi amaçlamaktadır. İlk başta, şehrin yukarı tarafındaki üç ana ölçümlenmemiş alt havzanın her birinde yağış-akış süreçlerini simüle etmek için HEC-HMS araçlarını kullanan hidrolojik modeller geliştirildi.

Ardından, 2B HEC-RAS modelinde 5 Aralık 2018 sel olayının deşarj hidrografları tanımlanmış ve çalışma alanının sel baskını haritaları oluşturulmuştur. İlk model, gözlemlenen taşkın haritası ile model taşkın haritası arasında %78'lik bir uyum iyiliği gösterir. Bununla birlikte, model daha sonra, uyum iyiliği oranı %84'e yükselene ve iki harita arasındaki bağıl hata (RE) %4,2'den %1,5'e düşene kadar Manning'in pürüzlülük katsayıları kullanılarak kalibre edilir.

Ayrıca, riskleri azaltmak açısından en uygun çözümü belirlemek için maliyet analizleriyle birlikte üç etki azaltma önleminin (yani beton kanal, rezervuarlar ve hem kanalın hem de rezervuarların entegrasyonu) teknik bir etki analizi yapılır. Optimum maliyetle sel. Sonuçlar, en düşük maliyetli beton kanalın 100 yıla kadar taşkınlara karşı koruma potansiyeline sahip olduğunu göstermektedir. Ancak 500

yıllık geri dönüş süresi gibi daha ekstrem olaylar için kanal kapasitesi sel sularını kanalda tutmaya yeterli olamamaktadır. Bu nedenle, taşkın farkındalığının artırılması ve erken taşkın uyarı sistemlerinin geliştirilmesi gibi yapısal olmayan ek önlemlerin de dikkate alınması gerekmektedir.

Anahtar Kelimeler: Hidrolik Modelleme, Hidrolojik Modelleme, Taşkın Yayılım Haritası, Dikmen, Kuzey Kıbrıs

To My Family and all who seek to make a positive change

ACKNOWLEDGMENTS

To begin, the author would like very much to express his gratefulness to supervisor Assist. Prof. Dr. Hasan Zaifođlu and co-supervisor Assist. Prof. Dr. Bertuđ Akintuđ for their supervision, unlimited support, guidance, criticism, and encouragement that certainly contributed to the completion of this research. Without them, this study would not have been possible and successful.

The author would also like to thank the officials in the Dikmen Municipality and Northern Cyprus Mapping Office for providing the required data sets for the study.

The author also wishes to express his gratitude to his friends and colleagues in the school and outside who made this experience unique and meaningful.

Last but not least, the author is highly grateful for all the support from his family members, especially his father Haji Noor Mohammad Yaqubi, his mother Haji Horezad Yaqubi, and his older and younger brothers. Without them, this whole journey would not have been possible.

TABLE OF CONTENTS

ABSTRACT.....	vii
ÖZ	ix
ACKNOWLEDGMENTS	xii
TABLE OF CONTENTS.....	xiii
LIST OF TABLES	xv
LIST OF FIGURES	xvi
CHAPTERS	
1. INTRODUCTION	1
1.1 Statement of the Problem	1
1.2 The Objective of the Study.....	8
1.3 Structure of the MSc Thesis	9
2. LITERATURE REVIEW	10
3. HYDROLOGICAL ANALYSIS METHODOLOGIES.....	16
3.1 Hydrological Analysis.....	16
3.1.1 Design Rainfall Hyetograph for Dikmen Urban Area	16
3.1.2 Hydrological Model Development.....	18
3.1.3 Reservoir Routing Process	21
3.2 Processing of the Digital Elevation Model (DEM) for Floodplain Area .	24
4. HYDRAULIC ANALYSIS METHODOLOGIES	25
4.1 History of HEC-RAS	25
4.1.1 1D HEC-RAS Flood Inundation Modeling	26
4.1.2 2D HEC-RAS Unsteady Flood Modeling Approach.....	29
4.2 Flood Model Development for Dikmen Study Area.....	36

4.2.1	2D - Flood Model Development in HEC-RAS	36
5.	STUDY AREA DESCRIPTIONS	47
5.1	Dikmen Urban Area as Case Study	47
5.2	Characteristics of the Dikmen Study Area	48
5.3	Climatic Conditions in the Study Area	51
5.4	Land Cover of the Study Area	52
5.5	The Data Sets of the Study Area.....	55
6.	HYDROLOGICAL MODELING RESULTS AND DISCUSSIONS	57
6.1	Hydrological Modelling.....	57
6.1.1	Formation of Design Rainfall Hyetograph	57
6.1.2	Flood Hydrographs Generation	59
7.	HEC-RAS FLOOD MODELING RESULTS AND DISCUSSIONS.....	67
7.1	Hydraulic Modelling Results	67
7.1.1	Dikmen’s 2018 – Flood Event Model Current Condition	67
7.1.2	50-, 100-, and 500-year Flood Maps For Current Condition	74
7.1.3	Mitigation Measure - M1: Concrete Channel.....	77
7.1.4	Mitigation Measure - M2: Reservoirs	89
7.1.5	Mitigation Measure - M3: Concrete Channel and Reservoirs.....	111
7.1.6	The Effects of the Channel on the Discharge Hydrographs	115
7.1.7	The Sensitivity Analysis of The Channel	117
8.	SUMMARY AND CONCLUSION	127
8.1	Summary and Conclusion	127
8.2	Recommendation For Future Studies	130
	REFERENCES	131

LIST OF TABLES

Table 4.1 Manning's Roughness Coefficient based on different Land Cover	41
Table 4.2 Vulnerability Thresholds For People, Vehicles, and Buildings.....	45
Table 6.1 Mean Annual Maximum Daily Precipitation of Boğaz Station for Different Return Periods.....	58
Table 6.2 Basin Characteristics Used in SCS UH Method in HEC-HMS.....	63
Table 6.3 Peak Discharges of Each Sub-basins Corresponding to Different Return Periods.....	64
Table 7.1 Manning's Roughness Coefficient n	69
Table 7.2 The Differences Between Observed and Modelled 2018 Flood Maps	69
Table 7.3 Open Channel Hydraulic Parameters.....	78
Table 7.4 Unit Cost Summary of the materials and labor works	85
Table 7.5 Details of The Excavation Cost Analysis	86
Table 7.6 Details of the Open Channel Cost Analysis.....	87
Table 7.7 Cost Analysis Details of the Closed Section of the Concrete Channel.....	87
Table 7.8 Formworks Cost Analysis Details	88
Table 7.9 Proposed Detention Reservoirs Characteristics	90
Table 7.10 Summary of the Flood Routing Analysis of Reservoirs Without Bottom Outlets	105
Table 7.11 Summary of the Flood Routing Analysis of Reservoirs With 1.0 m Diameter Bottom Outlets	106
Table 7.12 Reservoirs Description and Work Loads	109
Table 7.13 Reservoir Unit Cost.....	109
Table 7.14 Reservoir Cost Analysis.....	110
Table 7.15 Total cost of the Combined Mitigation Measures.....	114
Table 7.16 Changes in Peak Discharge.....	124

LIST OF FIGURES

Figure 1.1 Global Temperature Anomaly Between 1975–2021	2
Figure 1.2 Recorded Floods Events in the World and EU Since 1977	3
Figure 1.3 31 st December 2021 Flood in Nicosia Main Hospital.....	5
Figure 1.4 31 st December 2021 Flood in Nicosia.....	5
Figure 1.5 Dikmen During the 5 th December 2018 Flood.....	6
Figure 1.6 Dikmen During the 5 th December 2018 Flood Event	7
Figure 1.7 Dikmen Primary School Yard After the 5 th December 2018 Flood Event	7
Figure 1.8 Dikmen Primary School After the 5 th December 2018 Flood	8
Figure 3.1 Average Daily Percentage Distribution of the Recorded Rainfall in Boğaz Station.....	17
Figure 4.1 Energy Equation Representation	27
Figure 4.2 Unsteady State of the Flow Routing	28
Figure 4.3 Computational Grid Cells and Sub-Grid Cells	30
Figure 4.4 Computational Mesh in HEC-RAS 2D Modeling	34
Figure 4.5 2D - Computational Mesh Area of Dikmen Study Area.....	38
Figure 4.6 Building Polygons.....	39
Figure 4.7 Upstream Boundary Conditions Locations	40
Figure 4.8 Down Stream Boundary Conditions Locations	40
Figure 4.9 Combined Curve of Flood Hazard Assessment	44
Figure 5.1 Cyprus and Dikmen Area Location	48
Figure 5.2 Dikmen Sub-catchments Locations	49
Figure 5.3 Existing Condition of the Dikmen Basin	50
Figure 5.4 The Soil Characteristics Map of the Northern Cyprus.....	53
Figure 5.5 Soil Types of the Sub-basins.....	54
Figure 5.6 Dikmen Flood Plain Land Cover	55
Figure 6.1 The recorded Hyetograph of the Flood Day in Boğaz Station.....	58

Figure 6.2 The Estimated Average Hyetographs of Storms with 50-year, 100-year, and 500-year Return Period	59
Figure 6.3 DEM a) Dikmen Basin, b) Catchments Areas.....	61
Figure 6.4 Flow Direction Raster a)Study Area, b) Catchments Areas.....	61
Figure 6.5 Drainage Networks a) Study Area, b) Catchments Areas	62
Figure 6.6 Slope Raster of the a) Study Area, and b) Catchments Areas	62
Figure 6.7 2018 - Observed Flood Discharge Hydrographs	65
Figure 6.8 50-year Return Period Discharge Hydrographs	65
Figure 6.9 100-year Return Period Discharge Hydrographs.....	66
Figure 6.10 500-year Return Period Discharge Hydrographs.....	66
Figure 7.1 The Flood Maps of the 2018 Flood, Uncalibrated Model, and Calibrated Model	70
Figure 7.2 2018 - Flood Inundation Map.....	71
Figure 7.3 Flood Depths of the Model 2018 Flood	72
Figure 7.4 Maximum Flow Velocity Map of the 2018 Flood Event	73
Figure 7.5 a) Flood Inundation Map, b) Maximum Flood Depth, c) Maximum Flood Velocity Map of 50-year Event	75
Figure 7.6 a) Flood Inundation Map, b) Maximum Flood Depth, c) Maximum Flood Velocity Map of 100-Year Event	75
Figure 7.7 a) Flood Inundation Map, b) Maximum Flood Depth, c) Maximum Flood Velocity Map of 500-year Event	76
Figure 7.8 a) Proposed Channel Location c) Concrete Channel Sections	79
Figure 7.9 Flood Hazard of 2018 Flood Event. a) Before Channel, b) After Channel	81
Figure 7.10 Flood Hazard of 100-Year Return Period Flood Event. a) Before Channel, b) After Channel	83
Figure 7.11 Flood Hazard of 500-Year Return Period Flood Event. a) Before Channel, b) After Channel	84
Figure 7.12 Selected Reservoirs Locations.....	91
Figure 7.13 Top Sub-basin Reservoirs Cross Sections	92

Figure 7.14 Mid sub-basin Reservoirs Cross Sections	93
Figure 7.15 2018- Flood Routed Hydrograph After Without Bottom Outlets Reservoirs in Top Sub-basins	94
Figure 7.16 2018- Flood Routed Hydrograph After Reservoirs Without Bottom Outlets in Mid Sub-basins	95
Figure 7.17 2018- Flood Routed Hydrographs After Reservoirs with 0.5 m Bottom Outlets in Top Sub-basin	96
Figure 7.18 2018- Flood Routed Hydrograph After Reservoirs with 0.5 m Bottom Outlets in Mid Sub-basins	96
Figure 7.19 2018- Flood Routed Hydrographs After Reservoirs With 1.0 m Bottom Outlet in Top Sub-basin.....	97
Figure 7.20 2018- Flood Routed Hydrograph After Reservoirs With 1.0 m Bottom Outlets in Mid Sub-basins	97
Figure 7.21 2018- Flood Routed Hydrographs after Reservoirs With 1.5 m Bottom Outlet in Top Sub-basin.....	98
Figure 7.22 2018- Flood Routed Hydrograph After Reservoirs With 1.5 m Bottom Outlet in Mid Sub-basins.....	98
Figure 7.23 Reservoir W/O Bottom Outlet effects on 500-year Return Period Flood Hydrographs of Top Sub-basin.	101
Figure 7.24 Effect of Reservoirs W/O Bottom Outlets on 500-year Flood Hydrograph of Mid Sub-basin.....	102
Figure 7.25 Reservoir with 1.0 m Bottom Outlet effects on 500-year Return Period Flood Hydrographs of Top Sub-basin.	103
Figure 7.26 Effect of Reservoirs with 1.0 Diameter Bottom Outlets on 500-year Flood Hydrograph of Mid Sub-basin	104
Figure 7.27 RC Retaining Wall Recommended Geometry	107
Figure 7.28 RT3 Reservoir Front View.....	108
Figure 7.29 RT3 Side View of the Reservoir Structure	108
Figure 7.30 2018 - Flood Hazard Map After Channel and Reservoirs with 1.0 m Bottom Outlets.....	112

Figure 7.31 500-year Return Period Flood Map After Reservoirs and Channel Implications.....	113
Figure 7.32 Comparison of Outputs Hydrographs Without and With channel - 2018 Flood Event.....	116
Figure 7.33 Comparison of Outputs Hydrographs Without and With channel - 500-year Flood event	116
Figure 7.34 500-year Average Distribution Hyetograph	119
Figure 7.35 500-year Average Distribution Hydrograph.....	119
Figure 7.36 500-year Attempt-1 Distribution Hyetograph	120
Figure 7.37 500-year Attempt-1 Distribution Hydrograph.....	120
Figure 7.38 500-year Attempt-2 Distribution Hyetograph	121
Figure 7.39 500-year Attempt-2 Distribution Hydrograph.....	121
Figure 7.40 500-year Attempt-3 Distribution Hyetograph	122
Figure 7.41 500-year Attempt-3 Distribution Hydrograph.....	122
Figure 7.42 500-year Attempt-4 Distribution Hydrograph.....	123
Figure 7.43 500-year Attempt-4 Distribution Hyetograph	123
Figure 7.44 Flood Inundation Map of 500-year Attempt-4	125
Figure 7.45 500-year Flood Event. a) Before Channel, b) After Channel – Ave, c) After Channel - Attempt-4	126

CHAPTER 1

INTRODUCTION

1.1 Statement of the Problem

Floods are among the most common natural hazards with diverse socio-economic impacts on the environment and societies. The terms floods and flooding have always been associated with events that can cause damage and destroy houses and hydraulic structures such as levees, dams, bridges, culverts, channels, etc. Nevertheless, they also have a vital and integrated part in the geological history of the natural cycle on earth. Floodings in fluvial regions usually occur when the river experiences a constant and slow rise in water level and overflows from the riverbanks due to rainfall or snow melting into the floodplain areas. On the other hand, pluvial flooding, also known as flash floods, occurs as a result of extreme rainfall events in a short time over a basin with high mean slopes that lead the flood water to reach the town and cities shortly after the rainfall. Apart from these two types of floodings, hydraulic structure failures can also result in the occurrence of floods. Similarly, flooding can also occur in coastal areas due to hurricanes or tsunamis, which can be extremely devastating and damaging to the environment and cities (Mays 2010).

The rapid change in climate conditions, explicitly the temperature rise around the world, has increased the occurrence rate of many natural disasters that previously happened rarely around the world. Evidence shows that about two-thirds of the energy imbalance causing increases in the earth's temperature is linked to the human-induced overwhelming emission of carbon dioxide (CO₂) (Lindsey 2020). The rapid increase in global mean surface temperature, given in Figure 1.1, shows that the temperature rises have increased the possibility of occurrence and the intensity level of droughts and flood events. Warmer air with high-temperature vapors causes more

water, which can fuel more extreme storms and tropical cyclones along with severe flooding events around the globe (Banholzer et al. 2014).

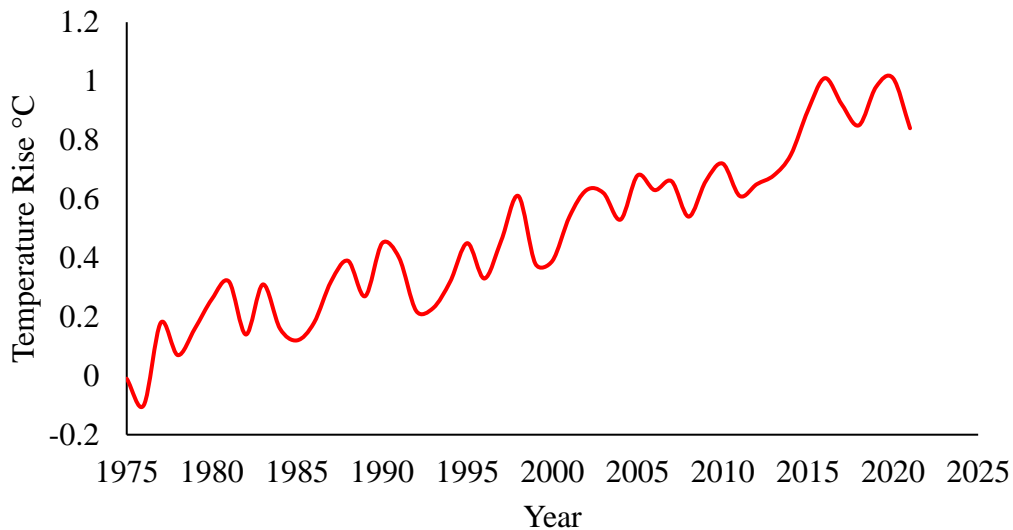


Figure 1.1 Global Temperature Anomaly Between 1975–2021

(Hannah Ritchie et al. 2020)

The recorded flood events in Figure 1.2 indicate a significant upward trend in flood events in the world and Europe, parallel to the increase in the global temperature. It shows that between 1977–1987, the total recorded global flood events worldwide were around 504. This number has risen to 1892 events between 2010–2021, which shows an apparent increase in the recorded floods, which can be similarly seen in the EU. The documented damages due to climate and water-related disasters in the past 50 years have shown a noticeable rise with the increase in occurrence and severity. In the last 50 years, the death casualty of only two significant flood-related events has reached up to 58700 deaths. Meanwhile, the total global economic losses due to flooding in the past 50 years since 1970 have surpassed 1.1 trillion dollars (WMO 2021).

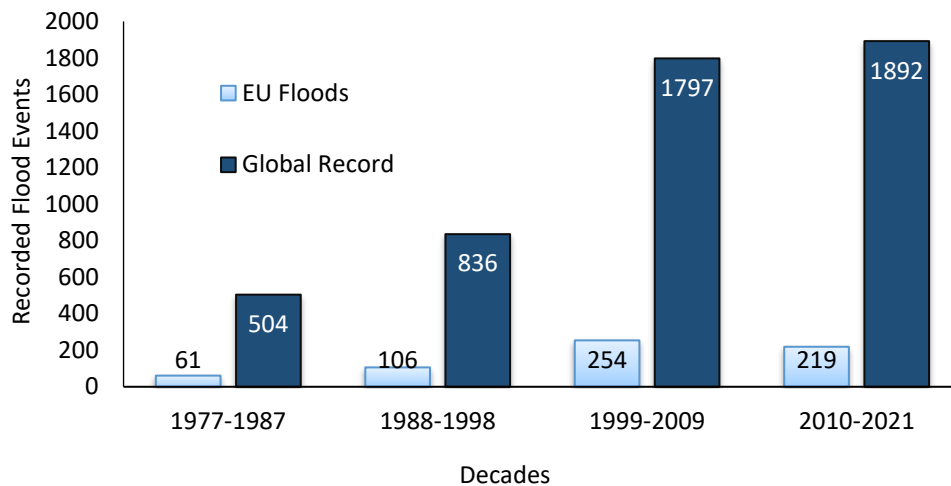


Figure 1.2 Recorded Floods Events in the World and EU Since 1977
(EM - DAT 2021)

According to the records of the WMO (2021), in the 1974 flood in Bangladesh, around 28,700 people died. Similarly, in another event in 1999 in Venezuela, approximately 30,000 people lost their lives. The economic losses due to flooding are also significant. For example, records of flood events in China in 1998, Thailand in 2011, and Korea in 1995 showed that those events caused about \$47.02, \$45.6, and \$25.11 billion in damages, respectively.

With climate change, extreme weather events are expected to occur more frequently and intensely in the future. Even the effects of climate change in terms of the increase in intensities and frequencies of natural disasters are expected to be higher in the Mediterranean region. According to the simulations, the temperature of the Mediterranean region will rise 20% more than the global average temperature by the end of this century (Lionello and Scarascia 2018). Cyprus, located in the Mediterranean region, is also under significant threat of that changes in the climate. The studies suggest that by the 2100s, the temperature on the island of Cyprus will rise between 4°C – 5°C more than the average global level (Zittis et al. 2020; Giannakis et al. 2020). This can lead to significant increases in the occurrence rate

and intensity level of extreme weather events, such as droughts and floods (Tabari 2020).

Some of the most devastating flood events in the past 30 years have caused millions of dollars in economic losses in Turkey. Hundreds of people lost their lives, and many more have been affected. For instance, in the 1995 flood event in Izmir, 61 people lost their lives, which caused a total economic loss of more than \$1 billion. Similarly, the 1979 Yeşilirmak flood event caused the death of nine people and damaged properties and infrastructures worth \$9 million in the area (Şahin et al. 2013). Additionally, the Black Sea region in Turkey is among the places where from time to time, flash floodings cause a significant number of victims and casualties, while triggering severe economic damages to the communities. For instance, the 2015 flash flood incident in Artvin which is located on the eastern coast of the Black. The Artvin flash flood came as a result of a 6-hrs rainfall storm. As a result of that storm, 11 people lost their lives, and the region suffered about 1 million dollars in economic loss and damages (Baltaci 2017). Furthermore, in August 2018 a catastrophic incident of a flash flood along with the landslide occurred in the Ordu Province in the black sea region in Turkey. In that, several people lost their lives or suffered serious injuries. Moreover, some important infrastructures such as bridges, houses, and roads were destroyed (Kocaman et al. 2020).

In Northern Cyprus, flood events have increased in magnitude and frequency. This increase is mainly linked to unplanned urbanization, climate change, and the country's lack of proper sustainable water management systems (Zaifoglu et al. 2019). For example, on the 18th of January, 2010 flood event in the village of Bostanci and Güzelyurt town caused approximate damage of 5 million TL in total, which occurred as a result of a 16-hour extreme rainfall event (Şahin 2013). The event on the 26th of February 2010 in Nicosia caused severe damage to the roads, hospitals, and people's properties (Zaifoglu et al. 2019). Similarly, the recorded event on the 9th of December 2014 was due to short but intense precipitation in Nicosia. It caused many roads to get closed and trapped students and teachers inside a high

school (Zaifoğlu 2018). Another recent example was the floods that occurred on the 31st of December 2021 in different parts of the country. The roads were severely damaged in Kyrenia, and the main hospital building was inundated in Nicosia, as shown in Figures 1.3, and 1.4.



Figure 1.3 31st December 2021 Flood in Nicosia Main Hospital
(Kibrisgazetesi 2021)



Figure 1.4 31st December 2021 Flood in Nicosia
(North Cyprus Now News 2021)

Dikmen, the study area of this research, has also been subject to floods in the past. One of the most devastating flash flood events happened on the 5th of December 2018. The event caused the collapse of a bridge, closed the roads to the upper part of Dikmen town, damaged the Dikmen primary school, flooded around 100 houses, and polluted the primary water source. The 2018 flood occurred directly from 10-hour intense rainfall, which exceeded a total rainfall depth of 172 mm in a day. Some negative consequences of that event can be seen in Figures 1.5, 1.6, 1.7, and 1.8.



Figure 1.5 Dikmen During the 5th December 2018 Flood

(Kibrisgazetasi 2018)



Figure 1.6 Dikmen During the 5th December 2018 Flood Event
(Kibrisgazetasi 2018)



Figure 1.7 Dikmen Primary School Yard After the 5th December 2018 Flood Event
(Cyprus-NEWS 2018)



Figure 1.8 Dikmen Primary School After the 5th December 2018 Flood
(Cyprus-NEWS 2018)

1.2 The Objective of the Study

The main objective of this study is to develop a flood model to identify the vulnerable areas to flooding under different rainfall scenarios. Also, the model is used to find and test suitable flood mitigation measures for the Dikmen town in Northern Cyprus. Furthermore, an extensive economic analysis of the identified measures is performed to find the feasibility and practicality of the solution alternatives. In the scope of this study, topographic data sets are collected and acquired from the Mapping Office in Northern Cyprus. Furthermore, a hydrologically accurate Digital Elevation Model (DEM) is created. The DEM is processed in ArcGIS software to delineate the basin, calculate several basin characteristics, and find the drainage network of each contributing sub-basin. The information from the ArcGIS is then used to develop a hydrological model using Hydrologic Engineering Center's–Hydrological Modeling

System (HEC-HMS). It is employed to generate flow hydrographs resulting from each sub-basins for different return periods.

Furthermore, 2D hydraulic models in Hydrologic Engineering Center's–Hydraulic Modeling System (HEC-RAS) software are developed to perform flood analysis. The flood model is calibrated based on the observed 2018 Flood event. Then it is used to understand the future flood conditions in the study area. Moreover, various mitigation measures are tested by using these flood models. The last part of this study contains an economic analysis of flood mitigation measures.

1.3 Structure of the MSc Thesis

This MSc Thesis is organized in the following manner:

- Chapter 1 contains the introduction to the thesis topic, problem statement, and main objective of the study.
- Chapter 2 covers the literature reviews of the recent developments in the field of flood management.
- Chapter 3 describes the hydrological modeling process and development of the rainfall hyetographs and flow hydrographs.
- Chapter 4 describes the methodologies used in the development of the two-dimensional (2D) hydraulic modeling
- Chapter 5 is about the description of the study area of Dikmen and the data sets that are used in this study.
- Chapter 6 is about the results and discussion of the hydrological analysis.
- Chapter 7 shows the hydraulic analysis results of various flood scenarios, including an experienced 2018 Flood event. In addition, it includes the analysis of adapted mitigation measures.
- Chapter 8 represents an overall summary and conclusion.

CHAPTER 2

LITERATURE REVIEW

The occurrence of floods along the riverine, coastal zone, and urbanized areas have always been an incorporated part of the earth's natural cycle. However, the increase in development and demand for housing leads to a rise in surface imperviousness, as a result, decreases soil infiltration capacities and increases the risk of flooding (Feng et al. 2021). Furthermore, extreme rainfall events, the leading cause of severe floodings, are now being experienced more frequently and more intensely than before due to changing climatic conditions (Mailhot et al. 2007). Therefore, the socio-economic losses and impacts of the flooding on the environment become severe (Cea and Costabile 2022). These challenges urged many scientists and institutions to perform studies containing management plans to reduce the flood risk and decrease the associated damages.

According to the flood directive of the EU (European Parliament 2007), flooding can cause damage to the environment, force people to displace, and even cause human fatalities. In general, the risk of flooding cannot be prevented, especially with climate change, and the chance of occurrence of these events is expected to increase. However, the associated risks can be decreased with proper steps and appropriate managerial plans. The main focus of an effective flood risk management plan should be on the prevention, protection, and preparedness of a region for potential flooding scenarios. For that purpose, flood maps are essential for identifying potential risks considering different rainfall scenarios of extreme, medium, and low probability of occurrences. In this study, the first step in acquiring flood inundation maps is the development of the hydrologic process by considering various characteristics of watersheds like land use/cover, soil properties of the land, and other physical features of catchments. However, generating a reliable hydrological model to simulate the flow from an ungauged catchment is a great challenge (Zaifoglu et al. 2019).

Nevertheless, many studies have utilized different methods that can be used in developing a hydrological model in HEC-HMS to mimic the outflow from a watershed with the use of empirical parameters such as curve number (CN), to calculate the losses in various basins types (Xiao et al. 2011; Ibrahim-Bathis and Ahmed 2016; Satheeshkumar et al. 2017; Al-Ghobari et al. 2020). After the hydrological modeling process, hydraulic models need to be developed to generate flood inundation maps of an interested area.

Various numerical modeling tools such as SOBEK, MIKE, and TUFLOW can present an overall view of the most vulnerable and critical areas to flood and show the risk associated with different flood events. However, the 2D capacity analysis of HEC-RAS software using the benchmark test developed by the UK's Joint Defra Environment Agency is done by (Brunner 2016). The results indicated that overall 2D HEC-RAS performed exceptionally well compared to the other models (Ongdas et al. 2020). For example, Mai and De Smedt (2017) developed an integrated hydrologic and hydraulic model to use in flood forecasting and to create a flood early warning system in Vietnam. In that process, the WetSPA modeling tool is utilized for the hydrological model generation to obtain a flow hydrograph from the Thua Thien-Hue basin in central Vietnam with an area of 2830 km². After that, the flow hydrograph is defined in an HEC-RAS model to generate flood maps that accurately represent the observed water surface levels. The result indicated that the integrated model could be used to predict future flood scenarios with inundation and depths.

Furthermore, the flood map of the Bostanli river basin, which is the main catchment with an area of 29.6 km² to the Bostanli Dam in Izmir, Turkey, is modeled with HEC-RAS. This hydraulic model showed that HEC-RAS can test the efficiency of the existing flood control structures, such as the Bostanli Dam in Izmir (Gül et al. 2010). Also, many other studies have used models to identify flood-prone zones in urban areas. For example, (Mihu-Pintilie et al. 2019) developed a 2D HEC-RAS model to simulate the streamflow of the Bistrita River within the urban and pre-urban regions in Bacau city in northeast Romania and generate multi-scenarios based flood hazard

maps. Similarly, Kumar et al. (2020) utilized Global Flood Monitoring System (GFMS) along with 2D HEC-RAS features to understand and delineate different flood inundation and flood risk zones in the Prayagraj region in India. Likewise, Rangari et al. (2019) developed a 2D HEC-RAS model and Geographic Information Systems (GIS) processing tool to generate flood depth and inundation maps, to classify the risk level from high to low for each part of the flooded area under various flood scenarios in Hyderabad, India. Meanwhile, Ongdas et al. (2020), in a case study on the Yesil (Ishim) River in Kazakhstan, showed that the 2D HEC-RAS models are capable of representing and simulating a past flood event with an acceptable accuracy level and can generate flood hazards maps considering various future flood conditions.

Flood hazard and risk maps can assist planners in understanding many aspects of flood risks and potential damages in a given area. These maps are critical for managing and reducing community and environmental concerns. This also aids in the adaptation and development of effective mitigation strategies. The commonly preferred structural mitigation strategies are constructing physical structures to redirect and regulate water via levees, dikes, diversion, and bypass canals, or storing flood water in large- or small-scale reservoirs.

Many studies have suggested and tested the effectiveness of different structural measures in reducing peak flow and flood inundation areas with the help of structural measures. For example, the flood management plan of the Danube river basin, which is shared in 19 different countries in Europe and covers a total area of 800,000 km², is adopted in Vienna, Austria, which usually has been exposed to flooding of the Danube river. The historically recorded floods in 1501 AC, or 16th and 17th centuries, are among the events in which the peak discharge reached about 14,000 m³/s. To prevent the potential damages of floods in Vienna, many plans have been proposed, including building lateral structures along the bank of the river or widening the river channel along the Danube river. However, the recently adopted measure, known as the New Danube project, involves constructing and excavating a canal with a length

of 21 km and a width of 210 m This project successfully protects the city against floods and leads to ecological improvements by creating a large green area inside the city (Kryžanowski et al. 2014).

Similarly, along the Danube river, about 62 km east of Vienna, is Bratislava, the capital city of Slovakia. Bratislava has also been experiencing the same flood regimes as Vienna city. The protection measures for Bratislava on both sides of the Danube river were first started to construct in 2007 and finished in 2010. The measures included the construction of dams, levees, concrete walls, and mobile wall elements to be placed in times of flooding. Similarly, Belgrade, the capital city of Serbia is further down along the Danube river about 450 km southeast of Bratislava. The flooding has also been causing severe economic damage to the communities and people there. The projects to protect Belgrade against the 1000-year return period flooding of the Danube river were first initiated in 1972 and finished in 1989. The completed projects include the reinforcement efforts on the river banks, the construction of new embankments, and three small water reservoirs along the path of the Danube river (Kryžanowski et al. 2014).

Furthermore, the consequent flooding in the Ichinomiya river basin in Japan has caused severe and destructive economic damage to communities living in those areas. To reduce the risks and decrease the financial losses, many plans, including the improvement in the conveyance capacity of the river and increasing the height of the embankments, have been implemented. However, none was successful enough, as the flood in September 1996 showed. Thus, a decision by the provincial government was taken to implement three extra structural measures that include a further increase in the embankment heights, smoothing the river bed to decrease the resistance, and construction of four retarding reservoirs to store flood water during the flood peak time. Dutta et al. (2006) showed that the newly proposed measures on the Ichinomiya river in Japan could significantly decrease flood risk against 50- and 100-year flood events and reduce the urban and agriculture damages by 70%.

Although structural measures have shown to have the capacity to control the flood and reduce the associated risks in many regions, in some situations, using solely structural measures is not enough. Thus, it would require structural efforts to get combined with non-structural flood control measures, such as efficient land planning, land regulation, development of flood awareness, and an early flood warning system to reduce the damages significantly (Kundzewicz 2002).

The Ministry of Agriculture and Forestry (MOAF) of the Republic of Turkey has also developed several flood management plans to reduce economic and environmental losses due to consistent flooding events throughout the country. Based on the 2019 report by the MOAF (Serdar Özcan 2019), flood risk assessment and management plans for Yesilirmak, Antalya, Susurluk, Ceyhan, and Sakarya basins have been completed. Appropriate structural and non-structural measures have been taken into action. For example, the Sakarya Basin's flood management and risk assessment plan against a 500-year return period flood have been presented. The project's first stage involved identifying the areas at risk, and several structural measures, including widening the river beds, constructing several retarding flood detention basins, and reinforcing the hydraulic structures. Also, in the flood management plan of the Sakarya Basin in Turkey, along with the structural measures mentioned above, the non-structural measures have been adapted, such as one flood early warning system in the center of Ankara, cleaning and restoration works of the river beds, and flood awareness efforts.

Additionally, in Northern Cyprus in recent years, limited efforts have been made to identify the areas at risk of flooding and propose the appropriate flood management strategies. For example, flood mitigation measures for the northern part of Nicosia and Gönyeli town are identified in an extensive study by Zaifoğlu (2018). In that study, the inflows to the Kanliköy and Gönyeli reservoirs have been collected from the hillside of the Kyrenia Mountains. After passing from the reservoirs, they flow through Gönyeli town and the northern part of Nicosia town. The hydrologic process of the flood model is simulated with the help of the HEC-HMS modeling tools to

generate the outflow from the ungauged reservoirs. The generated outflows are then defined in the 1D- MIKE 11 and 2D- MIKE 21 to create the flood maps of the area under different flooding scenarios. The identified and proposed structural measures that are capable of reducing the flood risk in Gönyeli town and the northern part of Nicosia consist of the construction of a new reservoir at the upstream side of the existing Kanliköy reservoir, increasing the crest elevations of the existing GÖnyeli reservoir and its capacity, and restoration of the creeks. The implementation of these measures has shown to have the ability to significantly protect the northern part of Nicosia against events up to a 500-year return period (Zaifoglu et al. 2019).

CHAPTER 3

HYDROLOGICAL ANALYSIS METHODOLOGIES

This chapter explains the adapted methodologies for hydrological analysis, considering different parameters and the availability of the data sets for the Dikmen Basin.

3.1 Hydrological Analysis

The primary goal of hydrological modeling is to create flow hydrographs for various return periods while accounting for rare extreme rainfall events to provide inputs to the hydrodynamic flood models. Due to the lack of streamflow data in the Top, Mid, and Low sub-basin catchments, the upstream flow input to the hydraulic model is generated by creating rainfall-runoff models using HEC-HMS hydrological modeling tools.

3.1.1 Design Rainfall Hyetograph for Dikmen Urban Area

The rainfall depth that would occur with a given occurrence frequency is potentially considered as a base value for the design of a structure, which is referred to as design rainfall. The design rainfalls for three scenarios (50-, 100-, and 500-year events) were chosen to reflect high, medium, and low probability instances in this study. The high probability rainfall design values are more commonly used in the design of hydraulic structures. However, to reflect the extreme cases of flooding that would occur rarely, 100-year and 500-year events, which are used to generate maps with higher associated risks, are also considered. In the first stage of constructing design rainfalls, a 24-hour rainfall distribution curve was derived from recorded rainfall data sets for the Boğaz station between 2010 and 2018. The recorded rainfalls are filtered

so that only the rainfall depth with a greater value than 10 mm is considered to create a representative hourly distribution of the rainfall. According to rainfall records and generated average distribution curve shown in Figure 3.1, around 80% of the rain falls in the first 8 hours after the storm begins, with the remaining 20% falling in the next 14 hours.

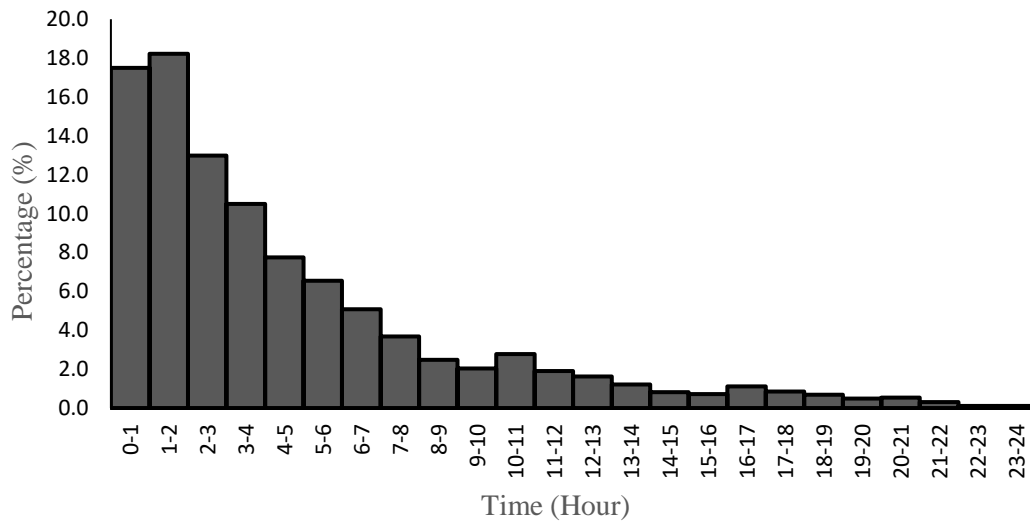


Figure 3.1 Average Daily Percentage Distribution of the Recorded Rainfall in Boğaz Station

Furthermore, to generate the design hyetograph that can be used in the hydrological model, the annual maximum daily rainfalls for each scenario (50-year, 100-year, and 500-year) are adapted from Zaifoglu et al. (2018). Herein, Boğaz station is selected as a representative station due to the closeness to the study area.

3.1.2 Hydrological Model Development

To convert the design rainfall to runoff, a model to represent this process is developed with the help of HEC-HMS software developed by the Hydrologic Engineering Center of the US Army Corps of Engineers (HEC-HMS 2022). To have a functioning model, a basin model in which various essential catchment characteristics and selected loss and transform methods need to be specified. Furthermore, the model also requires a meteorologic model and time series data components to introduce selected hyetograph with appropriate time increments for different rainfall scenarios.

Moreover, various loss methods that calculate the losses due to different factors, such as soil infiltration, evaporation, and other obstacles, must be selected. The available loss methods in the HEC-HMS are Green Ampt loss methods, Soil Conservation Services Curve Number (SCS-CN), and initial and constant loss methods. Furthermore, the transformation of the rainfall and generating runoff models can be performed using different methods. For example, the most common transformation methods in HEC-HMS are Soil Conservation Services (SCS), Clark's, and Snyder unit hydrograph methods. The baseflow that shows the prior stored precipitation in a watershed can be modeled using different available methods as well, such as the constant monthly-varying baseflow value method, exponential recession model, and linear reservoir volume accounting model. In the meteorological component, the properties related to meteorological conditions of the catchments like precipitation, evapotranspiration, temperature, or even specified hyetographs can be directly introduced (HEC-HMS 2022).

The methods listed below are chosen to perform the analysis and generate the rainfall-runoff components of the Dikmen study area. The selection of the methods is based on the availability of the information and data sets, practicality, and suitability of each method based on the climate and meteorologic conditions of the basin.

3.1.2.1 SCS Curve Number Loss Method

The Soil Conservation Curve Number (SCS-CN) method was initially developed in 1954 and has been revised many times by the Soil Conservative Services US Department of Agriculture. The method is widely used because of its simplicity and ease of application in modeling the rainfall-runoff process in ungauged watersheds (Mishra and Singh 2003). Besides, the method is one of the most commonly practiced loss methods in hydrological analyses (Ponce and Hawkins 1996). The SCS-CN method estimates the excess rainfall volume from the catchments as follows (Mishra and Singh 2003):

$$P_e = \frac{(P - I_a)^2}{(P - I_a) + S} \quad (1)$$

where P_e is the amount of excess rainfall, and P is the amount of accumulated rainfall depth in time t . Furthermore, I_a is the initial abstraction, which is the total sum of depression and interception, can be expressed as follows:

$$I_a = 0.2 * S \quad (2)$$

where S is the maximum potential retention.

Furthermore, the relationship between finding excess rainfall P_e can be expressed as follow:

$$P_e = \frac{(P - 0.2S)^2}{P + 0.8S} \quad (3)$$

To obtain S , curve number CN of the watershed can be entered in the equation (4).

$$S = \frac{25400}{CN} - 254 \quad (4)$$

CN for catchment can be determined based on the soil properties and land use characteristics in a watershed. Generally, the soil is categorized into four hydrological groups, starting from A with low runoff capability to D, which has the

highest runoff potential among other groups (NRCS Staff 2009; Mays 2010). Furthermore, in the catchment with different soil groups and characteristics that have different CN values, a composite $CN_{Combined}$ value for the basin can be calculated as follows:

$$CN_{Combined} = \frac{\sum(A_{Si} * CN_{Si})}{\sum A_{Si}} \quad (5)$$

where A_{Si} is the area of the sub-catchment with a homogenous curve number CN_{Si} value.

3.1.2.2 SCS Unit Hydrograph Transformation Method

The unit hydrograph (UH) developed by the Soil Conservation Service (SCS) is a dimensionless hydrograph created from the analysis of many watersheds. In the unit hydrograph UH procedure, the assumption is that discharge at any given time is proportional to the runoff volume. The time factors and the effect on the hydrograph shape are constant. The dimensionless UH is useful in estimating the runoff value from an ungauged catchment. Many agencies recommend facilitating the construction of a synthetic UH (NRCS Staff 2007). The equation needed to generate a UH from an ungauged catchment is given as (Mays 2010):

$$Q_{peak} = \frac{2.08 A_{cat}}{t_{peak}} \quad (6)$$

where Q_{peak} in m^3/sec represents the UH peak discharge from a watershed, while A_{cat} and t_{peak} represent the catchment area in km^2 and time to peak in hr that indicates rise time to the peak of UH respectively.

To calculate the time to peak t_{peak} (hr):

$$t_{peak} = \frac{T_{ro}}{2} + T_{lag} \quad (7)$$

Here, T_{ro} represents the excess rainfall duration in hr, T_{lag} in hr is the time needed to reach from the center of the mass of the rainfall excess to the peak discharge and can be calculated as follows:

$$T_{lag} = \frac{L^{0.8}(S + 1)^{0.7}}{1900 S_0^{0.5}} \quad (8)$$

where L is the mainstream channel length in ft, S is the maximum potential retention in inches, and S_0 is the mean slope of the catchment area in (%). Furthermore, the T_{ro} in hr can be calculated as:

$$T_{ro} = 1.33 T_C \quad (9)$$

$$T_C = \frac{5}{3} T_{lag} \quad (10)$$

Herein, the time of concentration T_C in hr is the necessary time for a particle to travel from the hydrologically most distant part of the catchment to the designated outlet point.

3.1.3 Reservoir Routing Process

One of the most extensively adopted structural measures is reservoirs to prevent and reduce the generated risks of flooding on river channels, levees, and floodplains in metropolitan areas. This method lowers the kinetic energy of flood waves, lowers the flood hydrograph, and delays the arrival of peak flood discharges (Fedorov et al. 2016). Furthermore, reservoirs can help limit stream erosion and provide some pollution control and management (Yanmaz 2018).

In a flow system, detention reservoirs hold inflow water. When the reservoirs' storage capacity reaches its maximum capacity, excess flow is released by an outlet, such as an emergency spillway or bottom outlet pipes. The presence of water storage systems can help to delay and reduce peak discharge. However, inflow hydrographs generated from a hydrological model are essential to design and test the efficiency

of one or more reservoirs in a system (Yanmaz 2018). The outflow curve routing method in HEC-HMS is designed to represent a reservoir with a known relationship between the storage capacity and the outflow rate (HEC-HMS 2022). However, this method allows the lump sum representation of all the discharges into a single storage-discharge relationship. This model is based on the concept of continuity, Eq. (11) (HEC-HMS 2022). Furthermore, a storage method for representing the primary relationship between the storage-stage and stage-discharges needs to be defined appropriately after selecting the appropriate routing method. Then, the model needs to provide the initial condition of the reservoir, stage-storage curve, and storage-discharge curve relationships.

The stage-storage relationship defines the volumetric difference for the changes in the elevation of the reservoir as a function of storage (S_R) in m^3 , surface area (A_R) in m^2 , and water elevation from the bottom of the weir (h_W) in m (Akan and Houghtalen 2003). The same relationship between the storage capacity and elevation of the reservoir can be generated using the ArcGIS 3D-Analyst tool.

$$\frac{\Delta S(t)}{\Delta t} = I_{(t)} - Q_{(t)} \quad (11)$$

$$S_{R2} = S_{R1} + \frac{h_{W2} - h_{W1}}{3} (A_{R1} + A_{R2} + \sqrt{A_{R1} * A_{R2}}) \quad (12)$$

In the continuity equation, $\frac{\Delta S}{\Delta t}$ represents the rate of change in reservoir storage S_R , $I_{(t)}$ inflow, and $Q_{(t)}$ is the outflow from the reservoir.

Furthermore, in the case of considering one or multiple bottom outlets, the stage-discharge relationship due to the existence of an orifice-type bottom outlet system can be calculated as:

$$Q_o = K_o a_o \sqrt{2gh_a} \quad (13)$$

where

$$Q_o = \text{Discharge} \left(\frac{m^3}{s} \right)$$

K_0 = Dimensionless orifice discharge coefficient.

a_o = Orifice area (m^2)

g = Gravitational acceleration ($\frac{m}{s^2}$)

h_a = Depth of water above the orifice center (m)

Moreover, the stage-discharge relationship of detention reservoir in a system with sharp crests spillways emergency evacuating system can be expressed as (Mays 2010):

$$Q_S = C_d \frac{2}{3} \sqrt{2g} B_C * H_C^{\frac{3}{2}} \quad (14)$$

where,

Q_S = Discharge from the spillway ($\frac{m^3}{s}$)

C_d = Dimensionless spillway discharge coefficient

B_C = Crest width (m)

H_C = Head above the crest level (m)

In the outflow curve routing method, a lump sum of the total discharges for the different stages of the reservoirs can be expressed using Eq. 15. In that Q_{sum} is the total amount of the discharge from the orifice-type bottom outlet and the emergency spillway concerning the changes in the elevation.

The established stage-storage and stage-discharge relationships, and initial conditions for each reservoir at the beginning of the storm event (e.g., full reservoir or empty reservoir), need to be inserted into the model. In the case of a multiple reservoir system, the outflow curve from the first reservoir can be used as inflow to the next one. The process continues until the last outflow hydrograph is generated from the outlet of the last reservoir in the system.

3.2 Processing of the Digital Elevation Model (DEM) for Floodplain Area

The flood modeling and management process in an urbanized area is a global challenge (Cea and Costabile 2022), owing to various physical obstacles such as roads, buildings, ponds, etc. The accurate representation of the ground conditions in a model in the form of topographic data formats can influence the environmental process in a model. On the other hand, acquiring high-resolution and precise topographic data is expensive and is one of the most challenging parts of developing a flood model in a 2D environment. Nevertheless, in this research study, the local mapping authorities provide the topographic data sets for the study area in scanned contour maps for every 5 m. The first stage was to digitize the paper-based maps into the digital format of the Digital Elevation Model (DEM), using the topo to raster method. Topo to raster function in ArcGIS is specifically designed to work intelligently with contour polylines to generate a digital map. This method also aids in the creation of DEMs that are hydrologically accurate and have proper drainage structures for accurately portraying streams. (Habib et al. 2020).

However, since DEMs only depict bare ground, a Digital Terrain Model (DTM) that includes buildings and roads is preferable for a more accurate representation of the metropolitan area in flood models (Zaifoglu et al. 2019). Therefore, the buildings' footprints and roads were provided by the authorities, which were then used to alter the DEM and generate the final DTM for the study area.

The first stage was to check whether the final DTM result was hydrologically accurate and free of sinks that could cause calculation mistakes. For that reason, the raster analysis was performed using the available hydrology tools in ArcGIS software to fill the potential sink points, generate a flow direction raster, flow accumulations map, stream network, and perform catchment delineation. Finally, the catchments were processed to determine the geometric and surface characteristics of the Dikmen basin.

CHAPTER 4

HYDRAULIC ANALYSIS METHODOLOGIES

This chapter shows the methodologies adapted in developing the flood model. The 2D-flood model is generated using the HEC-RAS software for hydraulic modeling and inundation map generation. Furthermore, the proposed mitigation measures are tested for flood protection in Dikmen urban areas.

4.1 History of HEC-RAS

HEC-RAS is among the first windows-based software developed by the Hydrologic Engineering Center (HEC) in the early 1990s. HEC-RAS, which stands for the Hydrologic Engineering Center – River Analysis System, was first released in 1995 as a replacement to the HEC-2 with the capability to perform relevant calculations to determine the water surface profile in a river system.

Since then, the capabilities of the HEC-RAS modeling tools have grown significantly. The earliest version of the software was only performing 1D-steady analysis. However, the 2001 January release of version 3.0 included the computation concerning 1D-unsteady analysis. Furthermore, with the release of version 5.0 in 2016, HEC-RAS gained the capability to perform 2D analysis systems which is an excellent tool for flood analysis in a location where the flow direction is difficult to determine (Alzahrani 2019). HEC-RAS V5.0 had some limitations in terms of modeling bridges and hydraulic structures into a 2D environment. However, with the release of the HEC-RAS V6.0, most of those limitations are now emitted. The currently freely available HEC-RAS version is V6.2, released in March 2022 not only performs 1D/2D steady/unsteady analysis systems, but can also perform rain on grid watershed model, modeling the hydraulic structures inside the 2D area, and

generate risk hazards maps with the help of the Raster Calculator embedded within the RAS-Mapper tools in HEC-RAS (HEC-RAS 2022).

4.1.1 1D HEC-RAS Flood Inundation Modeling

4.1.1.1 1D – Steady Flow Analysis Theorem in HEC-RAS

The early version of the HEC-RAS could simulate the flow inside a channel in a steady-state, gradually varied manner. The steady flow state describes a condition that a flow does not undergo any changes with time, meaning it constantly flows with the same magnitude. On the other hand, gradually varied flow states that the water surface profile of the flow is not changing with the changes in distance. The water surface profile calculation in a steady state is performed by solving the energy equation between two cross-sections in a channel, known as the standard step method. The energy grade line in Figure 4.1 governs the steady state between from upstream cross-section to the downstream cross-section of the flow, and its equation can be expressed as follows:

$$Z_{c2} + Y_{c2} + \frac{\alpha_{c2}V_{c2}^2}{2g} = Z_{c1} + Y_{c1} + \frac{\alpha_{c1}V_{c1}^2}{2g} + h_L \quad (15)$$

where Z_{c1} and Z_{c2} are the elevations of the channel bed from a hypothetical datum line, Y_{c1} and Y_{c2} illustrates the water surface elevation from the channel bed, V_{c1} and V_{c2} are the flow velocity, g is the gravitational acceleration, α is velocity weighting coefficients, and h_L is the headloss between two cross sections.

Furthermore, the losses in a channel are comprised of the losses due to friction and contraction and expansion of the channel in two consequent cross-sections. The headloss can be computed as:

$$h_L = L_C S_{Cf} + C \left| \frac{\alpha_{c2}V_{c2}^2}{2g} - \frac{\alpha_{c1}V_{c1}^2}{2g} \right| \quad (16)$$

where the L_C is the weighted reach length of the channel, S_{Cf} is the friction slope of the channel, and C represents the loss coefficients of the contraction or expansion between two cross-sections.

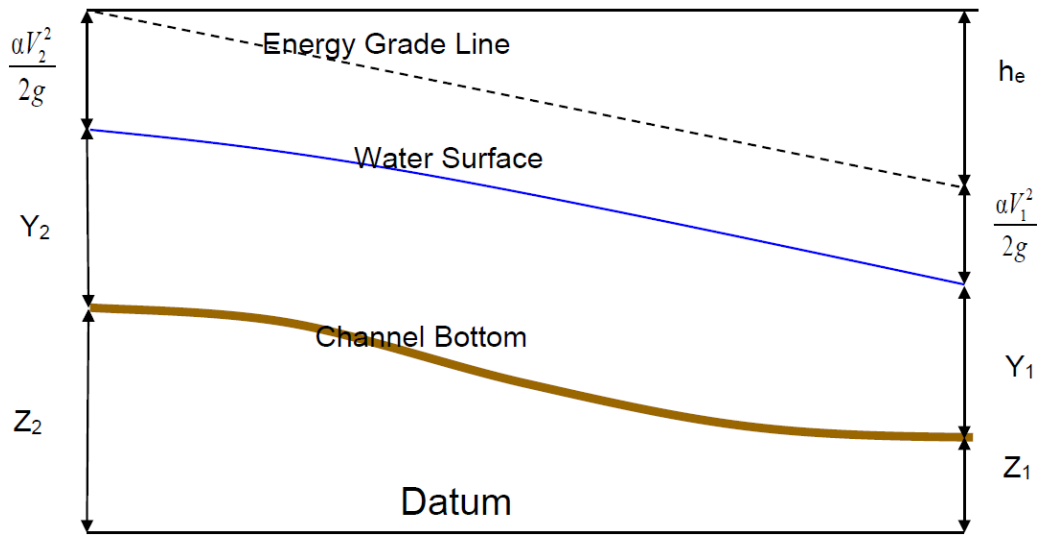


Figure 4.1 Energy Equation Representation (Brunner 2016b)

Moreover, the weighted reach length L_C is obtained with Eq. (17) using the left overbank L_{l-b} , right overbank L_{r-b} , main channel L_{cha} distances, and the flow averages Q_{l-b} , Q_{r-b} and Q_{cha} in left overbank, right overbank, and main channel, respectively (Brunner 2016).

$$L_C = \frac{L_{l-b}Q_{l-b} + L_{r-b}Q_{r-b} + L_{cha}Q_{cha}}{Q_{l-b} + Q_{r-b} + Q_{cha}} \quad (17)$$

4.1.1.2 1D – Unsteady Flow Analysis Theorem in HEC-RAS

The assumption that the flow is moving in a steady state is usually inaccurate with the natural channel flow. It usually flows in unsteady state conditions. Unsteady flow condition is the state in which the flow varies with time. Furthermore, the routing process of the unsteady flow is the process of determining the flow depths and

amounts in different locations of the channel at different times. In other words, the flow velocity, water depth, and discharge amount are all functions of the distances between two cross-sections along the channel path, as illustrated in Figure 4.2.

In HEC-RAS, the routing process of 1D unsteady flow is performed by solving the Saint-Venant equations, also known as the Shallow Water Equation (SWE), which Barre de Saint-Venant first developed in the late 1800s (Alzahrani 2019). The SWE is based on the conservation of mass, Eq. (18), and conservation of momentum, Eq. (19), when applied to a small control volume of fluid in a system.

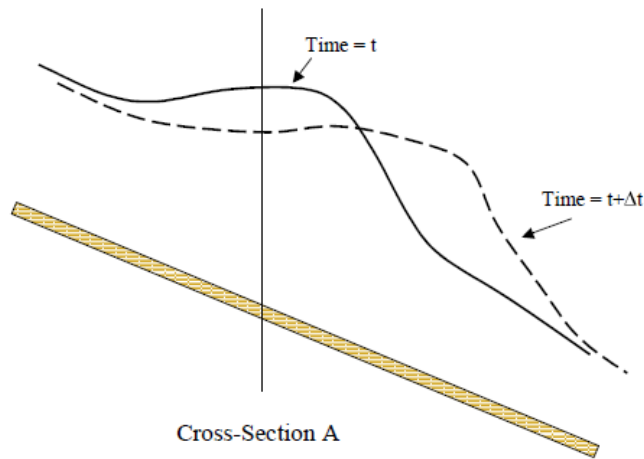


Figure 4.2 Unsteady State of the Flow Routing (Alzahrani 2019)

$$\frac{\Delta A_{ch}}{\Delta t} + \frac{\Delta Q_{ch}}{\Delta x} - q = 0 \quad (18)$$

$$\frac{\Delta Q_{ch}}{\Delta x} + \frac{\Delta Q_{ch} V_c}{\Delta x} + g A_{ch} \left(\frac{\Delta z}{\Delta x} + S_{cf} \right) = 0 \quad (19)$$

In these two equations, Q_{ch} is the discharge rate, A_{ch} is the cross-sectional area of the channel, t is the time, x is the horizontal distance along the channel path, q is the sink term, V_c is the flow velocity in the channel, g is the gravitational constant, S_{cf} represents the friction slope of the channel, and $\frac{\Delta z}{\Delta x}$ is the side slope of the channel.

4.1.2 2D HEC-RAS Unsteady Flood Modeling Approach

In the 2D HEC-RAS modeling approach, the fundamental concept is to discretize the channel or river plain with the adjacent plains with a collection of individual and connected cells known as grid cells or computational cells. Each computational cell contains various hydraulic information, such as the topographic elevation, roughness value, and slope frictions of the ground surface. The sub-grid bathymetry approach is used in HEC-RAS. In this approach, computational grid cells are formed from a combination of multiple GIS grid cells shown in Figure 4.3. A GIS sub-grid cell in HEC-RAS contains a unique elevation value of the ground. A collection of these cells can make up a terrain model representing a digitized ground condition model (Alzahrani 2019).

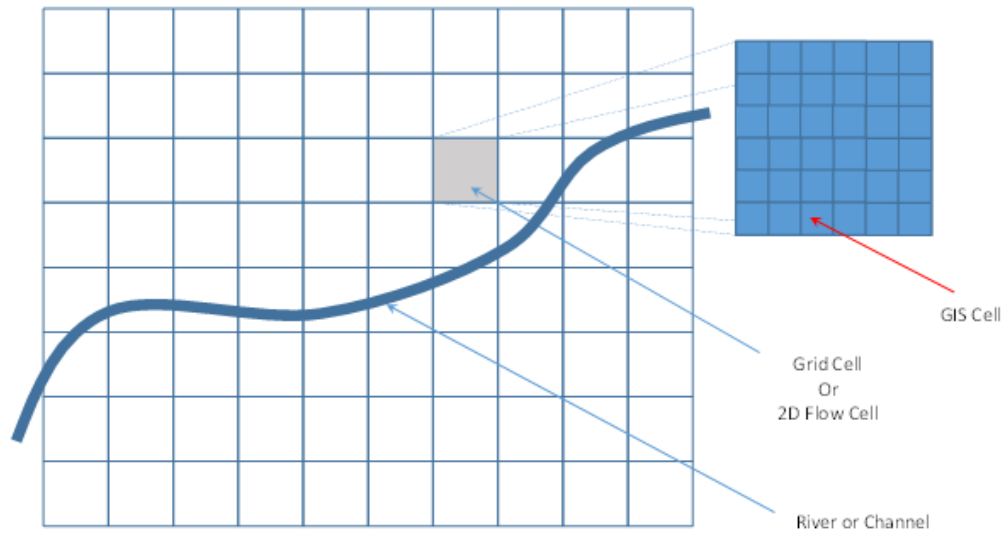


Figure 4.3 Computational Grid Cells and Sub-Grid Cells (Alzahrani 2019)

The sub-grid bathymetry approach is preferred to be used to enable the use of coarser grid cells even with high-resolution topographic data sets. The computation time and model size increase significantly if finer cell sizes are used. Furthermore, even with the coarser computation of cell sizes, the hydraulic properties, such as hydraulic radius, volume, and cross-sectional area, can be computed through mass conservation (Brunner 2016).

In the 2D model with unsteady flow conditions, the continuity equation is altered with the assumption that the flow is incompressible;

$$\frac{\partial H_w}{\partial t} + \frac{\partial(h_d u_x)}{\partial x} + \frac{\partial(h_d v_y)}{\partial y} + q_s = 0 \quad (20)$$

where H_w represents the water surface elevation, t is time, h_d is water depth, q_s is the source flux, u_x and v_y represent the velocity components in both x and y-directions, respectively.

However, when performing the 2D-HEC-RAS analysis, the user can select among the two available equations: The Shallow Water Equation (SWE) and Diffusion Wave Equation (DWE) (HEC-RAS 2022).

4.1.2.1 2D - Shallow Water Equations (SWE)

The 2D Shallow Water Equation is given as (Brunner 2016):

For x-direction:

$$\frac{\partial u_x}{\partial t} + u_x \frac{\partial u_x}{\partial x} + v_y \frac{\partial u_x}{\partial y} = -g \frac{\partial H_w}{\partial x} + v_t \left(\frac{\partial^2 u_x}{\partial x^2} + \frac{\partial^2 u_x}{\partial y^2} \right) - c_f u_x + f v_y \quad (21)$$

For y-direction:

$$\frac{\partial v_y}{\partial t} + u_x \frac{\partial v_y}{\partial x} + v_y \frac{\partial v_y}{\partial y} = -g \frac{\partial H_w}{\partial y} + v_t \left(\frac{\partial^2 v_y}{\partial x^2} + \frac{\partial^2 v_y}{\partial y^2} \right) - c_f v_y + f u_x \quad (22)$$

In Eq.s (21) and (22), v_t is the vertical Eddy viscosity coefficient, c_f is the bottom friction loss coefficient, and f is the Coriolis parameter.

Vertical Eddy viscosity can be calculated as (Brunner 2016):

$$v_t = D_{cons} h_d u_s \quad (23)$$

where, D_{cons} is the empirical non-dimensional constant, u_s is the shear velocity, and h_d is water depth. Furthermore, shear velocity can be computed (Brunner 2016):

$$u_s = \sqrt{g R S_e} \quad (24)$$

where R is the hydraulic radius in a cross-section area and S_e is the energy slope value.

The bottom friction coefficient can be calculated using Manning's equation:

$$c_f = \frac{n^2 g |V|}{R^{\frac{4}{3}}} \quad (25)$$

where n is Manning's roughness coefficient, V is the flow velocity, and R is the hydraulic radius.

4.1.2.2 Diffusion Wave Equation (DWE)

The Diffusion Wave Equation is a simplified version of the SWE equation, in which inertial terms are neglected in the horizontal momentum equation. The Diffusion Wave form of the momentum equation becomes;

$$\frac{n^2 |V| V}{(R(H_w))^{\frac{4}{3}}} = -\nabla H_w \quad (26)$$

Both sides are divided with the square root of their norm for simplification. Then, the equation can be rearranged into a more classical form:

$$V = \frac{-(R(H_w))^{\frac{2}{3}} \nabla H_w}{n |\nabla H_w|^{\frac{1}{2}}} \quad (27)$$

where V represents velocity vector, R is the hydraulic radius, ∇H_w is the surface elevation gradient, and n is Manning's roughness coefficient.

Furthermore, the diffusion wave equation can be expressed (Brunner 2016):

$$\frac{\partial H_w}{\partial t} - \nabla * \beta \nabla H_w + q = 0 \quad (28)$$

where ∇ is differential operational del and β can be computed as:

$$\beta = \frac{(R(H_w))^{\frac{5}{3}}}{n |\nabla H_w|^{\frac{1}{2}}} \quad (29)$$

4.1.2.3 Selection of the Appropriate Equation for Analysis

In HEC-RAS 2D modeling, selecting the appropriate equation for running a successful simulation and analysis depends on various factors. However, a general guideline is presented in the user manual (HEC-RAS 2022) for selecting an equation for the 2D analysis. The SWE and DWE method can both generate results in HEC-RAS. The main difference between these two equations is the model's file size and computational time step. In general, DWE can run with coarser time steps. Thus, the file size can be smaller. To decide on the selection of the computation equation, first, the model should be simulated with DWE. After that, a second model with the same characteristic, only this time with the SWE equation needs to be set up and computed. The outputs from both models should be compared. If there is a significant difference between the results, the model with the SWE equation is likely more accurate, and future considerations need to be taken accordingly.

However, regardless of the other situations, in some unique conditions that are listed below, the user needs to always run the model with the SWE equation (HEC-RAS 2022):

1. If the purpose is to model a dam break or flash flood analysis since the changes in flood waves are very rapid in these cases.
2. In locations with abrupt contraction and expansion.
3. Very flat sloping river system analysis.
4. If the model is influenced by tidal waves.
5. In the case of modeling flood propagation.
6. In the case of aiming to develop detailed velocity and water surface distributions at or near hydraulic structures.

4.1.2.4 Selection of Appropriate Mesh Size

Appropriate mesh size is among the most crucial factors in acquiring more accurate simulation results. The selection of the computation cells must be based on the terrain and the flow of water in the model. Each cell can have three, four, and up to eight sides, as shown in Figure 4.4. The model cells are detailed cross-sections converted into relationships between elevation-area, wetter perimeter, and roughness values. The critical key in choosing an appropriate mesh size is to ensure that cells are capable enough to capture all the high points of an object that disrupt the flow.

Another important thing is to consider the difference in the water surface elevation level (WSEL). Since only one WSEL value is computed in the center of cells, the larger the cells, the further the values of calculated water surfaces. Thus, smaller cells need to be selected in cases with a very high slope area to accurately capture the rapid changes in WSEL and flow velocity (HEC-RAS 2022).

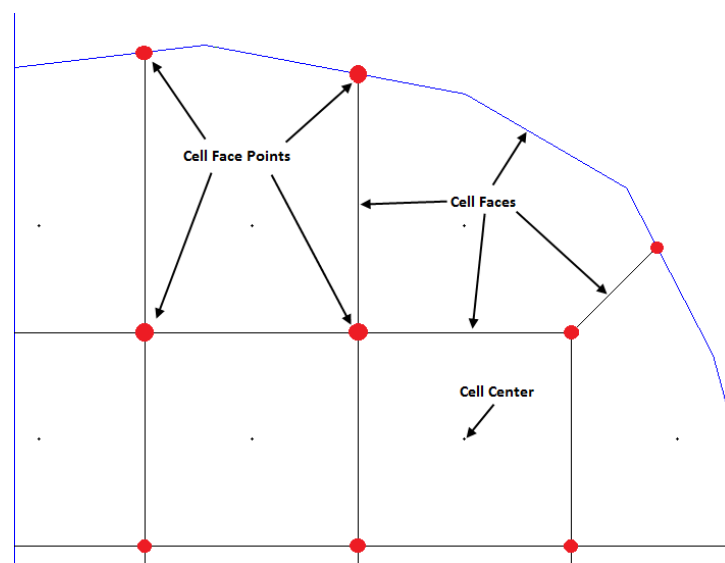


Figure 4.4 Computational Mesh in HEC-RAS 2D Modeling

4.1.2.5 Selection of Appropriate Computation Time Step

The selection of the time steps for computation also plays an important role in the model's accuracy. In HEC-RAS, the time steps can be introduced in two different ways (HEC-RAS 2022):

1. Fixed time step method, in which the simulation is performed with one single time step assigned throughout all the computation time.
2. The variable time step method has two options to work with (User-defined dates table and time step divisors and courant number method).
 - The user-defined method requires the user to introduce a table in the system with a base computation time step and a divisor integer number. After that, the program will automatically divide the base time step with the divisor. The time step is considered for the specific time and dates. This process requires much information regarding the event and the system.
 - On the other hand, Courant Number (C_n) is a dimensionless parameter that can define the maximum time step that simulation can take to maintain the model's stability (Mańko 2018). In general, in computational time step selection, the time step should be less than the travel time required between the two cells (Peng and Liu 2019). Depending on the equation that is selected for the simulation, (C_n) selection as a function of wave celerity (V_f), mean cell size (ΔX_c), and computational time step (ΔT) can be expressed (HEC-RAS 2022):
 - If the Shallow Water Equation - Eulerian-Lagrangian Method (SWE-ELM);

$$\text{If } C_n = \frac{V_f \Delta T}{\Delta X_c} \leq 1.0 \quad \text{Then } C_{n(max)} = 3.0 \quad (30)$$

Or

$$\text{If } \Delta T = \frac{\Delta X_c}{V_f} \quad \text{Then } C_n = 1.0 \quad (31)$$

➤ If Shallow Water Equation – Eulerian Method (SWE-EM);

$$\text{If } C_n = \frac{V_f \Delta T}{\Delta X_c} \leq 1.0 \quad \text{Then } C_{n(max)} = 1.0 \quad (32)$$

Or

$$\text{If } \Delta T = \frac{\Delta X_c}{V_f} \quad \text{Then } C_n = 1.0 \quad (33)$$

➤ If Diffusion Wave Equation Method (DWE);

$$\text{If } C_n = \frac{V_f \Delta T}{\Delta X_c} \leq 2.0 \quad \text{Then } C_{n(max)} = 5.0 \quad (34)$$

Or

$$\text{If } \Delta T \leq \frac{2\Delta X_c}{V_f} \quad \text{Then } C_n = 1.0 \quad (35)$$

4.2 Flood Model Development for Dikmen Study Area

This section describes developing a 2D HEC-RAS flood model along with all the necessary parameters for the Dikmen urban area.

4.2.1 2D - Flood Model Development in HEC-RAS

4.2.1.1 Computational Mesh Generation of the Study Area

The finite-volume scheme can be used in the HEC-RAS 2D modeling process. This algorithm allows the creation of computational meshes that have multiples from 3 side meshes up 8 sides. The mesh size can be entered in the model based on user preference (e.g., 5 m x 5 m). The automated tool divides the 2D area polygon, covers

the area, and creates computational meshes as shown in Figure 4.5. The polygon's boundaries are more related to the area of interest, previously performed trial model simulations, and the DEM information to indicate the potentially flood-prone areas. However, once the initial model is created, the boundary of the meshes can be extended or trimmed based on the need. The coverage of the unnecessary area can increase the mesh elements, computational time, and file size. In the model, a 2D area with a perimeter length of 8.5 km and an area of 2.30 km² is drawn around the study area to simulate the flow. Then, the automated mesh tool created 118593 total cells with an average face length of 4 m and a cell size of 19 m². Later in the created mesh, some adjustment and refinement region is added to precisely capture the high and low points of ground in terrain. This process was performed by adding the breaklines along the existing hydraulic structures or in locations where elevations are changing more rapidly (e.g., along the center of a channel, road, perimeter of a pond, or buildings, etc.). This helped the model to capture the variation in elevation to a great extent. Also, some regions may require finer mesh sizes. This can be done by creating a refinement region, where smaller cells can be introduced for higher accuracy in water elevation.

The building information was entered into the model as blocks with elevation, based on the building footprints that were provided to the authors by the Land Registry Office in Northern Cyprus. The provided building information was defined in ArcGIS software. Then the original DEM was modified to obtain a final DTM with building footprints. About 939 polygons for the buildings and structures were added to the terrain, as shown in Figure 4.6a. However, based on the google images of 2018, some modifications were made to the buildings using the modification tools in RAS-Mapper by adding some missing buildings to the DTM, as shown in Figure 4.6b.

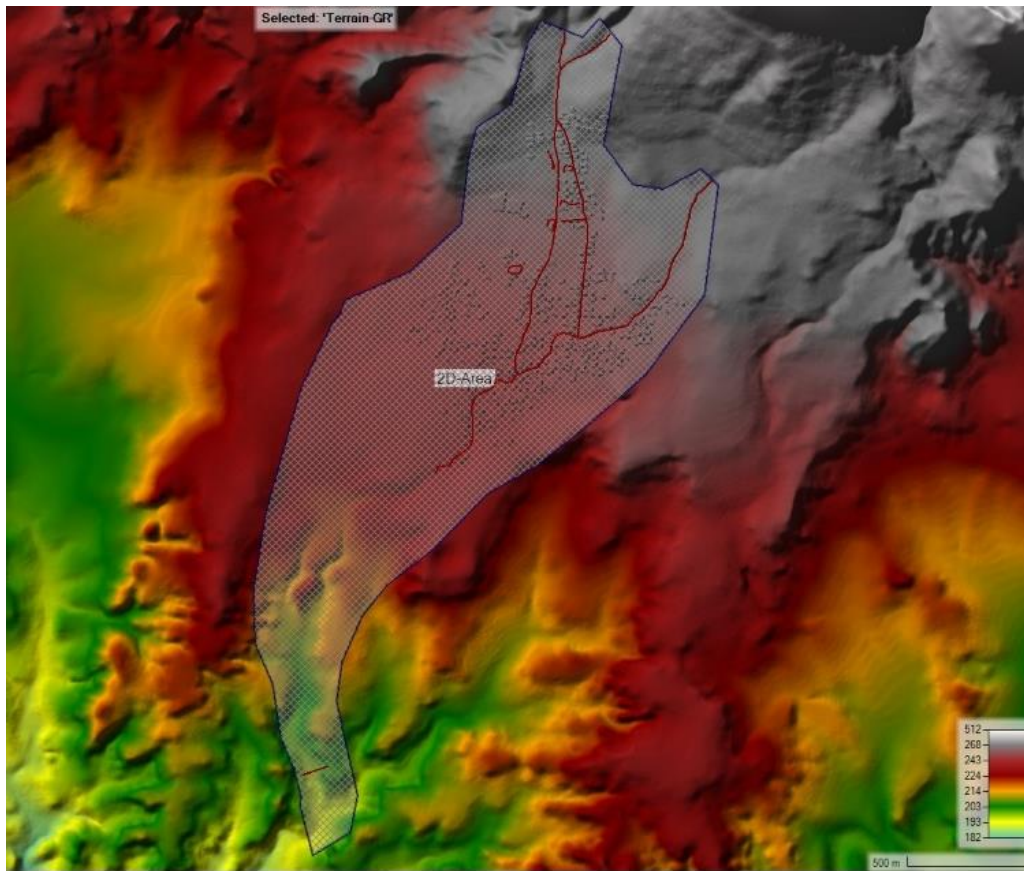


Figure 4.5 2D - Computational Mesh Area of Dikmen Study Area

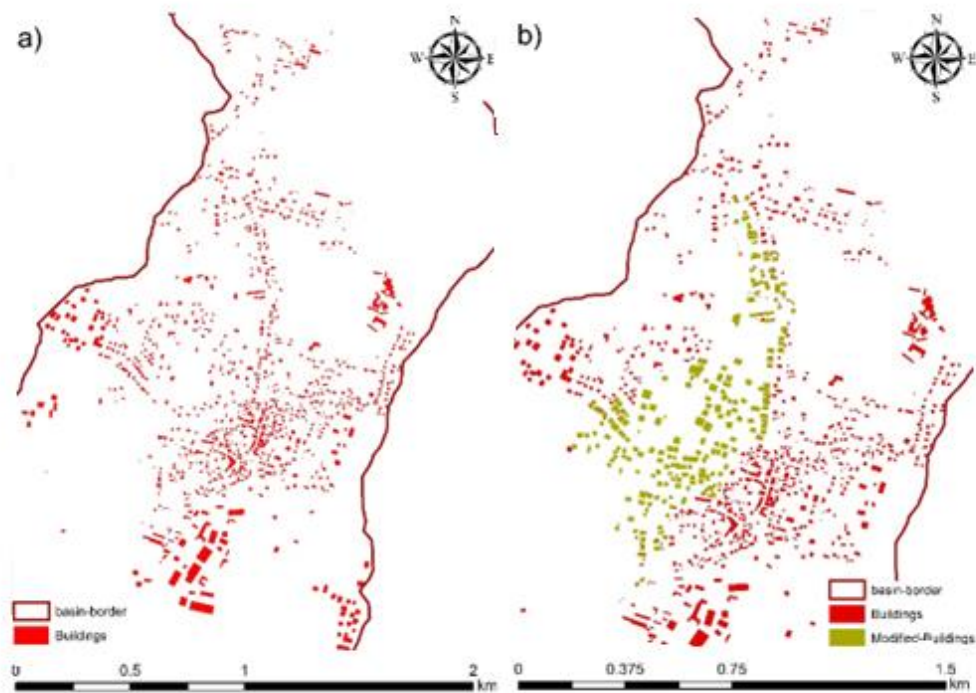


Figure 4.6 Building Polygons

4.2.1.2 Boundary Conditions Data

A 2D model requires a set of boundary conditions data, including information about incoming flow into the computational mesh and outgoing from the mesh. In this model, four boundary conditions (BCs) were introduced to the model for the flood modeling analysis. The three BCs were considered to contain the hydrographs that bring water into the system (Figure 4.7). Lastly, the downstream BC represents the water that would exit the system (Figure 4.8).

For the model, the hydrographs at the outlet of each sub-basin resulting from the 5th December 2018 Flood event were entered as an inflow in the three upstream BCs. Meanwhile, normal depth is selected for the downstream boundary conditions, and

a friction slope value of 0.029 is defined as a downstream boundary condition (DS-BC).

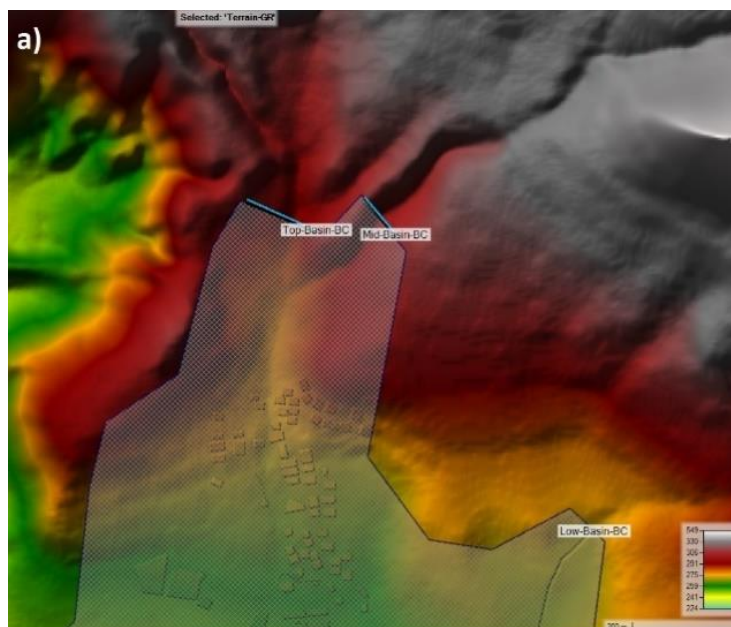


Figure 4.7 Upstream Boundary Conditions Locations

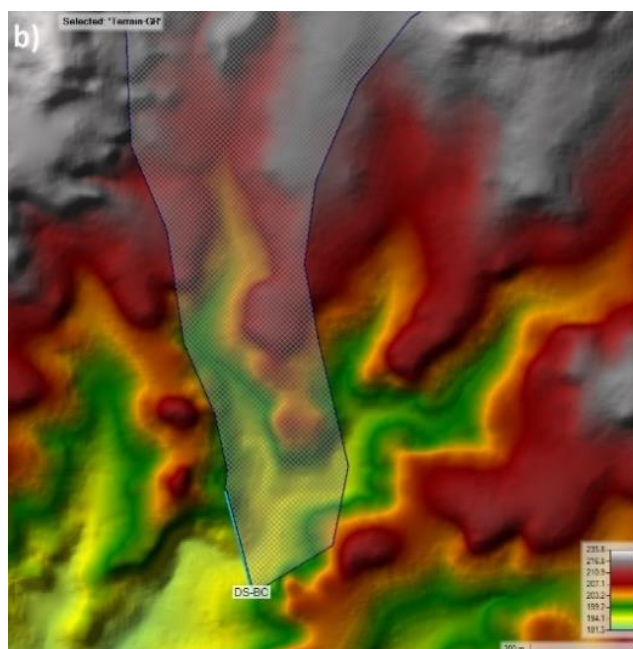


Figure 4.8 Down Stream Boundary Conditions Locations

4.2.1.3 Land Cover Classifications of the Study Area

Layers of land cover determine how resistant floodplains are to the flow of water in a region. The land cover layers are globally available in raster format for different locations. For example, Corine Land Cover (EEA and JRC 2011) for Europe has a resolution of 100 x 100 m. However, due to the low resolutions in cell size, in this study, land cover layer or Manning's roughness polygons are developed from the urbanized map's footprints containing the roads, cultivated lands, and residential. Manning's roughness coefficients for different types of land coverage are taken from Chow (1959), which are listed in Table 4.1. They are selected as initial Manning's roughness values and entered into the model.

Table 4.1 Manning's Roughness Coefficient based on different Land Cover

Land Cover Type	Manning's Roughness Coefficient, n
Asphalt Roads	0.013
Cultivated Lands	0.040
Residential Zones	0.080
Concrete Channel with the stone wall on the side	0.030

4.2.1.4 Calibration of the Flood Model

The calibration of the model is required after the development of the initial model. This can only be achieved by altering some model parameters to lower the differences between the observed and modeled data. One of the most commonly used methods in calibrating the 2D flood models is changing Manning's roughness values. This method has already been adopted and has given acceptable results in the literature (e.g., Mai and De Smedt 2017; Zaifoglu et al. 2019). Manning's coefficients of roads, residential areas, and cultivated land are chosen for calibration parameters in this study. Since there is no streamflow gauging station in the catchments and no record of the water levels for the 2018 reference flood, only the

observed inundation map of the 5th December 2018 is used as the reference map for the calibration. The Dikmen Municipality officials created the reference map after the event and provided it to the authors. However, since there is no other observed data of the recorded event, the validation process of the flood model was not possible. The editing features in RAS-mapper allow a user to create calibration polygons and specify and alter Manning's values in the calibration polygons. Therefore, the model can be tested if outputs match closely with the reference data, which is the observed flood extend the map of the 2018 Flood event.

To check the correctness of the model and find the difference between the model and observed maps, the relative error (RE) between the modeled (FA_{mod}) and observed flooded maps (FA_{obs}) can be calculated as (Zaifoğlu 2018):

$$RE = \frac{|FA_{obs} - FA_{mod}|}{FA_{obs}} \quad (36)$$

On the other hand, if the flooded region is over- or under-estimated in the model, the fitness rate F_{Stat} between the two maps can be used. Herein, FA_{com} is the area that overlaps and is wet both in the observed and modeled flood extend maps. It is computed as (Madhuri et al. 2021):

$$F_{Stat} = \left(\frac{FA_{com}}{FA_{obs} + FA_{mod} - FA_{com}} \right) * 100\% \quad (37)$$

Furthermore, F_{Stat} values range from 0 (indicating no match) to 100 (perfect match) between the modeled and observed flood maps.

4.2.1.5 Flood Hazard Assessment Methodology

In flood management, a hazard is usually defined as the main source of potential harm and a situation that can lead to losses. In this case, it means the potential of causing damage to the communities and people due to flooding in an area. Many factors must be considered while assessing the associated hazards of floods.

Predicting the flood characteristics, particularly flow specifications in a flood-prone area, can be a good starting point. The main flow characteristics that are typically more critical are the flow depth and flow velocity. However, a complete risk assessment also needs to cover other aspects, such as the social, environmental, and economic aspects (Smith and Cox 2019). Nevertheless, in this study, a more technical approach is taken to determine the magnitude of flood hazards in the Dikmen area under different rainfall scenarios, as the other aspects are challenging to quantify at this stage.

To define the risks of a flood event, it is essential to identify and study the characteristics of the flood (e.g., flood depth, flood velocity) in a flood-prone zone. One reasonably accepted method is to develop flood maps that produce data related to flood characteristics using numerical modeling tools to predict and assess areas vulnerable to floods. In a general sense, pedestrians, when they walk or when they are inside a vehicle or the buildings, are more likely in the way of harm and damage due to flood. Thus, the development of flood hazard assessment maps involves people's stability against a flood water flow, vehicle endurance in time of flooding, which can lose their stability due to friction, floating or sliding, and finally the building stability against an incoming wave of flood which can impose significant hydrostatic, hydrodynamic, uplifting, debris, erosion and scour forces (Smith and Cox 2019). The impact of severe flooding can be substantial. To assess the vulnerability of people either in their houses, cars, or pedestrians a curve was developed, which is known as the hazard vulnerability curve. The curve illustrates the threat levels to the communities (Figure 4.9). The curves also show the limits for the safety of people, vehicles, and buildings against a certain level of flood depth (F_D), flood velocity (F_V), and product of F_D and F_V (Smith et al. 2014). The product result of F_D and F_V in m^2/s indicates the upper limit for the combination of the two parameters, while F_D and F_V are showing the maximum upper limit of flood depth in m and flood velocity in m/s respectively.

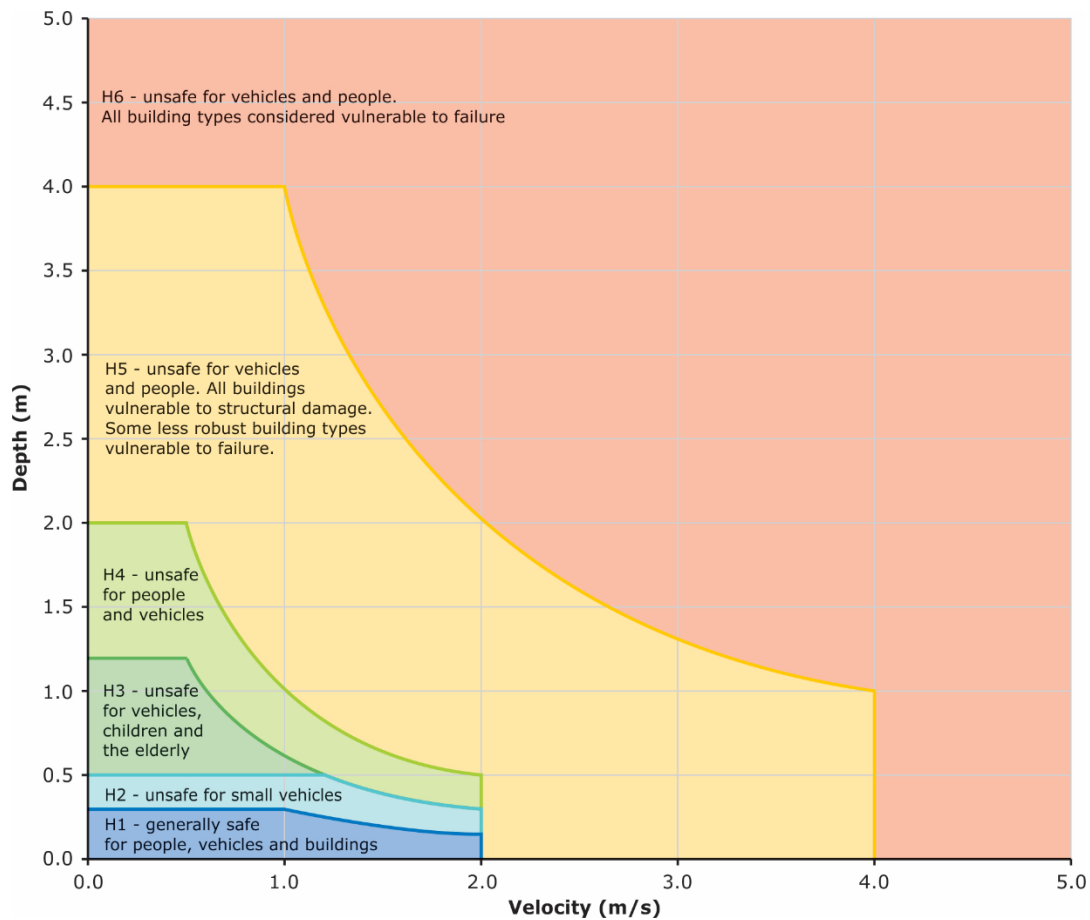


Figure 4.9 Combined Curve of Flood Hazard Assessment (Smith et al. 2014)

The HEC-RAS 6.0 modeling tool can generate flood risk maps based on the criteria introduced in Table 4.2, which can identify the area highly susceptible to threats and test the efficiency of mitigation measures in reducing the associated risk of flooding in a particular area.

Table 4.2 Vulnerability Thresholds For People, Vehicles, and Buildings

Level	F_D (m)	F_V (m/s)	$F_D \times F_V$	Description
H1	0.3	2	≤ 0.3	In General, Safe for People, Vehicles, and Buildings
H2	0.5	2	≤ 0.6	Unsafe for small size vehicles
H3	1.2	2	≤ 0.6	Unsafe for vehicles, children, and elderly people
H4	2.0	2	≤ 1.0	Unsafe for vehicles and People
H5	4.0	4	≤ 4.0	Unsafe for vehicles, people, and low-quality structures are subject to failure
H6	-	-	> 4.0	Unsafe for vehicles, people, and buildings are vulnerable to failure

4.2.1.6 Flood Mitigation Measures for Dikmen Urban Area

The main objective of this study is to propose solutions to the flood inundation problem in the Dikmen urban area. In this context, several flood mitigation measures have been discussed. For example, the diversion of the flow from the Top sub-basin to the west side of the Dikmen town. However, considering a diversion canal would create flooding to the industrial zone and town in the west of Dikmen. Thus, only three structural measures are examined for their efficiency against floods with 50-, 100-, and 500-year return periods. The proposed solutions are also tested against an experienced flood event on the 5th of December 2018. The first option is to assume the current conditions in the Dikmen urban area are kept, and the flood models are developed for 50-, 100-, and 500-year return periods. For the second option, a concrete channel having a depth of at least 1.8 m and a width of 4 m is proposed to link the flow coming from the Top and Mid sub-basins to the existing channel that carries water from the Low sub-basin to the downstream of the study area. In the third option, five reservoir ponds ignoring the bottom outlet contribution and with bottom outlet contribution are considered to be built inside the Top and Mid sub-basins to store the excess flood water during the peak period. Herein, the

effectiveness of the reservoirs is investigated. As the final option, the channel in the second option and the reservoirs in the third option are considered together to test their combined effectiveness against flooding. Furthermore, an extensive economic analysis is performed to find the monetary expenses for implementing these systems.

CHAPTER 5

STUDY AREA DESCRIPTIONS

5.1 Dikmen Urban Area as Case Study

Flash floods usually occur when extreme rainfall occurs on high slope small catchments. It typically does not take long before it reaches and exists the catchments and causes damage. Thus, the severity level of a flash flood is not only dependent on how much rainfall falls, but also on other factors, including the runoff with high velocity, the fast rise of water, and the transport of sediments that make these types of events hazardous (S̃pitalar et al. 2014). Dikmen urban area is located at the hillside of the Kyrenia mountain range in Northern Cyprus. It has occasionally been subjected to flash floods. With the increase in the experience of more extreme weather-related events around the world and Mediterranean region, the frequency of occurrence of these events, especially flooding events, is expected to rise as well (Banholzer et al. 2014; Benabdelouahab et al. 2020). The recent flash flood event that occurred on the 5th of December 2018 was one of the worst flood events that the residents in Dikmen have experienced. The storm event lasted for 10 hours and caused severe damage to the structures, environment, and water resources. The records in Boğaz Meteorological Station show that the area has experienced a rainfall depth of around 172 mm during 10 hours of rainfall.

The 2018 flood event caused the collapse of the crossing bridge, damaged around 100 to 120 houses, and polluted the area's water resources. Furthermore, it entered the proximity of the Dikmen Primary School, which caused one of its walls to collapse. The past experienced flash flood events in Northern Cyprus, especially in the Dikmen area, could be considered a warning that the intensity and severity level of these events have been worsening with time.

5.2 Characteristics of the Dikmen Study Area

Cyprus island is geographically located at latitudes of 30.33 to 35.41 and longitudes of 32.23 and 34.53. It is under the effect of a typical Mediterranean climate with hot summers and mild winters. The island is the third largest in terms of surface area in the Mediterranean sea after Sicily and Sardinia islands (Hunt et al. 2022). Dikmen (Dikomo) urban area is located in the city of Kyrenia in the north part of the island, known as the Turkish Republic of Northern Cyprus, which has an area of 3251 km² (Atasoy 2011). Figure 5.1 illustrate the global location of the Cyprus and Dikmen basin on the world and a local map.

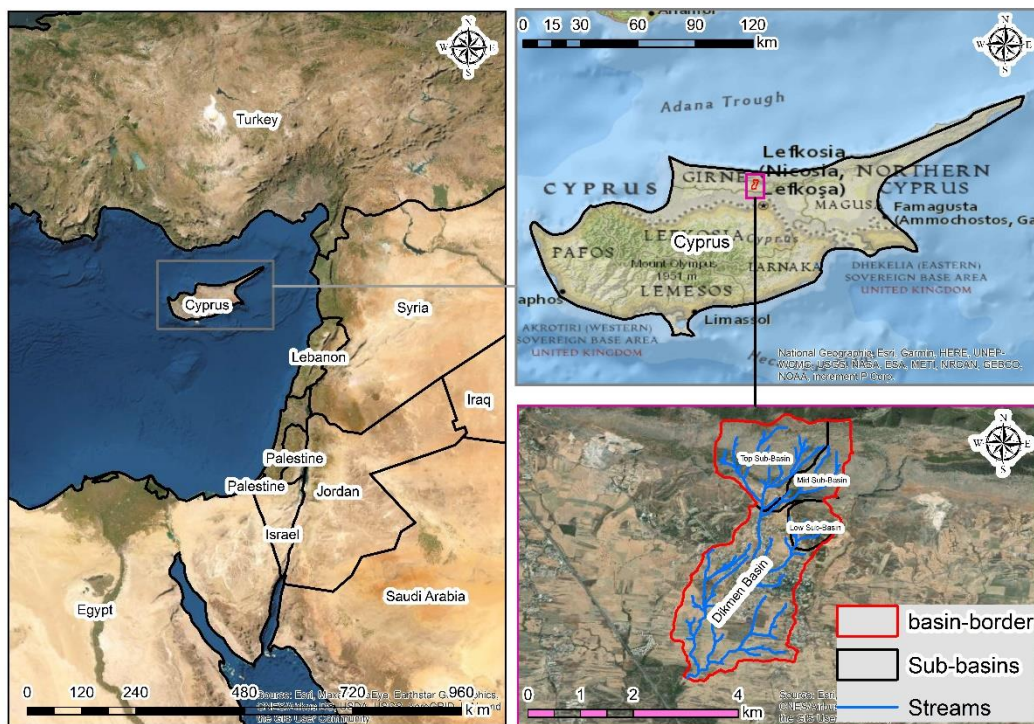


Figure 5.1 Cyprus and Dikmen Area Location

Dikmen urban area is located on the hillside of the Kyrenia mountain range. It is located at the latitude of $35^{\circ} 16' 24.56''$ N and longitude of $33^{\circ} 19' 24.86''$ E that spans from the top hills of the Kyrenia mountains to the major highway connecting Nicosia and Kyrenia cities. The study area is approximately 8 km^2 in size and divided into three sub-catchments (Top Sub-basin, Mid Sub-basin, and Low Sub-Basin), as shown in Figure 5.2. The water from these three sub-catchments flows through Dikmen's urban area. Usually, the streams in the Dikmen basin are ephemeral, which implies that water starts to flow in rainy seasons.

The flood flow passes through the urban area, and after crossing the highway between Kyrenia and Nicosia, it pours into the Gönyeli Reservoir. Currently, the only channel to carry water from the Low sub-basin is a concrete man-made channel with a length of 1.8 km. On the other hand, as shown in Figure 5.3, inside the black ellipse there is no channel to connect the Top and Mid sub-basins to the downstream side. Since the natural path of the creek is impaired because of the construction and the dense development along the path of the channel.

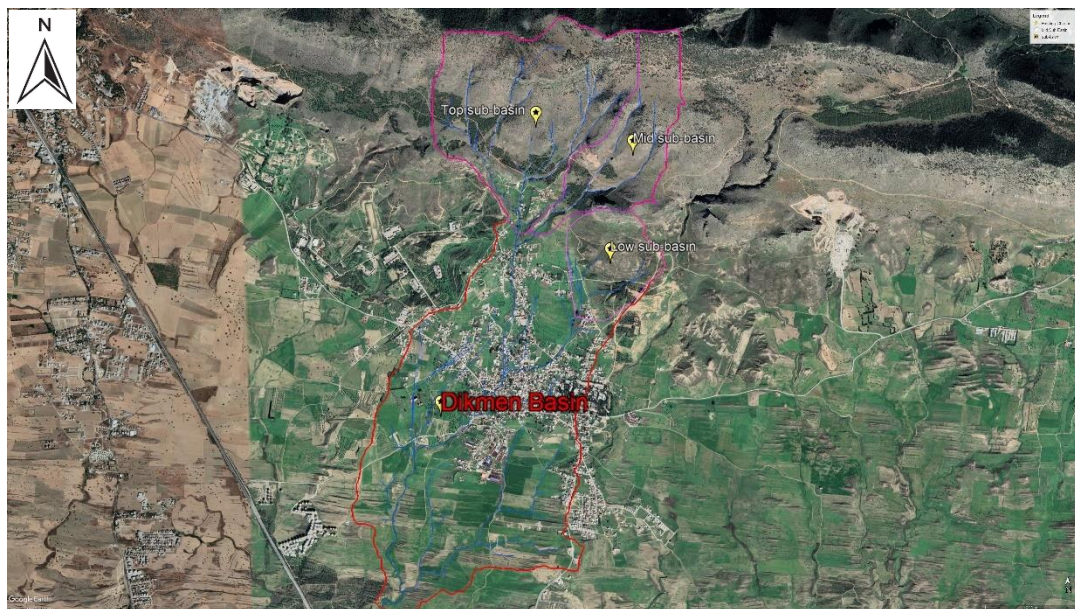


Figure 5.2 Dikmen Sub-catchments Locations

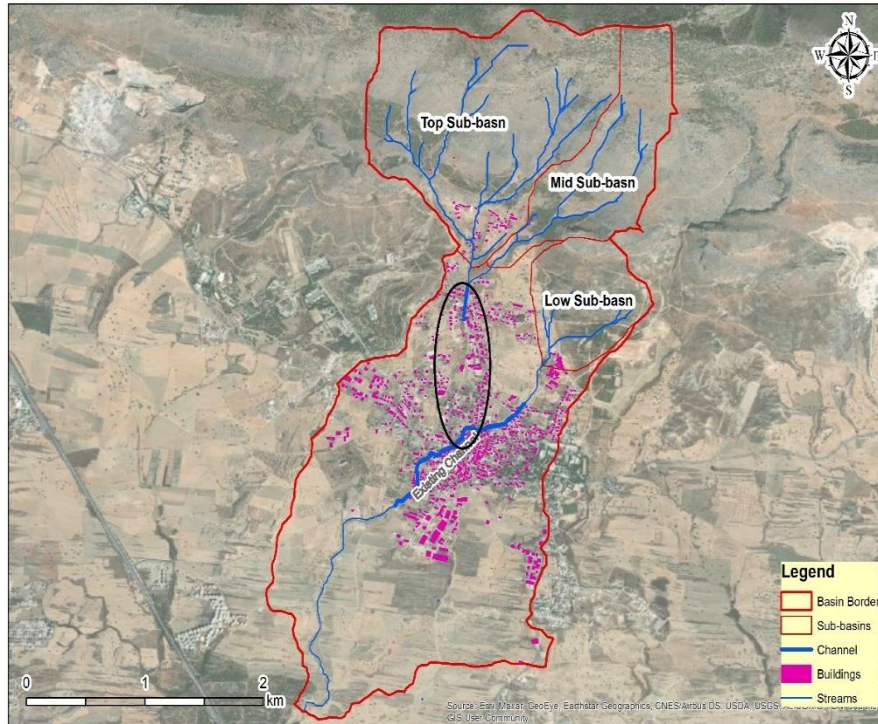


Figure 5.3 Existing Condition of the Dikmen Basin

The majority of incoming water to the Dikmen town is contributed by the three sub-basins located on the hillside of the Kyrenia mountains. The Top Sub-basin is the largest in the area of nearly 2 km² and has an average slope value of 41%, which contributes highly to the formation of flash floods in Dikmen. The Mid Sub-basin with an area of nearly 0.9 km² has a relatively smaller area and an average ground slope of around 42%. The Low Sub-basin has a surface area of approximately 0.6 km² and an average ground slope of 23%. The population and housing density are relatively dense in the floodplains and along the natural streams from the top two sub-basins. Recent flooding events and the subsequent damages have shown the high vulnerability of specific locations to flooding.

5.3 Climatic Conditions in the Study Area

Cyprus island, located in the eastern Mediterranean Sea, has a typical Mediterranean climate. The climate on the island is mild in winter, with limited rainfalls. However, the weather becomes very hot and dry in the summer. The island is made up of complex topography. The Kyrenia Mountains run parallel to the northern coasts of the island. Then Karpas Peninsula starts, which is one of the island's most distinctive geographical characteristics. Besides, the Mesaoria plain covers low-lying plains in the island's center. The Troodos Mountains cover the largest portion of southern Cyprus's southwestern regions. These variations in the topography of Cyprus differ the meteorological characteristics to a great extent (Zaifoğlu 2018).

The mean annual precipitation in Northern Cyprus varies from location to location. Typically it has a minimum value of 260 mm in the Western Mesaoria Plains and a maximum value of 550 mm at the Kyrenia Mountain Ranges. The mountainous parts of the study area in Dikmen can experience an annual mean precipitation value of around 470 mm. In the low-land, it can reach a depth of 300 mm in a year. Boğaz rainfall gauging station with a 300 m mean sea level elevation is selected as this study's representative rainfall gauging station. The mean annual precipitation (MAP) at the Boğaz Station from the recorded rainfall events between 1976-2015 is found as 400.5 mm (Zaifoglu et al. 2018).

One of the most remarkable flood events that caused significant disruption and damage to the Dikmen occurred on the 5th of December 2018. The recorded rainfall at Boğaz station indicates that on the 5th of December 2018, the area experienced a 10-hours intense rainfall. The recorded hourly rainfall shows that the rain started around 1 pm and lasted till 10 pm. The rainfall depth of 172 mm was recorded, which is very extreme considering the MAP in Boğaz station. Moreover, the mean annual maximum daily precipitation (MAMDP) of the Boğaz Station with a 100-year return period is 171 mm (Zaifoglu et al. 2018), which is lower than the experienced event in 10 hours in 2018.

5.4 Land Cover of the Study Area

In the hydrological analysis of a catchment, understanding and analyzing the soil characteristics is essential. The soil characteristic can influence the discharge amount from a watershed to a great extent. For instance, if the soil in a catchment consists of layers with high infiltration capacities, this can influence the flow values. As a result, the hydraulic model can predict a smaller inundation area since the runoff is lower compared to the catchments with soils that have low infiltration capacities.

The process of identifying and analyzing the soil types of the study area is performed based on a map Figure 5.4, provided by the Office of Agriculture in Northern Cyprus (Zaifoğlu 2018). Based on this map, silty clay loam, sand clay loam, and clay loam with loamy texture are the dominant soil types with low hydraulic conductivity and infiltration capacity in Northern Cyprus. In General, 109 types of soil series are listed on the map below, unique to Northern Cyprus.

In the scope of this study, the soil type map for the study area is extracted, and a new map given in Figure 5.5 is formed. According to Figure 5.5, the dominant soil types in the Dikmen sub-basins are Değirmenlik, Boğazici, and Marno Kalkar. Since the Boğazici and Marno Kalkar soil types have about 34%-36% of clay in their contents, the catchments are susceptible to having a very high runoff potential which increases the probability of the occurrence of flood events in Dikmen (Zaifoğlu 2018). Besides, the changes in land cover in the flood plain due to deforestation, urbanization, industrial zone development, etc., may increase the frequency of flooding and consequent severe damages.

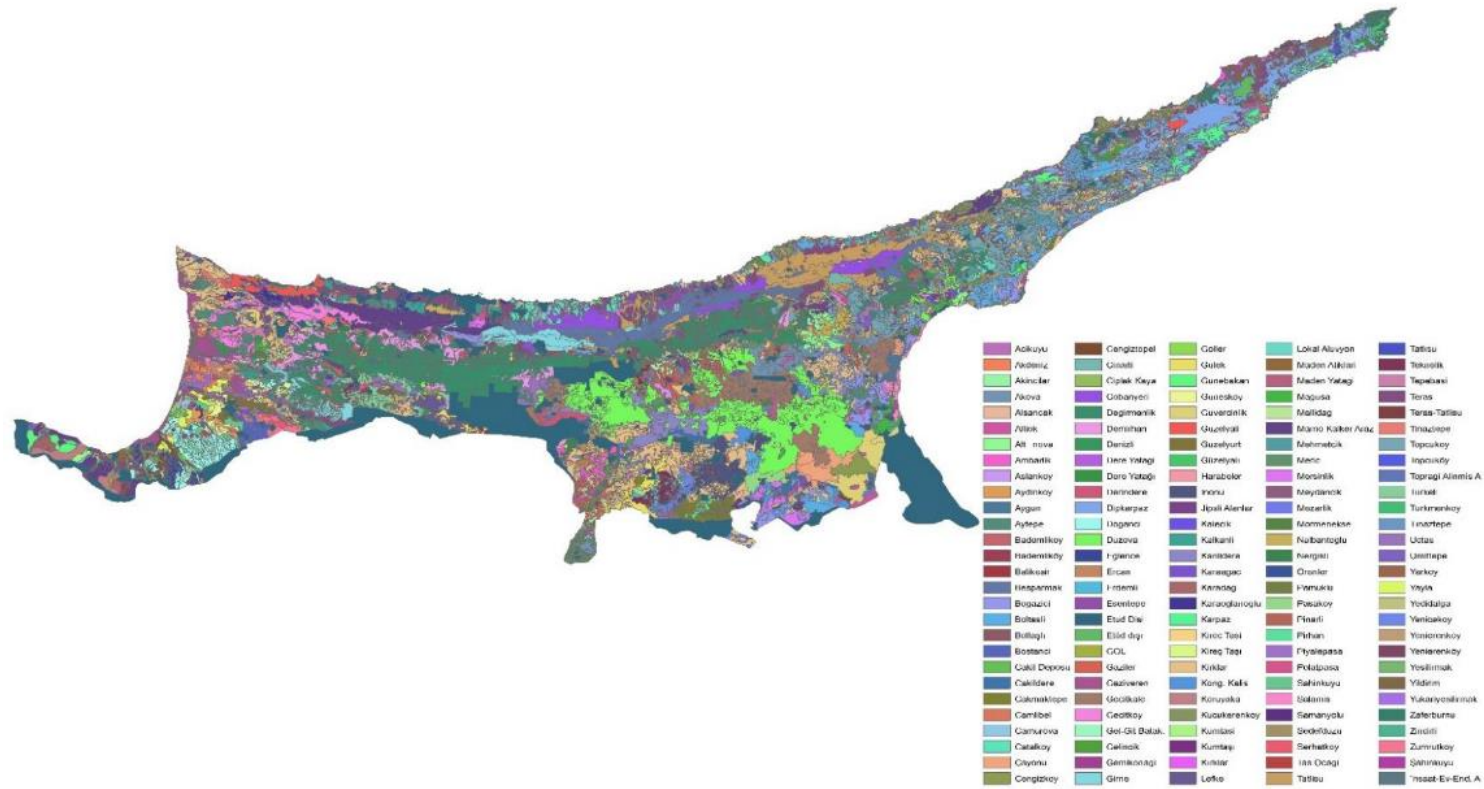


Figure 5.4 The Soil Characteristics Map of the Northern Cyprus

To accurately consider the impacts of the different land covers on the flood inundation map, Dikmen town's land cover is divided into five distinctive categories: buildings, residential zone, cultivated lands, roads, and concrete channels, as illustrated in Figure 5.6. There are 939 individual buildings, a total area of 2.11 km² identified as a residential area, and about 4.60 km² area covered by the lands of cultivation and agriculture.

The study area has a channel with a length of 1.8 km that passes through the Dikmen center and carries water from the Low sub-basin area to the downstream part of the town. However, there is no functional channel to safely convey the collected water from the Top sub-basin and Mid sub-basin apart from a 200 m channel upstream of the floodplain. After the channel ends, the water starts to disperse in the Dikmen urban area, which has been one of the leading causes of severe flood damage even with a small rainfall event.

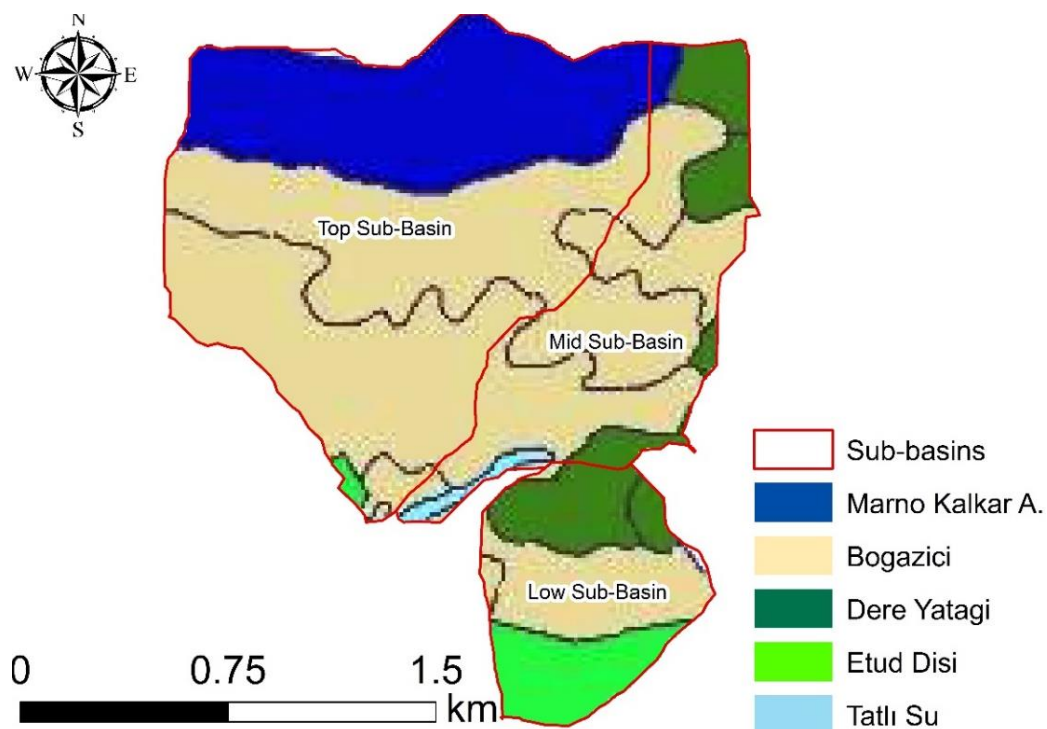


Figure 5.5 Soil Types of the Sub-basins

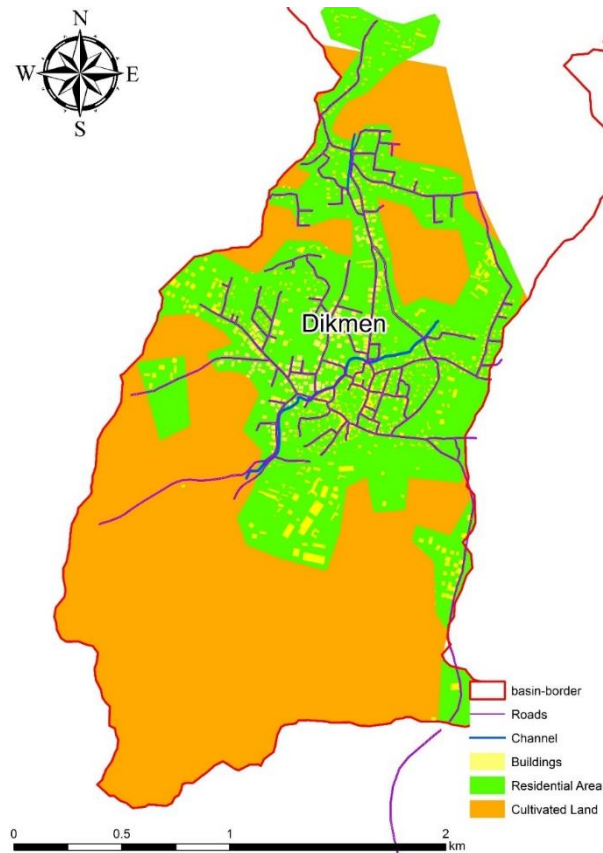


Figure 5.6 Dikmen Flood Plain Land Cover

5.5 The Data Sets of the Study Area

The reliability of the data sets is critical for any analysis involving water-related projects (e.g., water resources management, flood modeling, and the design of hydraulic structures). In this regard, having a dependable source of data that can reliably estimate hydrological extremes is critical (Tabari 2020). However, long-term hydrological data records are still unavailable in many parts of the world, particularly in areas where the socio-economic repercussions of weather-related events are significant (Srinivasan et al. 2015).

The rainfall data were gathered from Zaifoglu et al. (2018), in which a set of quality control checks was done and showed that the rainfall series were quality-controlled,

homogeneous, and complete. Also, in that study, Northern Cyprus was divided into five homogeneous sub-regions, and the mean annual maximum daily precipitation series (MAMDP) were used to determine the precipitation depths corresponding to different return periods ranging from 2-year to 500-year. Boğaz rainfall gauging station with the coordinate of $35^{\circ} 28' 8.25''$ N latitude and longitude of $33^{\circ} 28' 4.84''$ E is chosen for hydrological data representation since it is fairly close to the study region. However, because the data is in the form of maximum daily precipitation in (mm/24-hr), finer scaled data sets are needed to simulate rainfall-runoff models. Thus, an hourly rainfall distribution for 24 hours encompassing the observation period of the 2010-2018 water years is calculated using Boğaz hourly rainfall records. Finally, a 24-hour design hyetograph is constructed for the meteorological model in rainfall-runoff simulation.

Another kind of data that must be included for flood modeling is topographic information regarding ground conditions. The digital terrain model, or DTM, is a fundamental component of ground data that can represent the reality of the ground surface and calculate flood depths, inundation, and risk assessment maps based on slope, drainage, and other surface features (Arrighi and Campo 2019). The recent advancement in utilizing high-resolution remote sensing technology has transformed flood modeling. However, still obtaining high precision data sets with very high accuracy (e.g. light detection and ranging (LIDAR), aerial photography with drones, hyperspectral, and synthetic aperture radar) are costly (Yan et al. 2015).

CHAPTER 6

HYDROLOGICAL MODELING RESULTS AND DISCUSSIONS

This chapter includes the results and related discussion regarding the hydrological analyses and the formation of the needed topographic maps in the digital elevation model (DEM) format.

6.1 Hydrological Modelling

6.1.1 Formation of Design Rainfall Hyetograph

To create a design rainfall hyetograph for the study area, Boğaz Station, located at a distance of 3.5 km from the Dikmen center, is selected as the representative rainfall gauging station. On the other hand, since the Intensity-Duration-Frequency (IDF) curve of Boğaz station is unavailable, the storm hyetographs for different return periods (50-year, 100-year, and 500-year) are created from the Mean Annual Maximum Daily Precipitation (MAMDP) data sets given using the average daily distribution of rainfall shown in Figure 3.1. Furthermore, the 2018 Flood event storm in Dikmen had a rainfall depth of 172 mm in 24 hours, and the observed hourly distribution of the storm is given in Figure 6.1. Based on the recorded data, the area experienced intense rainfall with a peak intensity of 56.2 mm/hr, which happened 8 hours after the rainfall started. The recorded rainfall of the 2018 Flood event showed that about 63.4% of rainfall had fallen in the first 6-hrs of the rainfall. Meanwhile, the average daily rainfall distribution curve indicates that about 73.5% is expected in the first 6-hrs.

To develop rainfall hyetographs for high, medium, and low probability cases, the MAMDP series of Boğaz Station is adopted from Zaifoglu et al. (2018), which are listed in Table 6.1. Then, the hourly hyetographs for 50-year, 100-year, and 500-year

storms are generated by distributing the MAMDP values based on the average daily distribution of the Boğaz station (see Figure 3.1). The hyetographs are given in Figure 6.2.

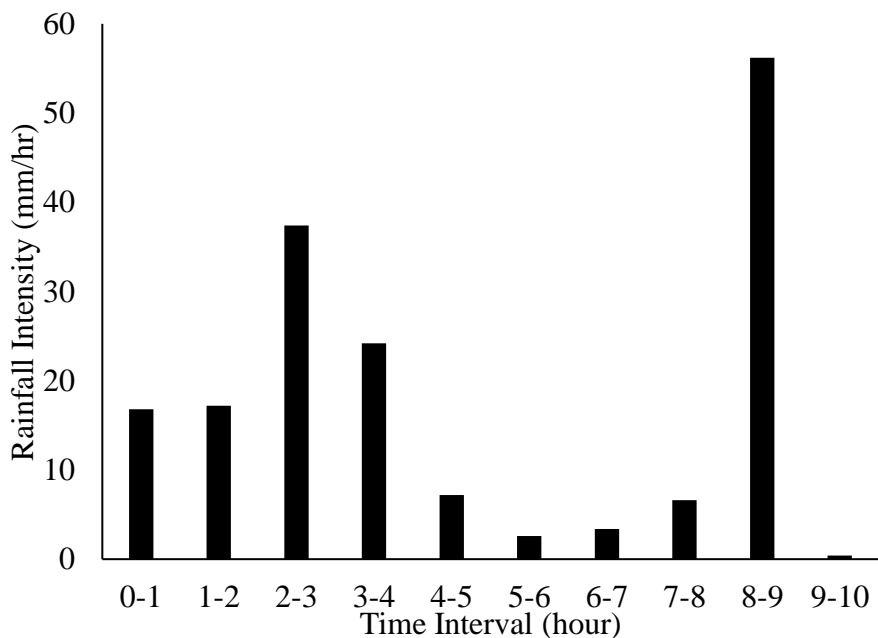


Figure 6.1 The recorded Hyetograph of the Flood Day in Boğaz Station

Table 6.1 Mean Annual Maximum Daily Precipitation of Boğaz Station for Different Return Periods

Return Period (Year)	MAMDP (mm/day)	Occurrence Probability in a year (%)
50	151.7	2.0
100	171.0	1.0
500	215.1	0.2

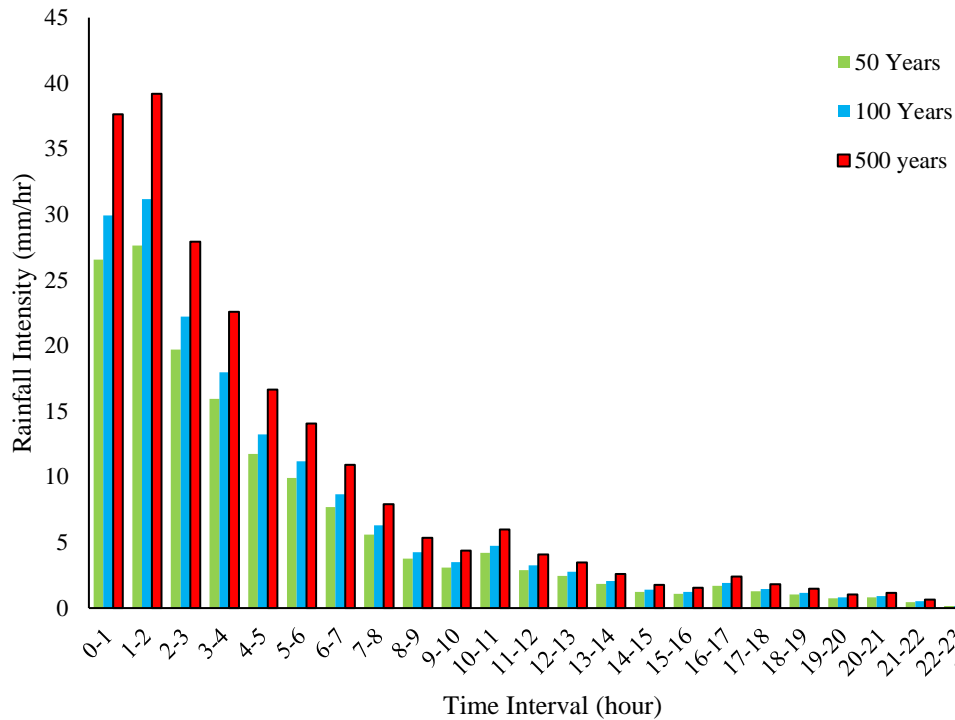


Figure 6.2 The Estimated Average Hyetographs of Storms with 50-year, 100-year, and 500-year Return Period

6.1.2 Flood Hydrographs Generation

6.1.2.1 Sub-basins Pre-processing in ArcGIS

Flood hydrographs under various conditions are used as the main inflow input into the hydraulic model to generate flood maps. However, since the catchments in the Dikmen town are ungauged, there is no record to show how much discharge developed in each catchment during a specific time. Therefore, the outflow hydrographs must be generated synthetically. One of the most widely used methods to create synthetic hydrographs from an ungauged catchment is the SCS Unit Hydrograph method adapted in this study. This method helps to develop flood hydrographs based on the physical characteristics of the catchments. However, pre-

processing the catchments' topographic data was required to generate representative hydrographs for different cases. In the process, depressionless DEMs are developed with the help of ArcGIS processing tools. In that process, the Hydrology tools in ArcGIS are used to obtain the necessary information related to the catchments.

In the first step, DEM for the Dikmen basin and the upstream catchments (Top sub-basin, Mid sub-basin, and Low sub-basin) are generated using 1:25,000 and 1:5,000 topographic contour maps of the area (Figure 6.3). Next, the sink points in the DEM that can cause an error in the processing are identified and removed using the Fill tool in GIS. After removing the sink points, the flow direction raster is created that shows the direction in which the flows are moving based on the topographic characteristics of the ground (Figure 6.4). Moreover, drainage networks are obtained using the flow accumulation function of Hydro tools that can illustrate the path and number of cells that discharge into other cells (Figure 6.5). Similarly, the slope raster is created using the Surface function of the Spatial Analyst tools in ArcGIS (Figure 6.6). The slope function calculates the gradient steepness from each cell of the DEM raster. Based on the percent rise indication of the slope, 0 means a flat surface, and 100 percent surface has a 45-degree slope (ESRI 2022).

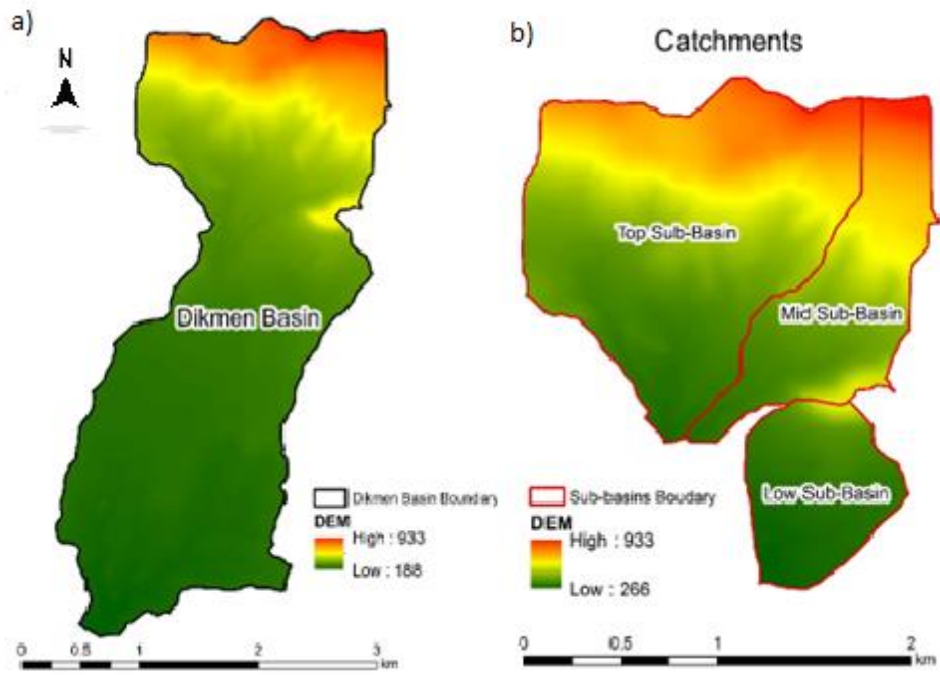


Figure 6.3 DEM a) Dikmen Basin, b) Catchments Areas

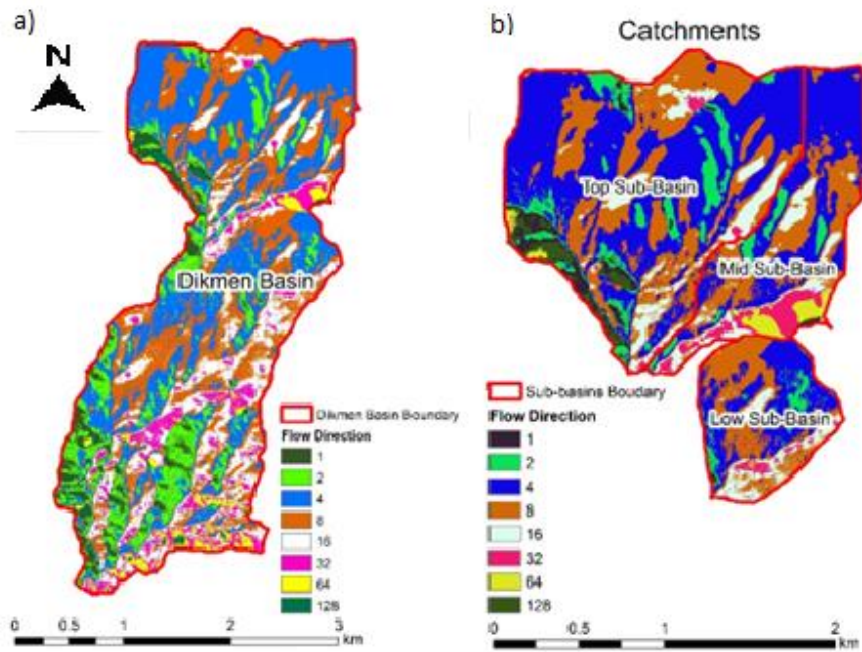


Figure 6.4 Flow Direction Raster a) Study Area, b) Catchments Areas

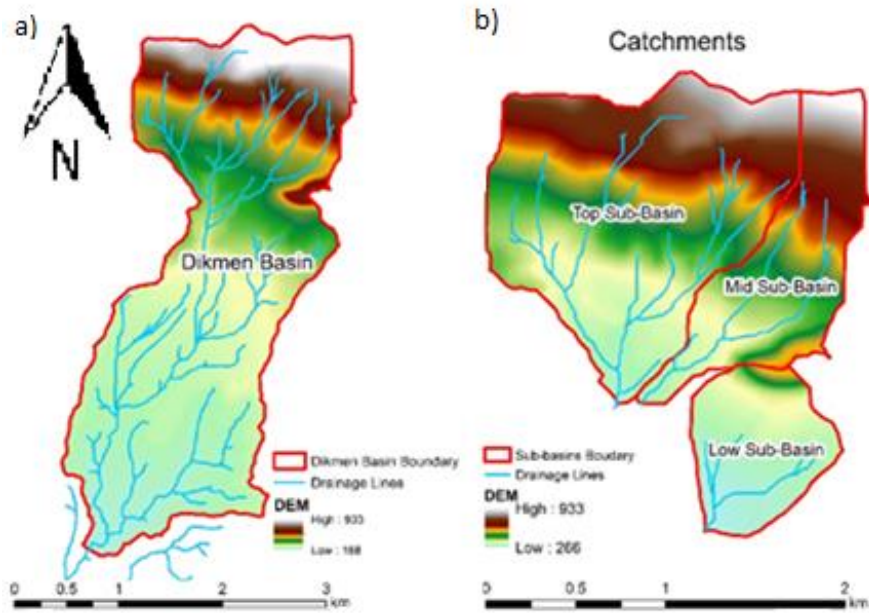


Figure 6.5 Drainage Networks a) Study Area, b) Catchments Areas

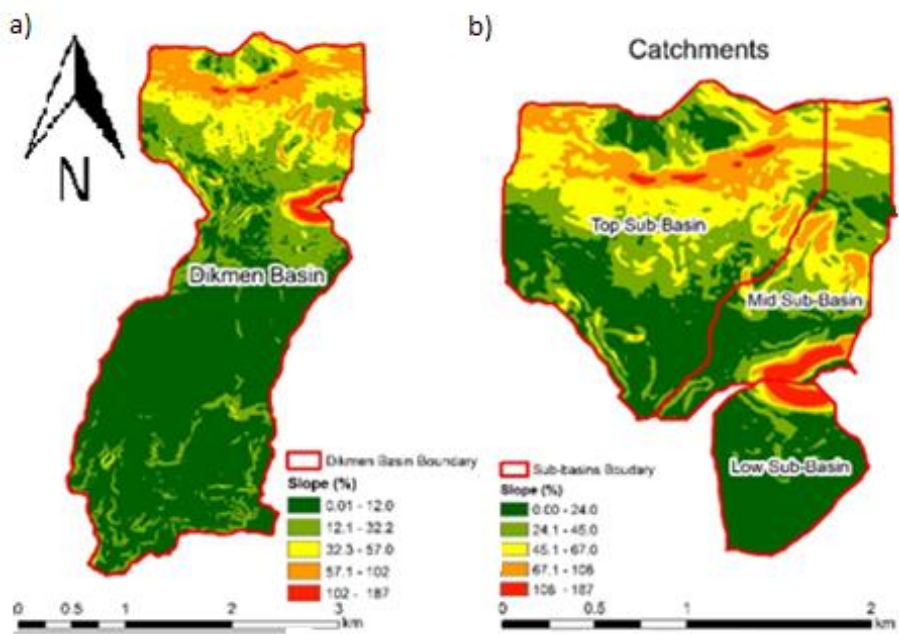


Figure 6.6 Slope Raster of the a) Study Area, and b) Catchments Areas

6.1.2.2 Sub-basins Hydrological Modelling in HEC-HMS

The generation of outflow hydrographs into the floodplain using the SCS-UH method requires identifying a composite CN number that can be adapted from the literature based on different soil characteristics. The soil map of the sub-basin in Figure 5.5 shows that most of the soils inside the three main catchments (Top sub-basin, Mid sub-basin, and Low sub-basin) are the soil types of Boğazici and Marna Kalkar. Boğazici and Marna Kalkar have higher clay contents, which results in high runoff potential. Therefore, the hydrological soil group (HSG) D is selected to represent the soil types with the highest runoff potential among others (Zaifoğlu 2018). The other essential catchment parameters (i.e., slope, flow length, area) are obtained using the ArcGIS processing tools, and the summary of all the information needed to perform the SCS-UH method in HEC-HMS is listed in Table 6.2.

Table 6.2 Basin Characteristics Used in SCS UH Method in HEC-HMS

UH-Parameters	Top Sub-Basin	Mid Sub-basin	Low Sub-basin
CN	89.2	90.0	92.1
S (cm)	3.1	2.8	2.2
S _s (%)	40.5	44.0	25.1
t _{lag} (h)	0.19	0.18	0.12
t _p (h)	0.22	0.21	0.14
t _r (h)	0.04	0.04	0.03
L (km)	2.48	2.54	1.25
A (km ²)	2.16	0.83	0.51
Q _P (m ³ /s)	20.75	8.4	7.7

In Table 6.2, S represents potential maximum retention in the basin, L is flow length, t_{lag} is lag time, t_c is concentration time in each basin, A is the area of the catchment, S_h is the mean watershed slope in percent, t_p is time to peak, t_r is effective rainfall duration, and Q_{peak} is peak discharge of UH. The design hyetograph of each storm event with different return periods (see Figure 6.2) and the generated basin characteristics (see Table 6.2) are entered into the HEC-HMS model to create the runoff hydrographs respective to different return periods. Table 6.3 lists the peak discharges resulting from various events for each sub-basin.

Table 6.3 Peak Discharges of Each Sub-basins Corresponding to Different Return Periods

Return Period (Year)	Peak Discharge Q_{peak} (m^3/s)		
	Top sub-basin	Mid sub-basin	Low sub-basin
2018 - Flood	32.5	12.5	7.8
50	13.7	5.4	3.5
100	16.0	6.2	4.0
500	21.0	8.2	5.2

The outflow hydrographs generated from the hydrological analysis of each sub-basins due to the occurrence of the 2018 Flood event in Dikmen are illustrated in Figure 6.7. Moreover, the outflow hydrographs resulting from hydrological analysis of rainfall events with 50-year, 100-year, and 500-year return periods are also given in Figures 6.8, 6.9, and 6.10, respectively. The generated hydrographs are then defined as the inflows into the 2D HEC-RAS models to create the flood inundation maps corresponding to high, medium, and low probability flood events.

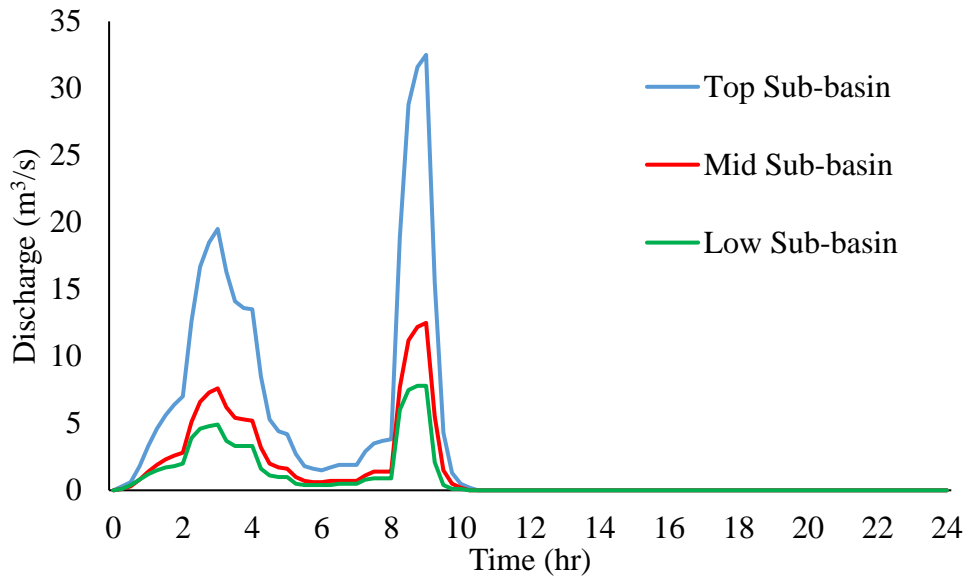


Figure 6.7 2018 - Observed Flood Discharge Hydrographs

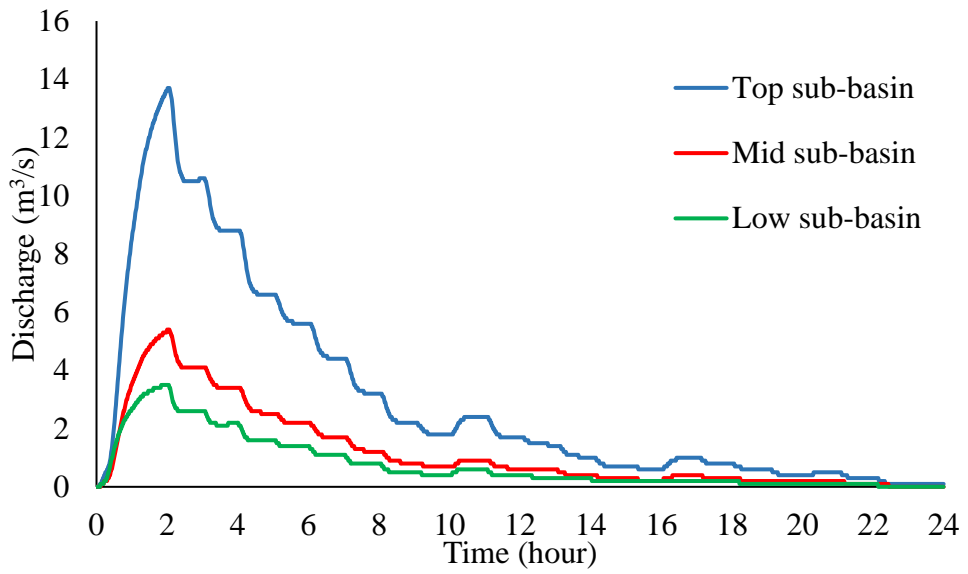


Figure 6.8 50-year Return Period Discharge Hydrographs

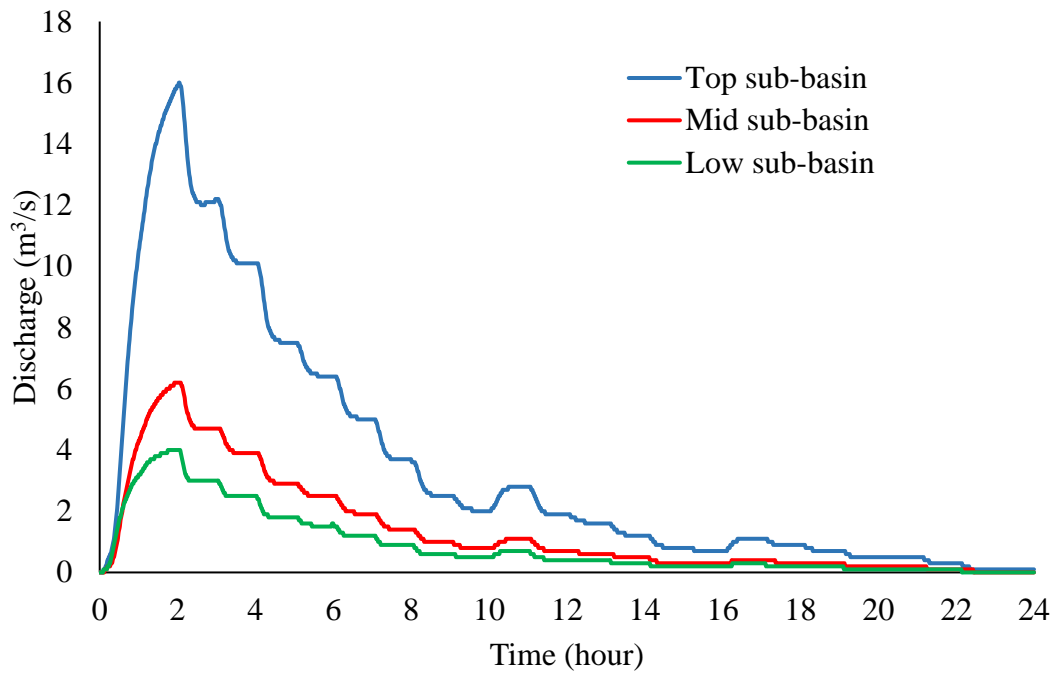


Figure 6.9 100-year Return Period Discharge Hydrographs

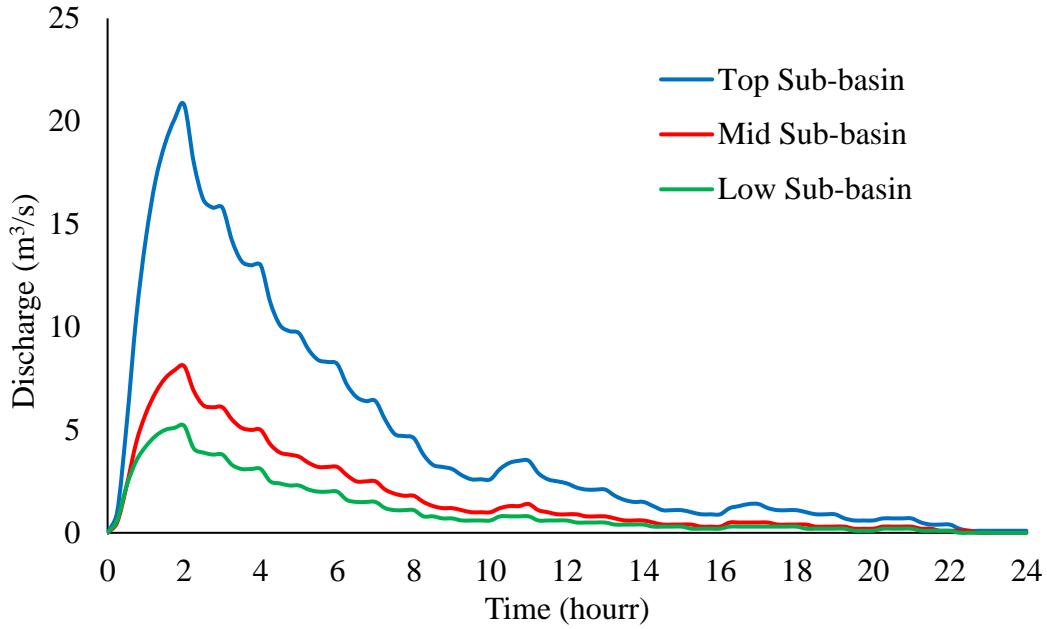


Figure 6.10 500-year Return Period Discharge Hydrographs

CHAPTER 7

HEC-RAS FLOOD MODELING RESULTS AND DISCUSSIONS

7.1 Hydraulic Modelling Results

In the Dikmen town's flood modeling process, 16 different models are developed and analyzed using HEC-RAS software. The obtained outputs from the flood modeling involve flood inundation, flood depth, flood velocity, water surface elevation layer, and flood hazard maps for the observed 2018 Flood event and future flood scenarios. As input for the boundary conditions, the inflow hydrographs corresponding to each flood event are introduced at each sub-basin outlet in the 2D flood model.

7.1.1 Dikmen's 2018 – Flood Event Model Current Condition

Flood models that can predict the potential damages of flooding to the environment and urban areas are cost-effective tools that help the developer recognize vulnerable areas, design the infrastructures and mitigate the damages accordingly. However, the flood models' accuracy depends on many factors, including the accuracy of topographic and hydrological data and the experience of the model developer. Thus, model calibration is necessary to increase the accuracy of generated flood maps (Huxley and Ryan 2016).

In this study, the initial 2D model of the 2018 Flood event was carried out using the primary information regarding Manning's roughness coefficients (n), which indicates the resistance of the ground surface to the flood water. The initial values are given in Table 7.1. The values are initially selected based on the existing literature corresponding to each land cover identified and mapped for the Dikmen study area. To consider the ground conditions in the model, the initial hydraulic model in HEC-RAS was carried out on a DEM with a cell size of $5\text{m} \times 5\text{m}$

interpolated from a contour map with the 5 m contour interval. The obstacles, such as houses and buildings, are integrated into the model as blocks having different elevations. This process was carried out based on the footprints of the buildings provided by the local authorities. Later, it was compared with 2018 satellite images of the area and modified further to increase the reality of the building numbers and locations.

Moreover, the computational time step of the initial model was set to 5 sec, the base output interval to 10 sec, the Courant Number (C_n) to 1, and the equation were set as SWE. The hydrographs resulting from the hydrological analysis of the 2018 rainfall hyetograph in HEC-HMS are entered as the upstream boundary conditions for each sub-basin into the 2D HEC-RAS model. Meanwhile, the normal depth indicating the channel bed's friction slope with a value of 0.029 is defined as the downstream boundary condition.

The observed flood extend map of the 2018 Flood event in Figure 7.1 was taken as a reference for the calibration process of the flood model. The map indicates that the recorded observed area by the authorities is around 0.45 km². After the successful computation of the initial model, the result of the 2D model showed a close correlation in the goodness-of-fit statistics between the modeled inundation map and the observed flood map for the 2018 Flood event. About 78 % of the flood extend map in the initial attempts was captured, as given in Table 7.2. However, the relative error (RE) between the two maps was around 0.042. In order to increase the overlapping between two maps and decrease the RE rate, the calibration process was carried out by altering local Manning's roughness coefficients (see Figure 6.2) in residential areas and roads, and the calibrated Manning's values are given in Table 7.1. In the calibration process, the 2D HEC-RAS model was run with modified roughness values, and the results were compared with the observed flood extend map. The comparison results of the final model and the observed map in Table 7.2 indicate an increase in goodness-of-fitness statistics, up to 84%, and a decrease in the RE to 0.015. In the end, a significant part of the residential areas, Dikmen Primary

school, roads, and cultivated areas were flooded during the 2018 Flood event, as shown in Figure 7.1.

Table 7.1 Manning's Roughness Coefficient n

Classifications	Uncalibrated n Values	Calibrated n Values
Cultivated Areas	0.04	0.04
Residential Areas	0.08	0.09-0.11
Roads	0.013	0.0145
Channel	0.03	0.03

Table 7.2 The Differences Between Observed and Modelled 2018 Flood Maps

Flood 2D Models	The Goodness of Fit Statistics		
	$A_{\text{modelled}} \text{ (km}^2\text{)}$	RE	F (%)
Uncalibrated Flood Model	0.434	0.042	78
Calibrated Flood Model	0.460	0.015	84

The statistical result between the modeled inundation area and the observed flood map of the 2018 Flood event indicates that the model can sufficiently reflect the reality of the flood extend map. Thus, considering the calibrated 2D HEC-RAS model, relative maps showing the inundation, maximum flood depth, and maximum flood velocity map of the 2018 Flood event are given in Figures 7.2, 7.3, and 7.4, respectively.

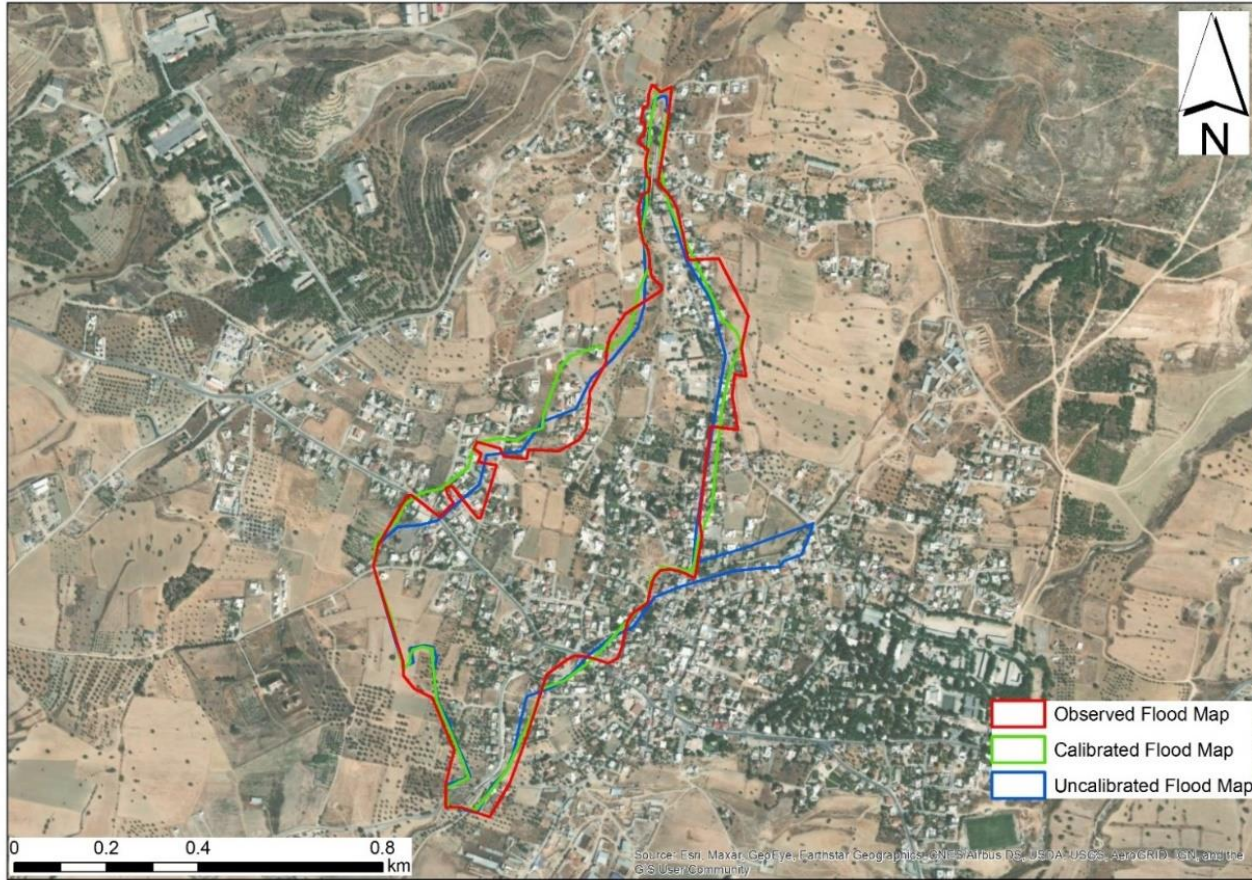


Figure 7.1 The Flood Maps of the 2018 Flood, Uncalibrated Model, and Calibrated Model

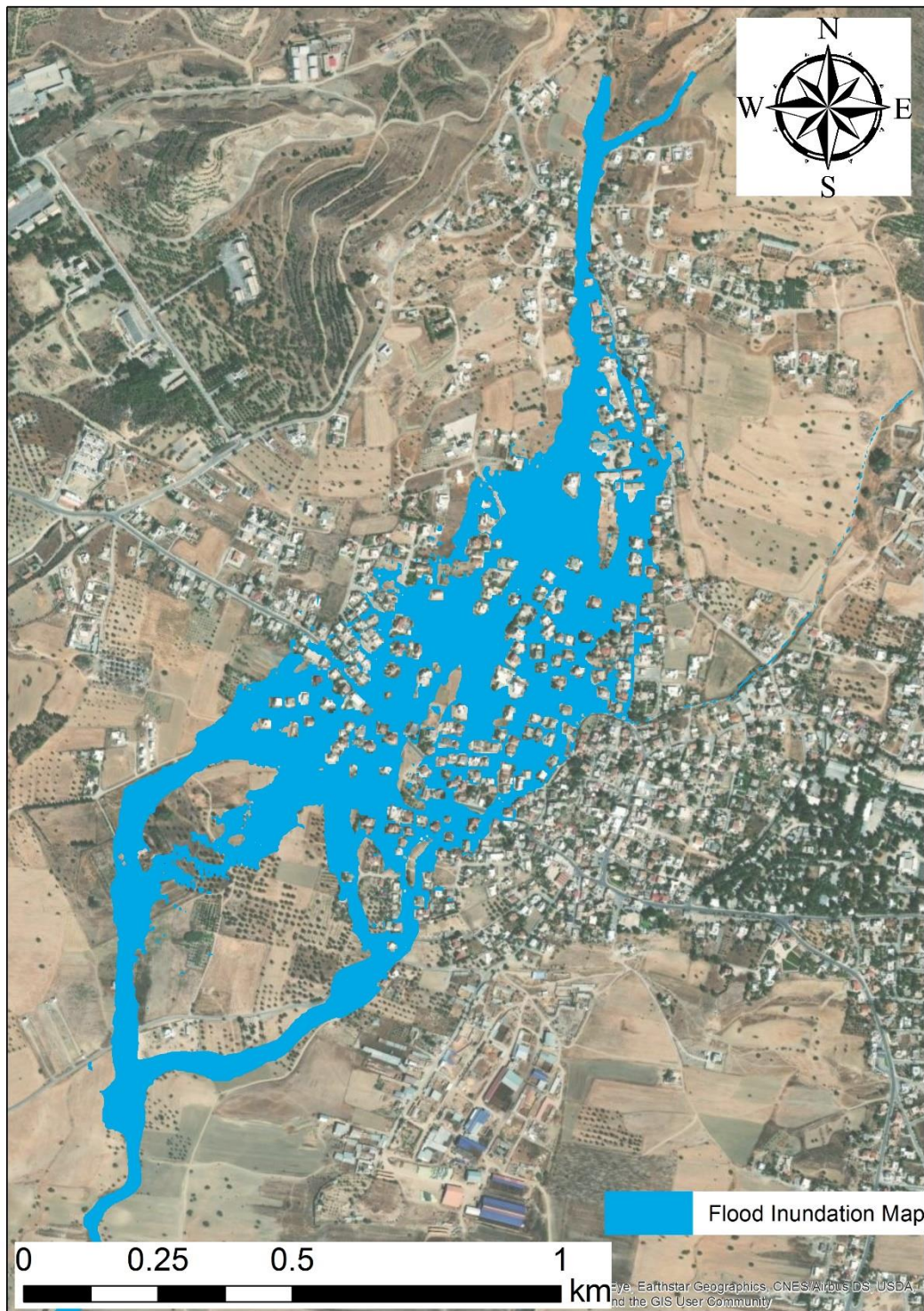


Figure 7.2 2018 - Flood Inundation Map

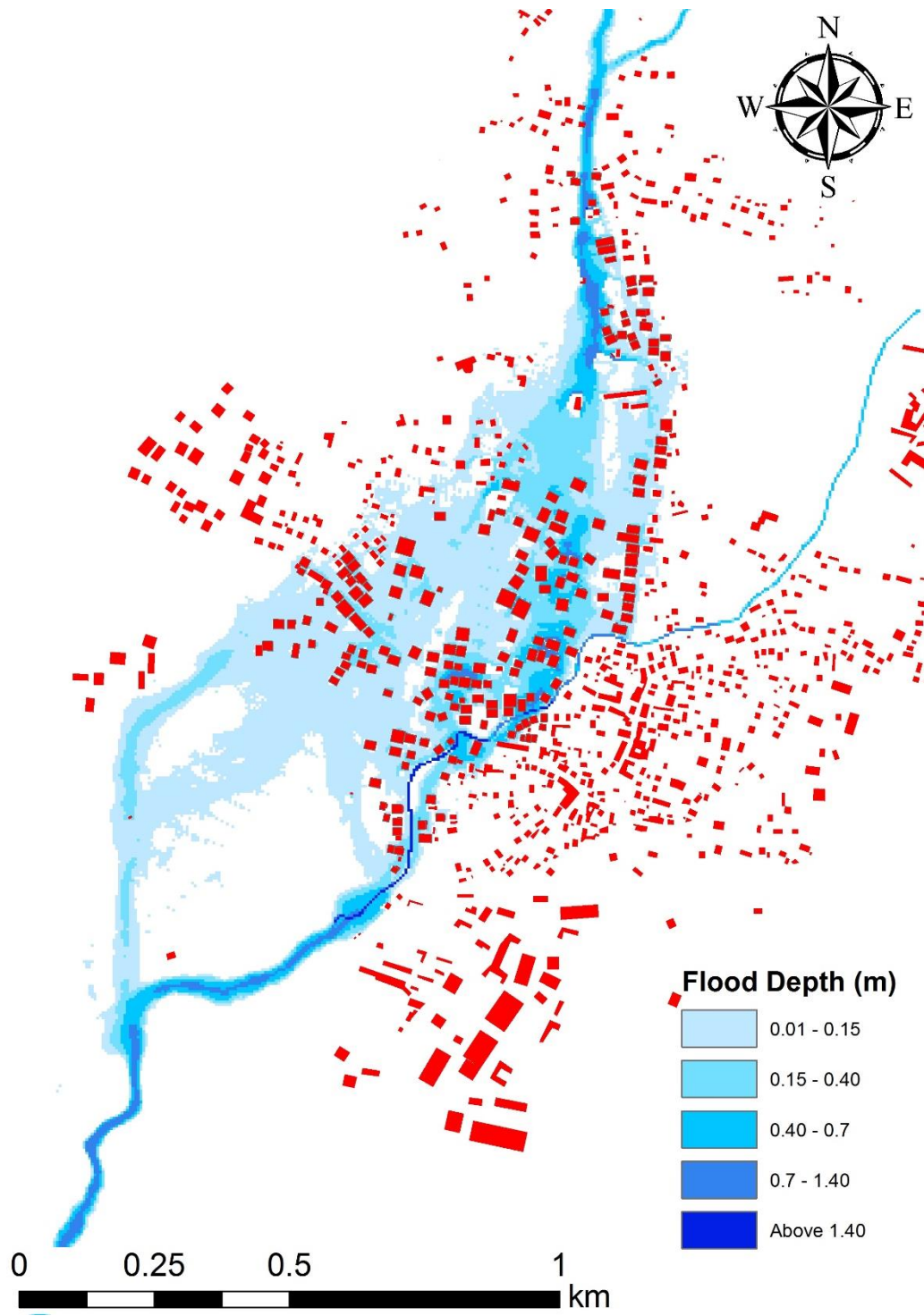


Figure 7.3 Flood Depths of the Model 2018 Flood

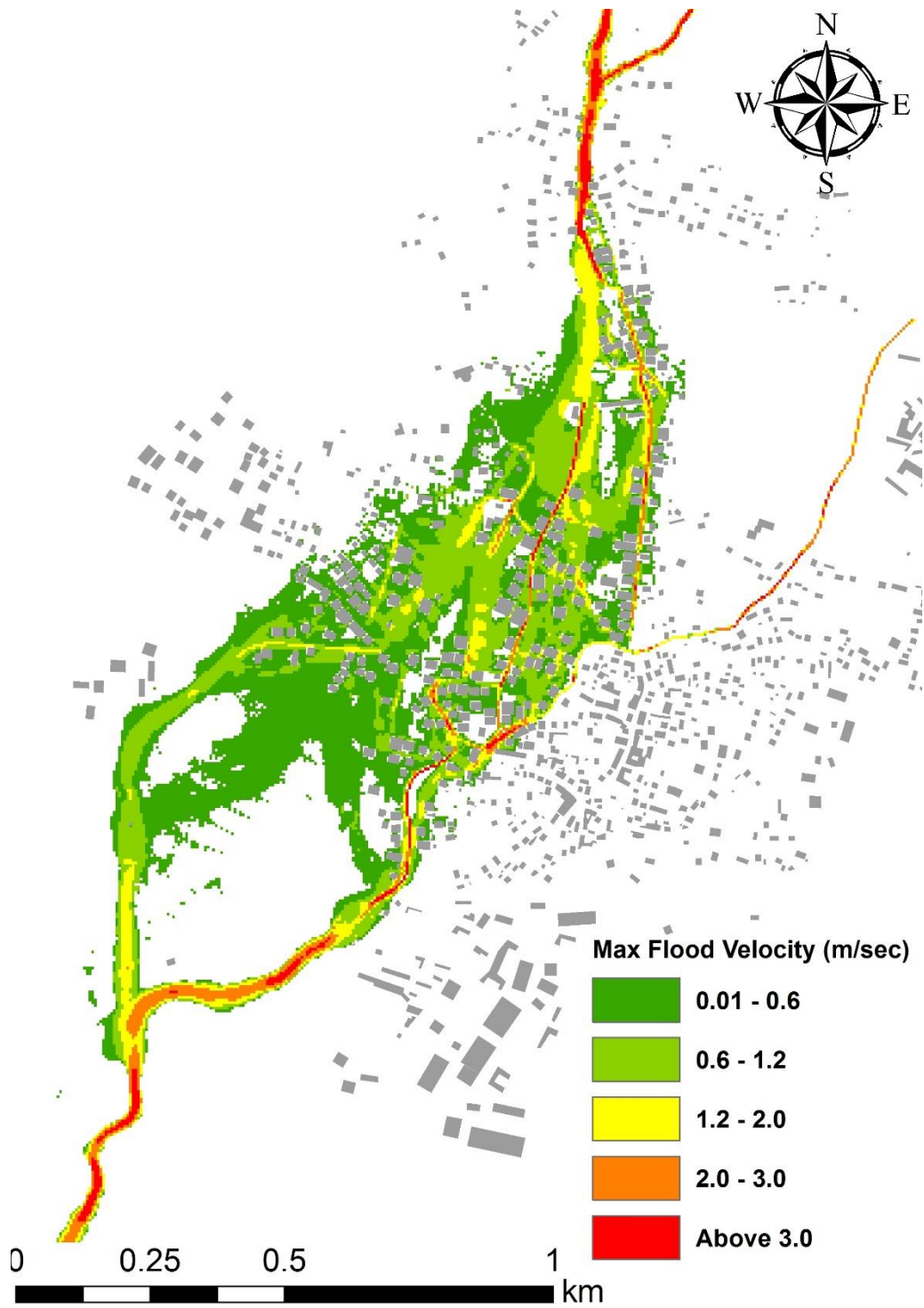


Figure 7.4 Maximum Flow Velocity Map of the 2018 Flood Event

7.1.2 50-, 100-, and 500-year Flood Maps For Current Condition

The 2D HEC-RAS features allow flood map generation based on the inputs provided to the model. After successfully calibrating the model, the calibrated model was adapted as the base for future prediction of flood events with different return periods. The hydrographs generated from the hydrological model based on rainfall events with 50-, 100-, and 500-year return periods are entered as the upstream boundary conditions. The other settings of the model, including the land covers, the calibrated Manning's values, the model computation settings, etc., were kept the same as the calibrated model.

The maps shown in Figure 7.5 indicate that the Dikmen town under a rainfall event with a 50-year return period would experience serious damage. The 50-year return period flood extent map (Figure 7.5a) covers almost the same area as the 2018 Flood event. However, the flood depth map in Figure 7.5b signifies some differences in various locations. For example, the 2018 Flood model shows that depth values in the upstream areas have reached up to 0.8 m. However, those values are close to 0.45 m in the flood model of the 50-year rainfall event. Similarly, the maximum flow velocities in Figure 7.5c are lower in the case of a 50-year flood. Nevertheless, it can pose a serious threat to the community.

The flood inundation map of rainfall events with a 100-year return period shown in Figure 7.6 indicates a slight increase compared to the 50-year map. Meanwhile, it covers a smaller area than the 2018 Flood event, since the peak value of the 2018 Flood event is higher than the peak discharge value of a 100-year return period flood. On the other hand, generated results indicate that flood velocity and flood depth maps of the 500-year return period (Figure 7.7) are higher than the events with 100-year as expected.

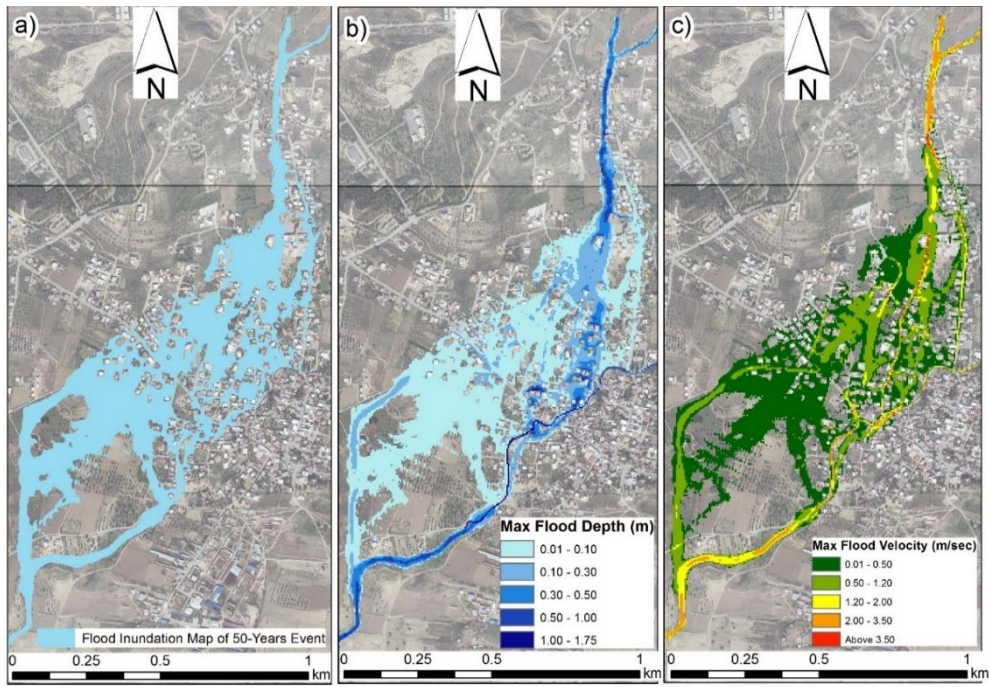


Figure 7.5 a) Flood Inundation Map, b) Maximum Flood Depth, c) Maximum Flood Velocity Map of 50-year Event

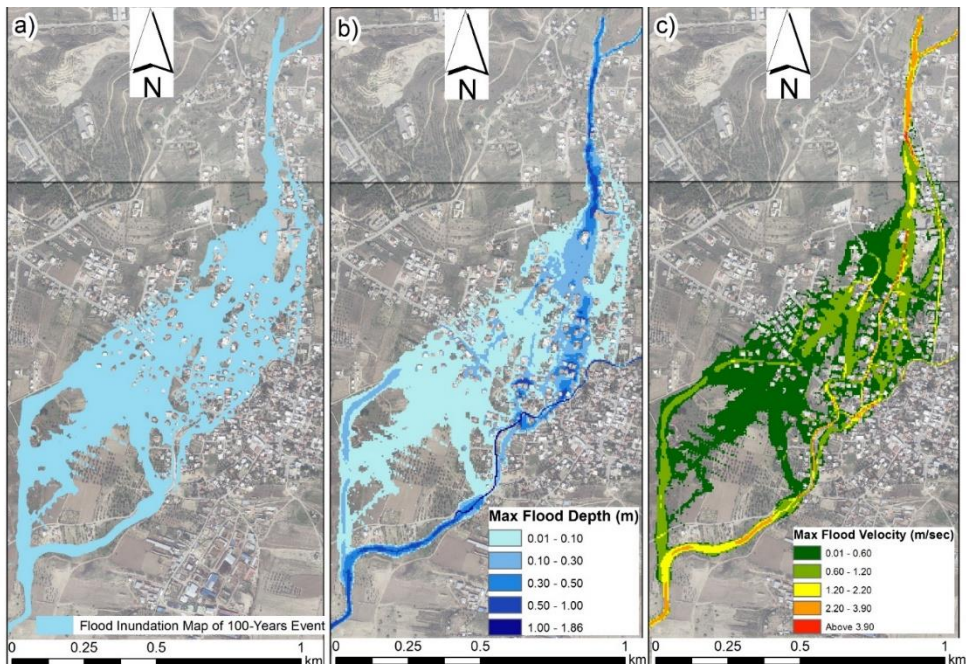


Figure 7.6 a) Flood Inundation Map, b) Maximum Flood Depth, c) Maximum Flood Velocity Map of 100-Year Event

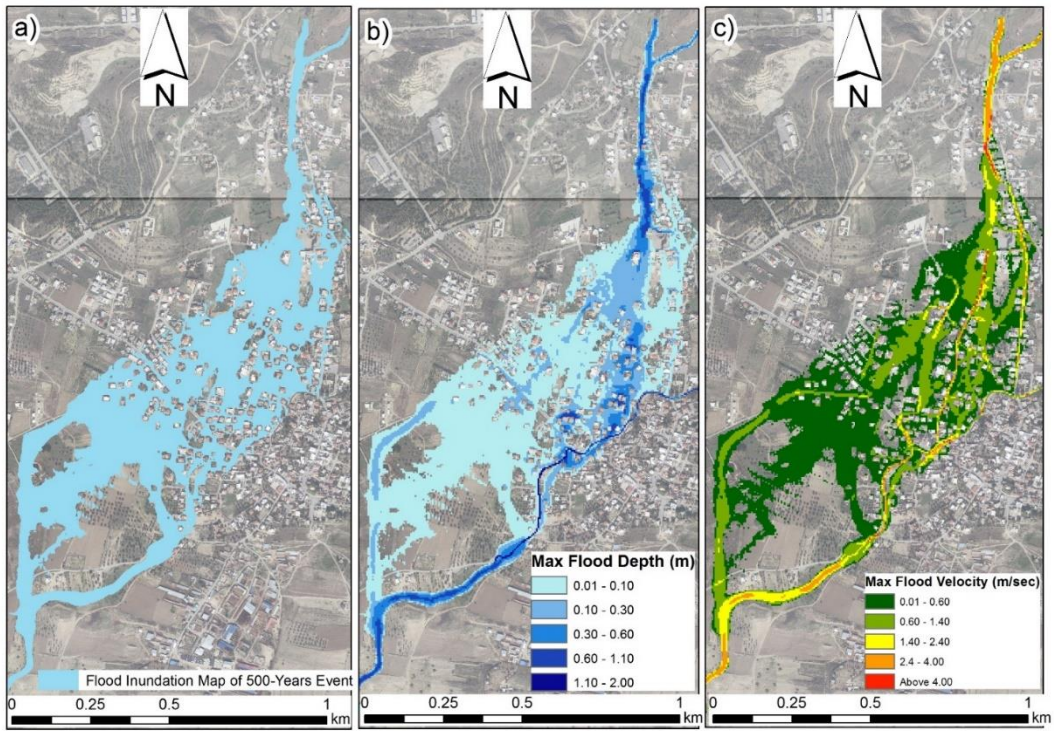


Figure 7.7 a) Flood Inundation Map, b) Maximum Flood Depth, c) Maximum Flood Velocity Map of 500-year Event

7.1.3 Mitigation Measure - M1: Concrete Channel

The initial assessment of the area and the model results showed that one of the main reasons for the frequent floods in Dikmen town is the impaired channel path due to unplanned urbanization developments. Therefore, constructing a channel is considered the first mitigation measure (M1) to carry water from the Top Sub-basin and Mid Sub-basin. However, various factors, including the land regulations and ownership surrounding the channel and the channel's path, limit the channel's width and depth.

The proposed channel characteristics involved the construction of a rectangular open channel that has a concrete bed with a length of 900 m, as shown in Figure 7.8. The walls of the open channel are made of rubble stones as this is the area's widely used and commonly available material. For the remaining distance of 135 m, the channel top will be covered as it goes under a road before it joins the existing concrete channel in Dikmen. The proposed channel width (W), channel depth (D), mean slope (S_0), and Manning's roughness values (n_1 and n_2) for stone and concrete walls are listed in Table 7.3. The initial 1D HEC-RAS analysis result showed that an open channel with a given design characteristic (Table 7.3) has a maximum capacity of 24 m³/s. Meanwhile, the closed part of the concrete channel with concrete walls has a mean slope of $S_0 = 0.028$, and roughness coefficient of $n_2 = 0.013$ for concrete culverts according to Mays (2010). A concrete channel with the characteristics given has a capacity of up to around 90 m³/s.

Table 7.3 Open Channel Hydraulic Parameters

Channel Parameters	Values
n_1	0.03
n_2	0.013
S_0 (Varying)	0.012 - 0.033
W (m)	4.0
H (m)	1.8

However, the main objective is to test the effectiveness of the channel as a flood control measure. Hence, the channel with specific characteristics was incorporated into the 2D HEC-RAS model using Terrain Modification Tools in Ras Mapper. Following the incorporation of the channel into the model, a series of breaklines were added to enforce the cell faces along the linear features of the channel, such as the bank line and centerline to align the flow meshes with the channel path. This approach increased the accuracy of the flow computation in the channel. It ensured that the overflow only occurs when the channel capacity reaches its maximum level. Similarly, in the junction point of the two channels, a refinement area with 1/10 of the normal size of meshes in the 2D area was created for higher accuracy and better alignment in the flow transition from the connecting channel to the existing channel (HECRAS 2022). The results, after running the 2D HEC-RAS model with a time step of 1 sec, Courant number $C = 1$ with SWE as the selected computational equation, and the incorporation of the concrete channel with a 2D model indicate that the overflow occurs from the channel banks at the location with lowest slope value $S_0 = 0.012$ when the inflow hydrograph values are around $26 \text{ m}^3/\text{s}$ of discharge.

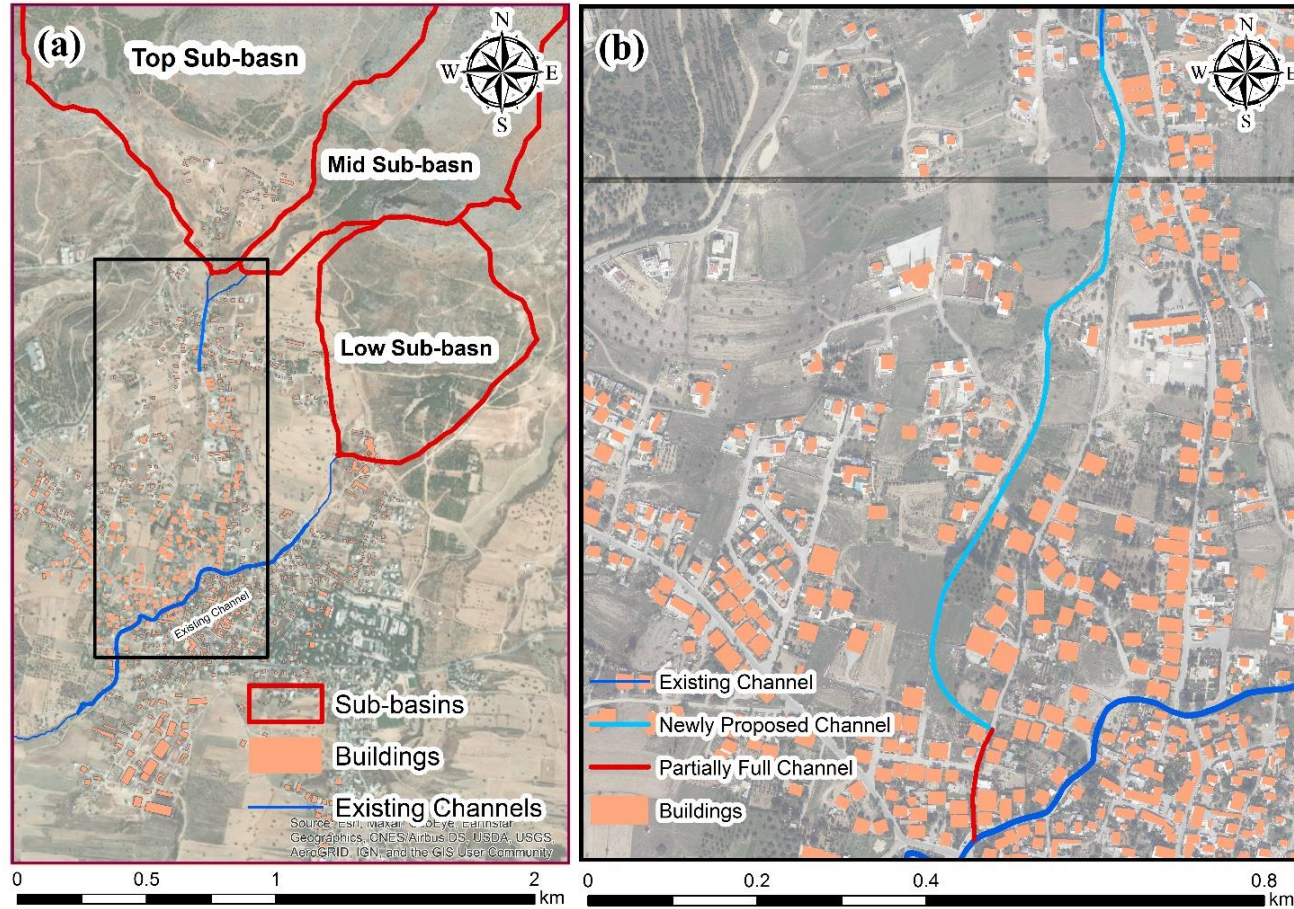


Figure 7.8 a) Proposed Channel Location c) Concrete Channel Sections

7.1.3.1 Channel Impacts Against 2018 - Flood Event

In the first scenario, the proposed channel efficiency is tested against the experienced extreme flood event in 2018. That event which was unique and had a total rainfall depth of 172 mm in 10 hours, caused severe damage to the urban areas in Dikmen town. The result of the hydrological model indicates that the event had two resultant peak discharge values from both the Top sub-basin and Mid sub-basin outflows. The first peak discharge value was around 27.1 m³/s, and the second was about 45 m³/s. If the same event occurred with the same traits again, the majority of the flood, due to the first peak, would be carried with the channel. However, in the event of the second peak arrival with a magnitude of 45 m³/s, some areas will be at risk of flooding. The flood hazard map before and after the channel in Figure 7.9 indicates that when the second peak of 45 m³/s arrives, a large part of the urban area in Dikmen is safe against flooding with the channel. However, in the lower and top part of the channel, the inflow exceeds the maximum channel capacity and start to inundate the urban area.

Moreover, the generated flood hazard maps shown in Figure 7.9 indicate significant differences between the flood hazard maps of the 2018 Flood event, without channel (Figure 7.9a) and with the channel (Figure 7.9b). The result points out that before the channel, a significant part of the study area, especially on grounds with low roughness values such as roads, has hazard thresholds of H6, which implies that it is unsafe for people, vehicles, or structures. However, after the proposed channel, the hazard level of those locations mostly decreases significantly, especially in the upstream part of the study area. On the other hand, in some locations with a lower slope of the channel bed, the downstream side of Dikmen town would still be in danger of flooding.

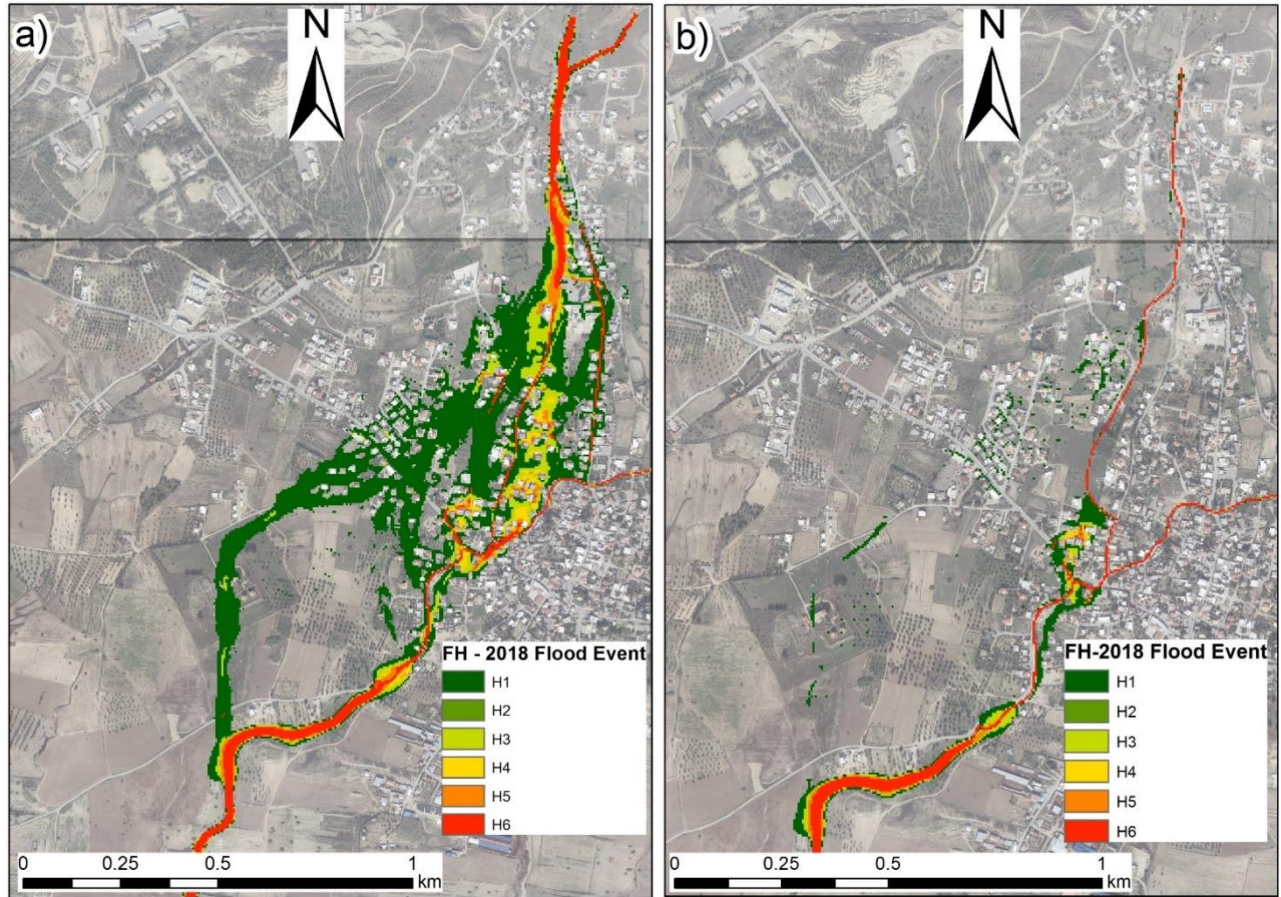


Figure 7.9 Flood Hazard of 2018 Flood Event. a) Before Channel, b) After Channel

7.1.3.2 Channel impact Against, 50, 100, and 500-year Flood Events

In this section, the impact of the concrete channel is considered against 50-, 100-, and 500-year return period rainfall events. The generated flood hazard maps indicate that the construction of the channel would significantly decrease the hazard level of the flooding due to the events having 50- and 100-year return periods. As shown in Figure 7.10, the 100-year flood hazard maps before and after the channel indicate the changes between the conditions before and after the channel's implication.

However, the total peak discharge from the flood hydrograph of the Top sub-basin and Mid sub-basin in case of a 500-year return period flood event is around $29 \text{ m}^3/\text{s}$. Since the channel has a capacity of $26 \text{ m}^3/\text{s}$, the proposed channel can carry about 90 % of the total incoming flow. After the channel integration into the terrain, the expected result was a significant decrease in the flood inundation and hazard maps, as shown in Figure 7.11, and a decrease in the vulnerability of the previously flood-prone areas. A considerable reduction is detected between the flood hazard maps of a 500-year return period with and without the channel in Figure 7.11a and Figure 7.11b, respectively.

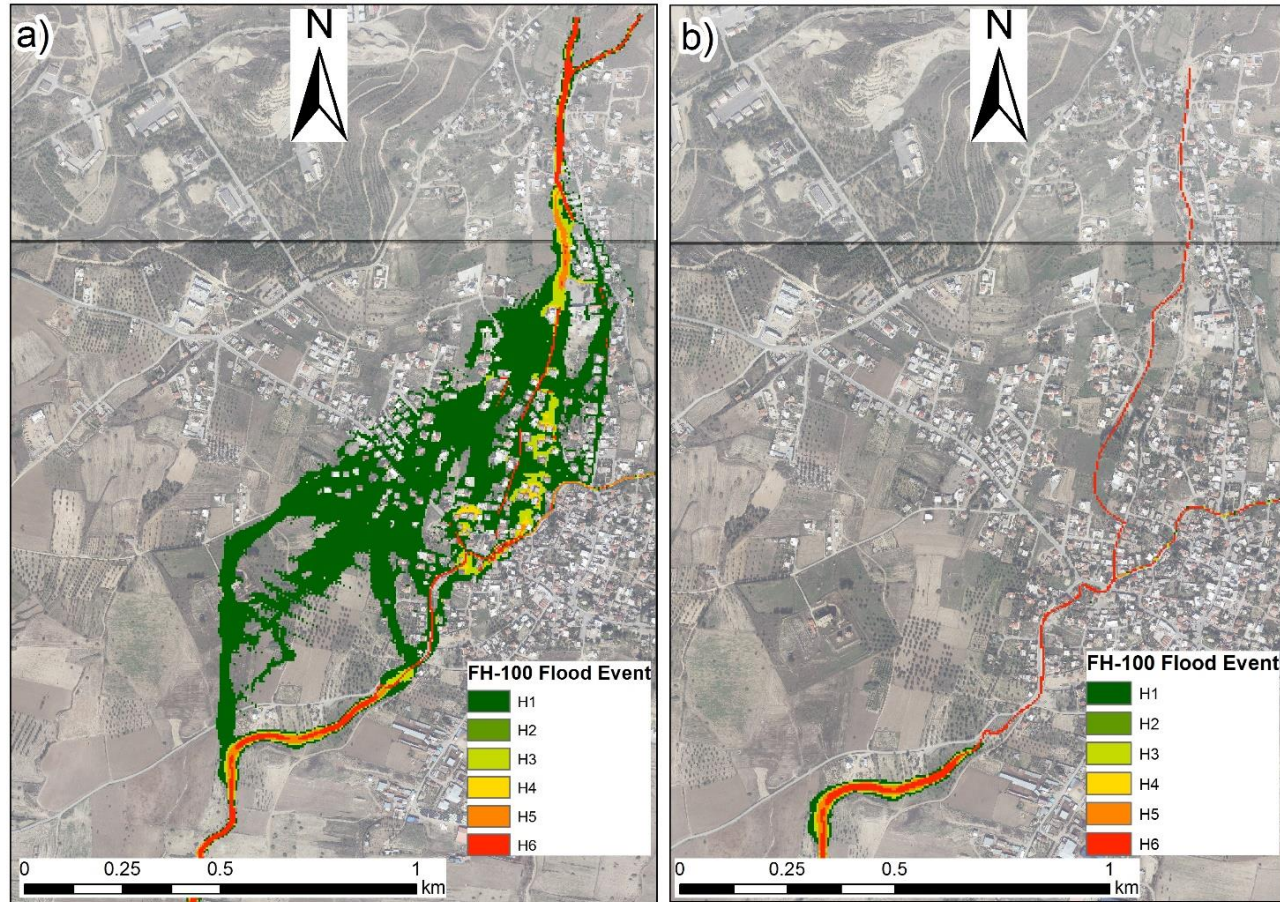


Figure 7.10 Flood Hazard of 100-Year Return Period Flood Event. a) Before Channel, b) After Channel

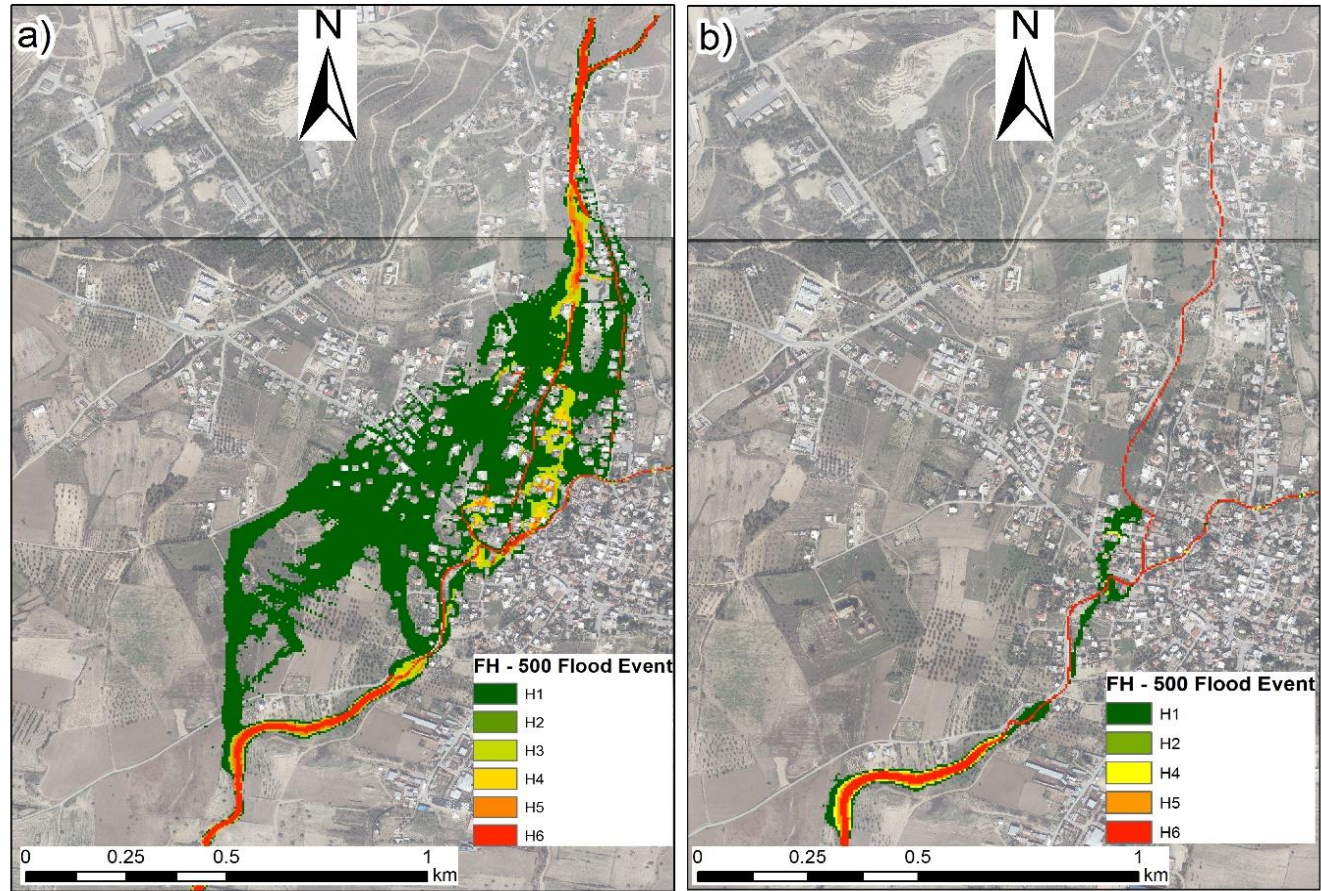


Figure 7.11 Flood Hazard of 500-Year Return Period Flood Event. a) Before Channel, b) After Channel

7.1.3.3 Cost Analysis of the Concrete Channel

This section includes the cost analysis of a rectangular concrete channel with a net width (4 m) and net height (1.8 m). The components include excavation costs, walls, concrete, and formwork costs. The unit costs are taken in the Turkish Lira (TL) local currency from the price list provided by the local authorities in Northern Cyprus (Tok. 2022) given in Table 7.4. Unit costs include material costs, labor costs, and contractor profit costs.

Table 7.4 Unit Cost Summary of the materials and labor works (Tok 2022)

List No	Description (Turkish)	Description (English)	Unit	Cost (TL/Unit)	Cost (\$/Unit) ¹
1.2	Makine ile radye temel kazısı	Excavation with Machine	m ³	59.0	3.3
5.3	Beton C 20/25	Concrete C 20/25	m ³	1,265.0	70.3
5.5	Beton C 25/30	Concrete C 25/30	m ³	1,350.0	75.0
7.1	donatılarının İşlenmesi	Reinforced Steel works	Ton	24,000.0	1,333.3
8.1	İstinat duvarı betonarme kalıbı	Retaining wall Formwork	m ²	150.0	8.3
40.12	Kırma Dağtaşı ile harçlı duvar örülmesi	Building a mortar wall with crushed mountain stone	m ³	2,653.0	147.4

¹ 1 USD = 18 TL (Average Exchange rate in August 2022).

The total excavation cost can be calculated as follow:

$$C_x = (b_c y_c L_c) C_{uxa} \quad (38)$$

where C_x is the excavation costs, b_c is the width of the channel, y_c is the height of the channel for the rectangular channel, and L_c is the total channel length. The volume of excavated soil amount is noted as V_x . The excavation unit cost, C_{uxa} is listed in Table 7.4, which equals 59 TL/m³ or 3.3 \$/m³. The details of the calculation are listed in Table 7.5.

Table 7.5 Details of The Excavation Cost Analysis

L_c (m)	B_c (m)	y_c (m)	V_c (m ³)	C_{uxa} (TL/m ³)	C_{uxa} (\$/m ³)	C_x (\$)
900	4.6	2.1	8694	59	3.3	28,497
135	4.6	2.1	1304.1	59	3.3	4,275
					Total	\$ 32,772

The concrete channel wall with a length of L_{oc} will be constructed with stones and mortar, as it is among the commonly available materials in the area. In Table 7.4, the unit cost of a 0.3 m thick stone wall with mortar C_{usw} is given as 147 \$/m³. Meanwhile for the channel concrete bed with 0.1 m thickness and C20/25 grade, the unit cost C_{bt} is given as 70.3 \$/m³. The overall costs of the channel walls C_{sw} and channel bed C_b are given in Table 7.6.

Table 7.6 Details of the Open Channel Cost Analysis

Open Channel	L_{oc} (m)	W_w (m)	y_c (m)	V_{sw} (m^3)	C_{usw} (TL/ m^3)	C_{usw} (\$/ m^3)	C_{sw} (\$)
2 side Walls	1800	0.3	1.8	972	2653	147	143,262
	L_{oc} (m)	C_w (m)	C_{bt} (m)	V_{bc} (m^3)	C_{usb} (TL/ m^3)	C_{ub} (\$/ m^3)	C_b (\$)
Channel Bed	900	4	0.1	360	1265	70.3	25,300
Total							\$ 168,562

Moreover, for the closed section of the channel, both side walls, the bottom slab, and the top slab of the channel are considered to be constructed with reinforced concrete in the form of a culvert. The concrete considered in the analysis is made of crushed quarry stone with reinforced steel with a grade of C25/30. The side walls, top slab, and bottom slab design of the culvert are considered based on the recommendation given in FDOT (2013). The total cost of the culvert, C_c is calculated based on the total concrete volume (V_{con}). The unit cost of the C25/30 concrete C_{uc} is given 1350 TL/ m^3 or 75 \$/ m^3 in Table 7.4. Considering the given information, excluding the cost of steel, the final cost is calculated in Table 7.7.

Table 7.7 Cost Analysis Details of the Closed Section of the Concrete Channel

Closed Channel	L_{cc} (m)	T_w (m)	H (m)	V_c (m^3)	C_{uc} (TL/ m^3)	C_{uc} (\$/ m^3)	C_c (\$)
2 side Walls	270	0.3	2	162	1350	75	12,150
	L_{cc} (m)	T_w (m)	W (m)	V_c (m^3)	C_{uc} (TL/ m^3)	C_{uc} (\$/ m^3)	Total (\$)
Top Slab	135	0.2	4	108	1350	75.0	8,100
Bottom Slab	135	0.2	4.4	119	1350	75.0	8,910
Total				389 m^3			\$29,160

In order to determine the total cost of the reinforced steel required for the project, the amount of steel must be calculated first. A detailed reinforcement design is required to obtain the actual amount. However, this project is based on the assumption that about 150 kg of steel is usually needed for every 1 m³ of concrete in the construction of the retaining walls (Ugochukwu et al. 2020). Based on that assumption, for the 389 m³ volume of concrete required for the closed section of the channel, about 58.3 tons of reinforced steel is required. The unit cost of steel given in Table 7.4 is 1333 \$/ton. Thus, the total cost of the steel needed for the project is \$77,760.

The formwork cost analysis for the top slab and side walls is considered for each 1 m² of the surface area of the walls and the top slab. The formworks unit cost C_{fwu} equal to 8.3 \$/m² is given in Table 7.4. The total amount of the formworks surface area is 540 m² for the top slab works and 972 m² for both side walls. Table 7.8 illustrates the formworks cost analysis.

Table 7.8 Formworks Cost Analysis Details

Formworks	Lcc (m)	Bc (m)	yc (m)	A (m ²)	C _{FWU} (TL/m ²)	C _{fwu} (\$/m ²)	C _{FW} (\$)
Top Slab	135	4	0.2	540	150	8.3	4,500
2 side Walls	135	4	1.8	972	150	8.3	8,100
Total							12,600

Based on the cost analysis of the individual section of the channel, which includes the excavation cost, stone wall cost, open channel concrete bed cost, closed section total concrete cost, reinforcement steel cost for the closed section, and formworks cost for the closed section of the channel, the total cost of the channel reaches to the amount of \$320,853.

7.1.4 Mitigation Measure - M2: Reservoirs

Storing rainwater effectively recharges the underground aquifer and provides irrigation water to the farmers during the dry seasons. On the other hand, using reservoirs in flood control is also common practice, which can contribute to mitigating the potential damages imposed by floods. Meanwhile, reservoirs can also contribute to developing resilient and sustainable communities. Generally, there are two types of flood control reservoirs: dry and wet. Dry reservoirs are usually constructed for flood control. They have no water before the arrival and occurrence of a flood. In contrast, wet reservoirs contain water before the occurrence of flood events.

The limitations and constraints in the catchment areas limit the size and locations of the reservoir. Therefore, considering these factors, several alternative locations for flood control reservoirs were tested, and the final locations were selected for further investigation. For instance, after primary analysis, it has been determined that the topographic conditions in the catchments and existing properties (e.g., houses) would not allow the construction of one large reservoir in each sub-basin. In addition, the catchments' high ground surface slope limits the reservoir storage surface area. Thus even with the increase in the reservoir height, reservoir storage capacity does not increase significantly.

In the first step, the stage-storage relationships and storage-discharge relationships of several reservoirs in the various potential locations are generated. Based on these relationships, the selected reservoirs' final locations are determined, as shown in Figure 7.12. One small-size reservoir, RT1, one medium-size reservoir, RT2, and comparatively one large-size reservoir, RT3, were selected to be considered for flood control purposes in Top Sub-basin (see Figure 7.13). Furthermore, one small-size reservoir, MR1, and comparatively one large-size reservoir, MR2, were deemed reasonable for flood control in the Mid sub-basin, as shown in Figure 7.14. The details and characteristics of each selected reservoir are given in Table 7.9.

To represent the effect of the individual reservoirs on flood control, the Top sub-basin was divided into two parts of Western Top sub-basin with an area of 0.92 km² and the Eastern Top sub-basin (ETS-B) with a surface area of 1.23 km². The other hydrological parameters were kept the same as in the hydrological model. The new hydrographs were generated from the original hydrological model in HEC-HMS for flood routing analysis.

Table 7.9 Proposed Detention Reservoirs Characteristics

Basin	Name	Height (m)	Operating Level (m)	Length (m)	Orifice (m)	Crest Length (m)	Max Storage (m ³)
Top Sub- basin	RT1	7	5.5	46	1.0	12	6180
	RT2	12	11	43	1.0	12	7840
	RT3	12	11	54	1.0	12	30912
Mid Sub- basin	MR1	7	6	45	1.0	10	2000
	MR2	13	12	74	1.0	10	24000

The reservoir routing process requires setting the initial condition of the reservoir. Several prior studies have indicated that the impacts of full reservoirs on attenuating the peak time and discharge are very insignificant (Gül et al. 2010; Kaboosi and Jelini 2017). Based on that analogy, the impact analysis of the flood control reservoirs on flood hydrographs was performed, assuming that before any extreme event, the reservoirs are all empty and their full storage capacity is available.

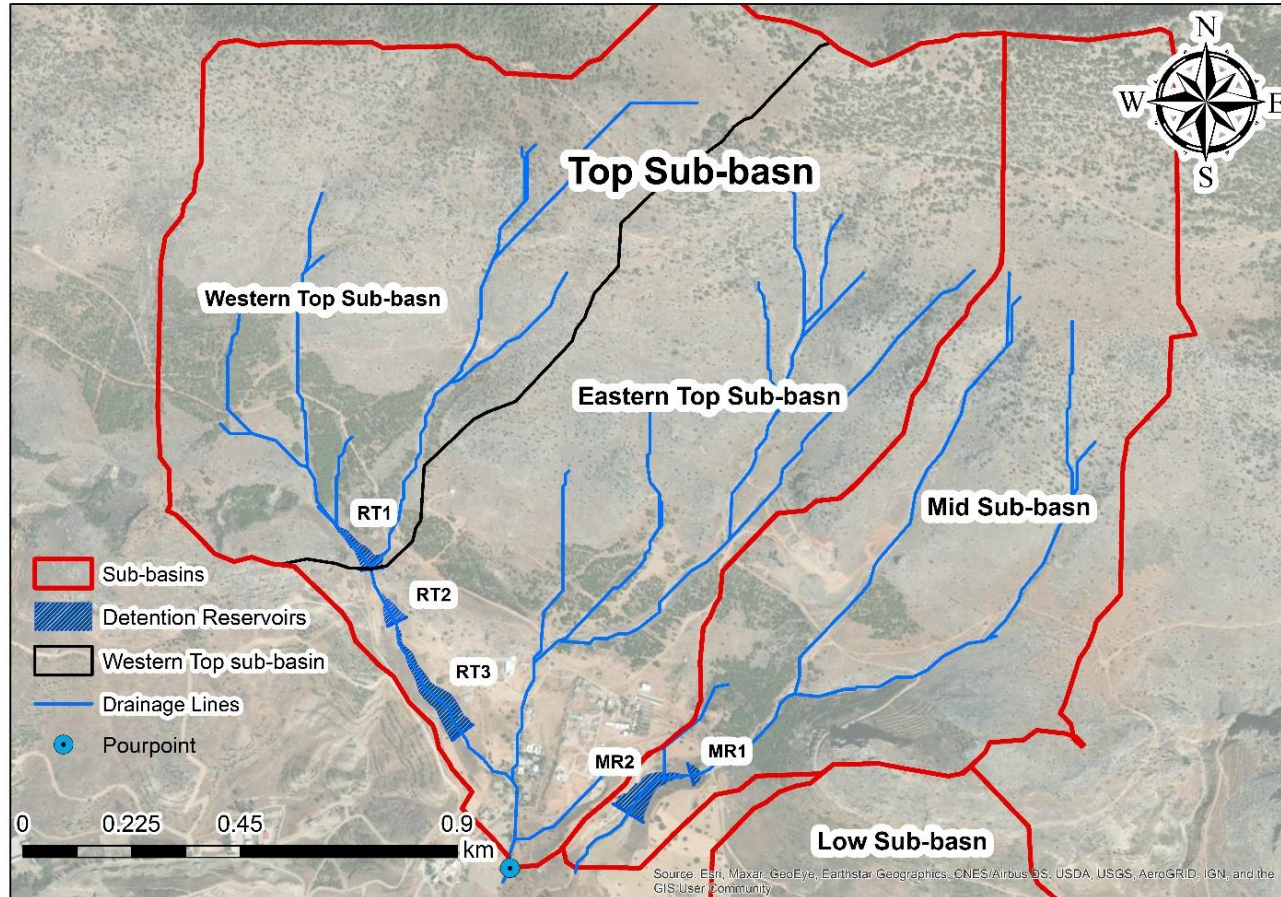


Figure 7.12 Selected Reservoirs Locations

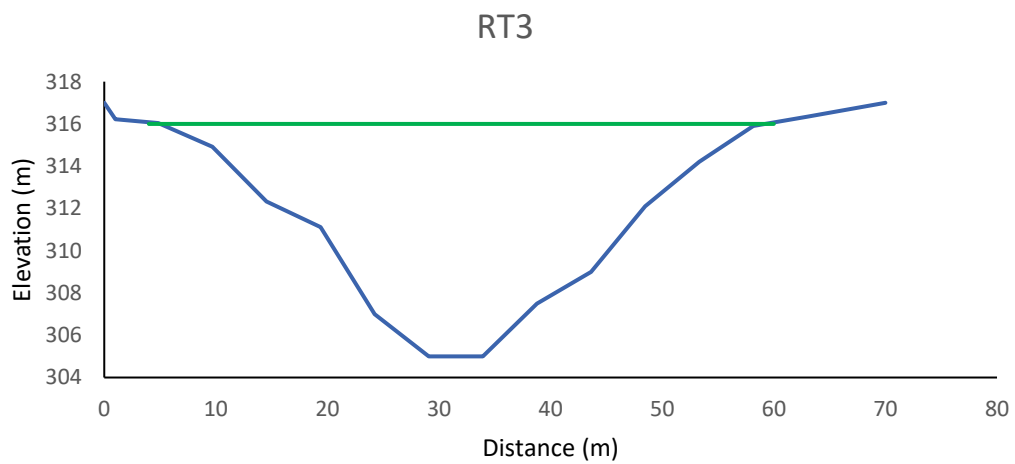
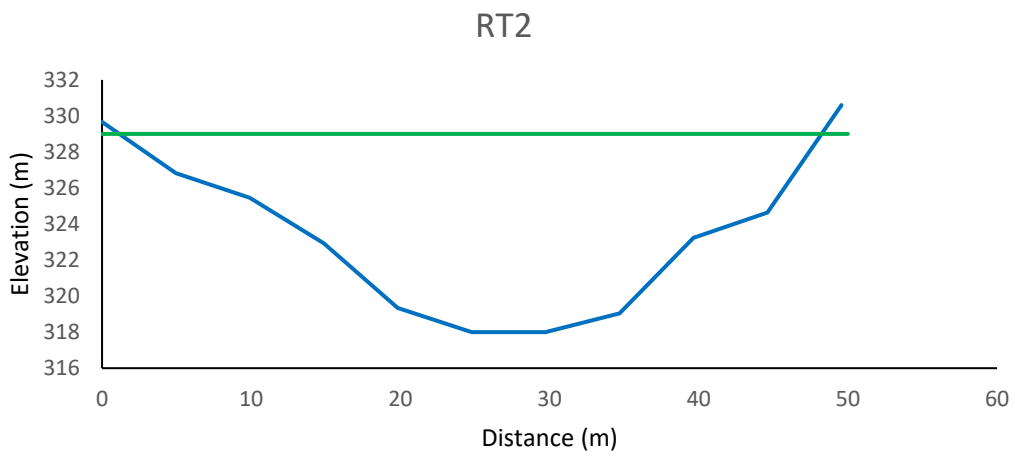
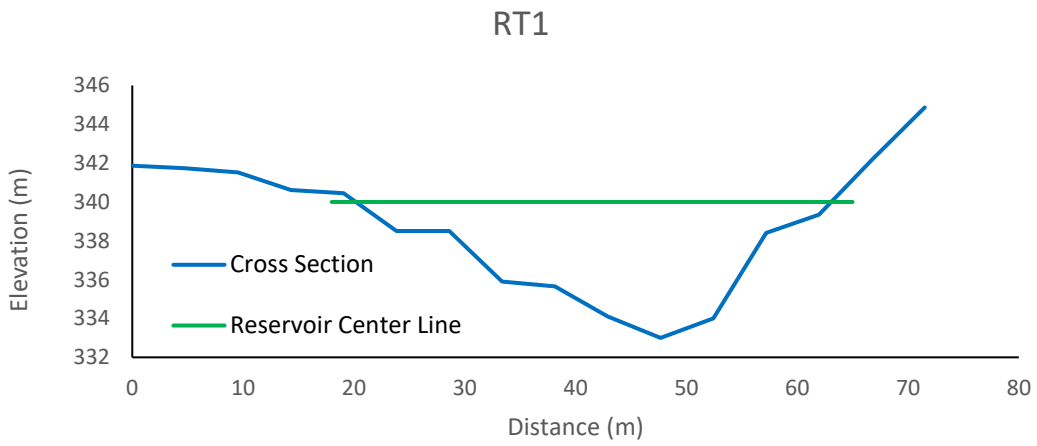


Figure 7.13 Top Sub-basin Reservoirs Cross Sections

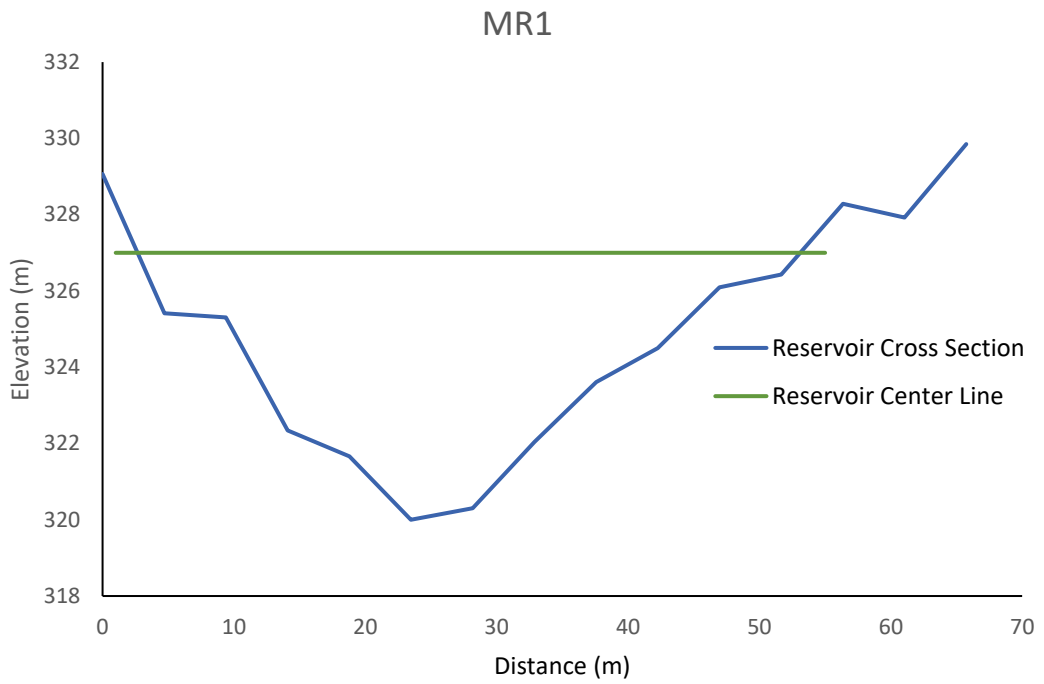


Figure 7.14 Mid sub-basin Reservoirs Cross Sections

7.1.4.1 Reservoirs Impact Against 2018 - Flood Event

In the first part of this section, the flood routing analysis is performed on a case similar to the event of the 2018 Flood. At first, the potential risk reduction of the reservoirs ignoring the significant impacts of the bottom outlets is considered. The analysis results indicated that the reservoirs without a bottom outlet in the Top sub-basin and Mid sub-basin slightly decreased the first peak value of the 2018 Flood hydrograph, as shown in Figures 7.15, and 7.16 respectively. However, with the arrival of the second peak discharge, the reservoirs fail to provide attenuation to both the second peak value and the second peak flood arrival time. Based on the obtained hydrographs after the flood routing, the results showed that the flood inundation map would not experience any change.

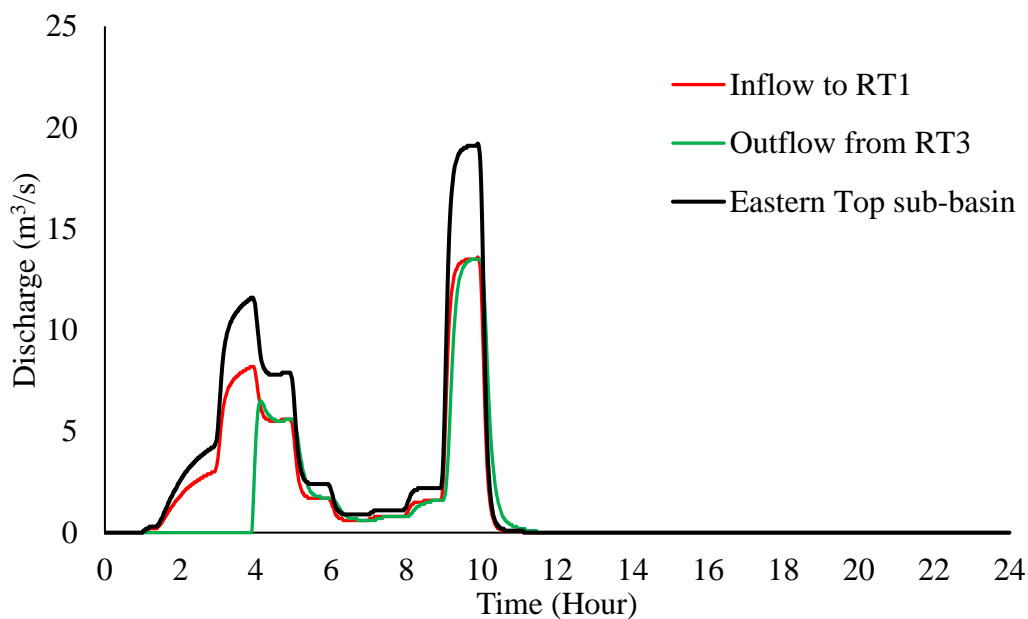


Figure 7.15 2018- Flood Routed Hydrograph After Without Bottom Outlets Reservoirs in Top Sub-basins

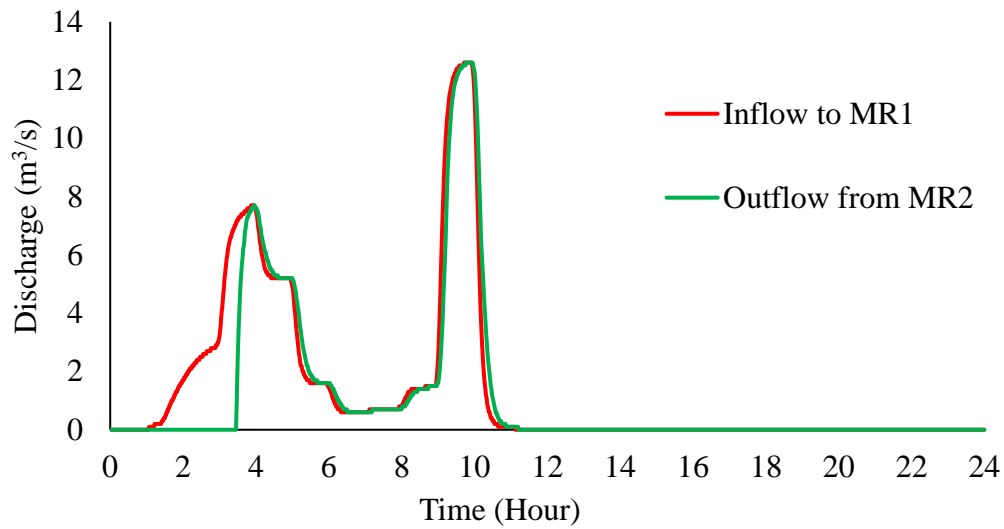


Figure 7.16 2018- Flood Routed Hydrograph After Reservoirs Without Bottom Outlets in Mid Sub-basins

On the other hand, in the second part of this section, the impacts of each reservoir with three different bottom outlet options with diameters of 0.5 m, 1.0 m, and 1.5 m are investigated separately. In option 1, the flood routing of reservoirs with 0.5 m diameter outlet in the Top and Mid sub-basins are assessed, and the results are given in Figures 7.17, and 7.18 respectively. For option 2, the results of the flood routing of the reservoirs with 1.0 m pipe as the bottom outlet for the Top sub-basin and Mid sub-basin are illustrated in Figures 7.19, and 7.20 respectively. In option 3, the impacts of the reservoirs with a 1.5 m bottom outlet on the 2018 Flood event discharge hydrographs from the Top sub-basin and Mid sub-basin are given in Figures 7.21, and 7.22 respectively.

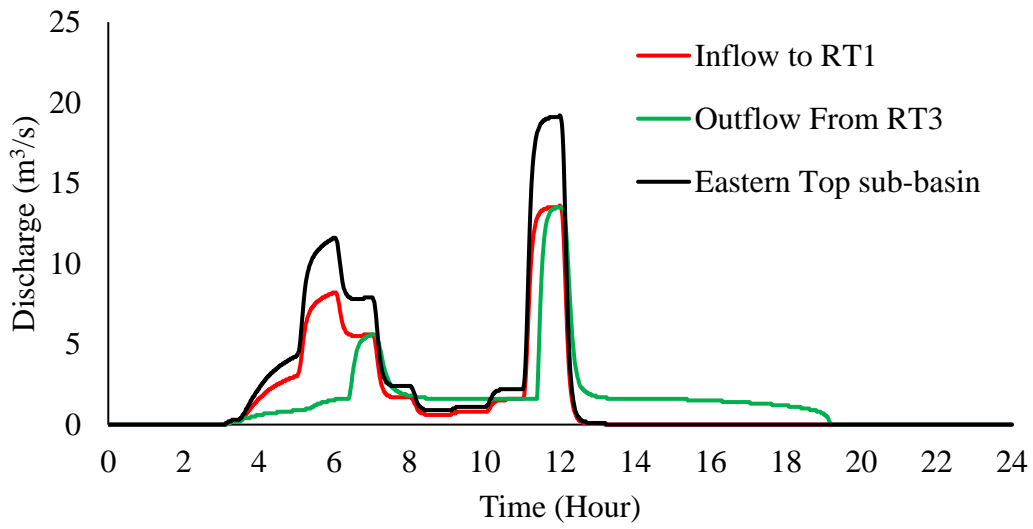


Figure 7.17 2018- Flood Routed Hydrographs After Reservoirs with 0.5 m Bottom Outlets in Top Sub-basin

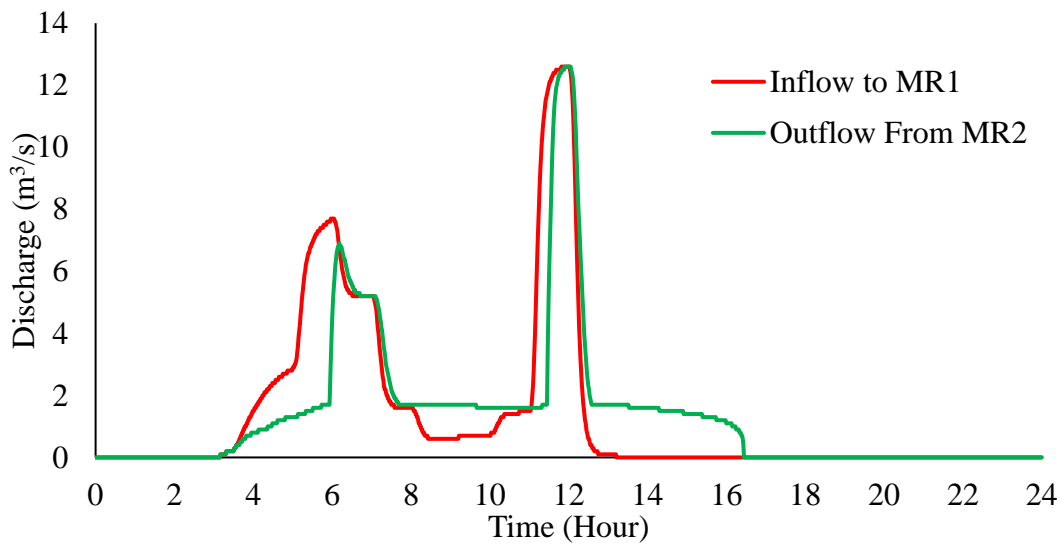


Figure 7.18 2018- Flood Routed Hydrograph After Reservoirs with 0.5 m Bottom Outlets in Mid Sub-basins

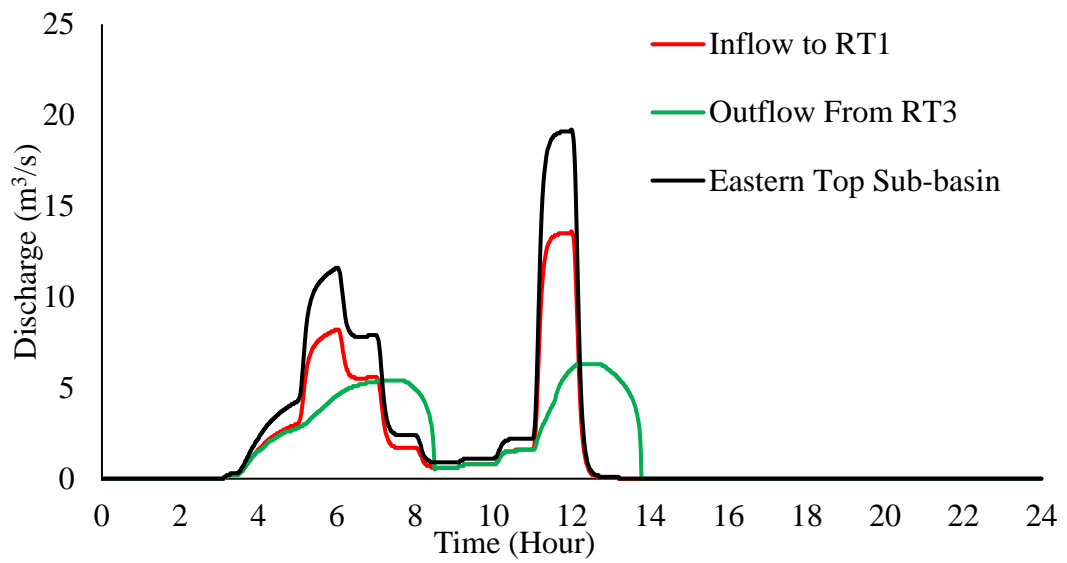


Figure 7.19 2018- Flood Routed Hydrographs After Reservoirs With 1.0 m Bottom Outlet in Top Sub-basin

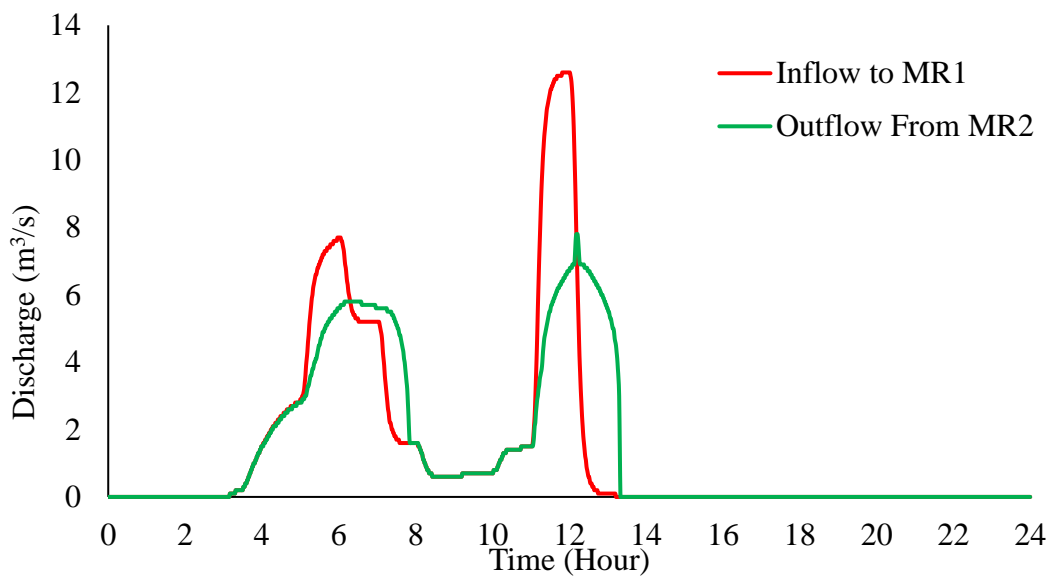


Figure 7.20 2018- Flood Routed Hydrograph After Reservoirs With 1.0 m Bottom Outlets in Mid Sub-basins

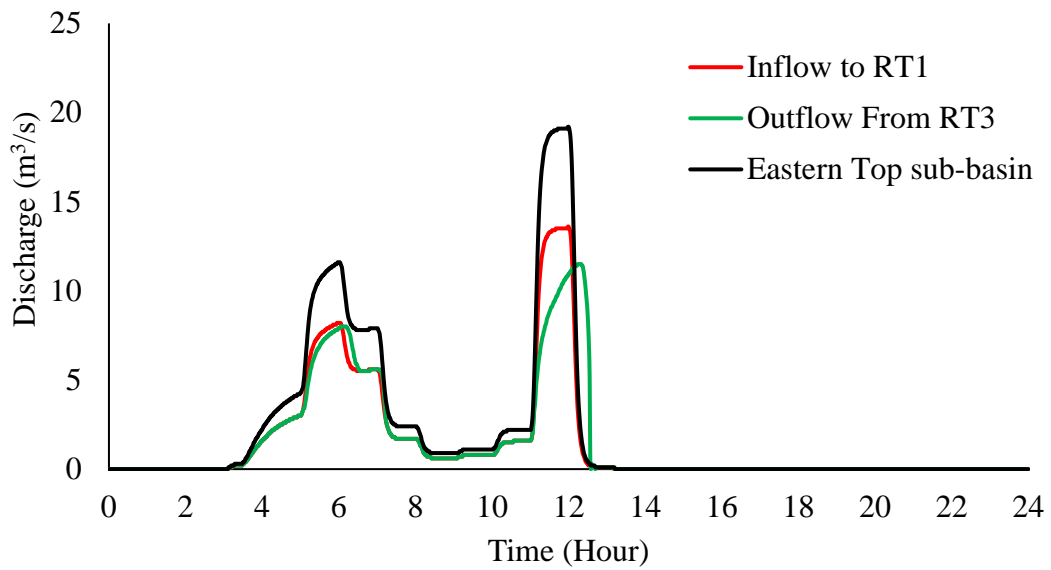


Figure 7.21 2018- Flood Routed Hydrographs after Reservoirs With 1.5 m Bottom Outlet in Top Sub-basin

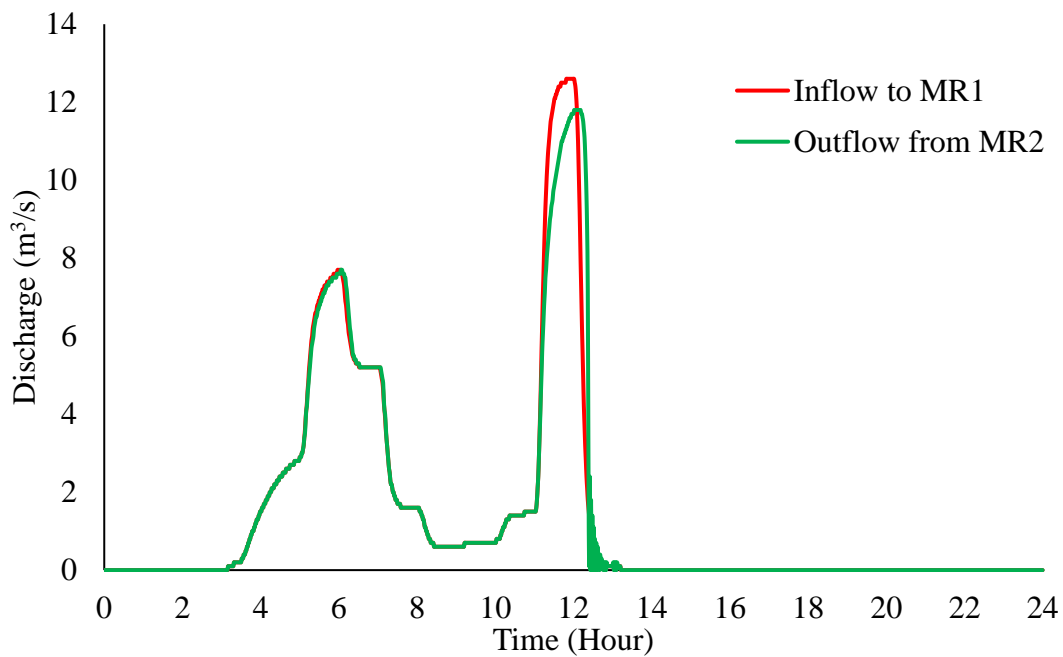


Figure 7.22 2018- Flood Routed Hydrograph After Reservoirs With 1.5 m Bottom Outlet in Mid Sub-basins

Based on flood routing analysis and outflow hydrographs of the three options, option 2, including the reservoirs with a 1.0 m diameter bottom outlet, generates the most optimum result in terms of attenuating the peak discharge values and peak time, as also seen in Figure 7.19. The results show a decrease in the peak discharges of the Top sub-basin from 32.6 m³/s to 24.7 m³/s. Similarly, in the reservoirs with a 1.0 bottom outlet, a considerable reduction in the releases from the Mid sub-basin onto Dikmen town can be seen in Figure 7.22. For instance, without reservoirs, the peak value of the outflow from the Mid sub-basin is 12.6 m³/s. However, the peaks drop to 7.3 m³/s after passing through MR1 and MR2 reservoirs with a 1.0 m bottom outlet.

7.1.4.2 Reservoirs Impact Against 50-, 100-, and 500-year Flood Events

The result of the flood routing analyses of reservoirs to reduce the peak discharge and delay the arrival of the floods for the events of 50-, 100-, and 500-year return periods are presented in this section. The results indicate that the effects of the reservoir without the bottom outlets are generally insignificant. For example, in the case of a 500-year return period flood event, as shown in Figure 7.23, the peak inflow into the RT1 reservoirs is 8.7 m³/s. After reservoir routing in the Top sub-basin, the peak discharge from RT3 drops to 7.6 m³/s. While there is about 1 m³/s reduction from inflow rate into RT1 to outflow from RT3, there is no significant shift in peak time occurrences. On the other hand, due to topographic limitations and the high slope on the eastern side of the Top sub-basin shown in Figure 7.12, the reservoir construction does not have a significant impact in terms of flood control. However, it may serve as sediment control and contribute to recharging the groundwater sources.

Similarly, as seen in Figure 7.24, the results indicate that the construction of the reservoirs without bottom outlets on the Mid sub-basin will not have any considerable effect on the flow rate, the volume of inflow, and the delaying of flood

arrival time. Thus, about 28.1 m³/s of combined flow from the Top and Mid sub-basins will pass through the residential town without any changes in the flow rate or volume. The summary of the flood routing analysis covering all scenarios considering reservoirs without the bottom outlets is presented in Table 7.10. Here, W/O/R refers to the condition without a reservoir, and W/R stands for with a reservoir case.

The main reason behind the low reservoir capacity is the topographical conditions of the ground and constraints on the storage capacity of the reservoirs. However, the construction of the reservoirs can undoubtedly store a good amount of water for irrigation purposes. Moreover, the reservoirs can also work as sediment and pollutants control structures that can make the community more resilient to flooding and recharge the underground water resources.

Moreover, the flood routing analysis results considering reservoirs with optimum-sized bottom outlets of 1.0 m indicate that in the case of a 500-year return period, the flow rate from the Top sub-basin experiences significant reduction, as shown in Figure 7.25. For example, the peak discharge from the Top sub-basin decreases from 21 m³/s to 17.3 m³/s. Similarly, the inflow from the Mid sub-basin drops from 8.2 m³/s to 6.2 m³/s, as shown in Figure 7.26. Table 7.11 presents the impacts of the reservoirs with 1.0 m bottom outlets on 50- and 100-year flood hydrographs.

The results of the flood routing for the reservoirs with a 1.0 m diameter bottom outlets compared to the reservoirs without the bottom outlets are significant. However, still considerable water would discharge into the town and cause flooding even in the events having low return periods.

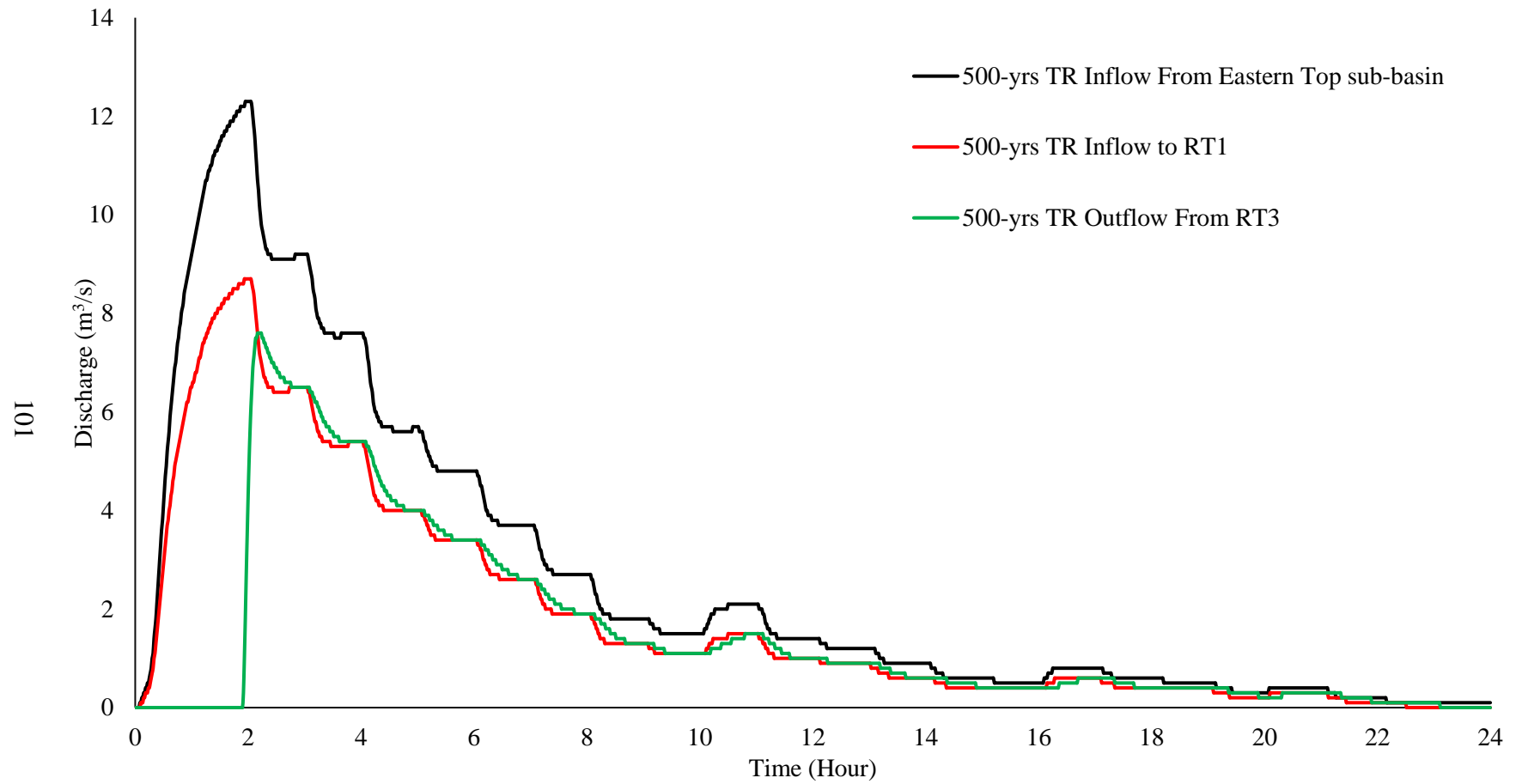


Figure 7.23 Reservoir W/O Bottom Outlet effects on 500-year Return Period Flood Hydrographs of Top Sub-basin.

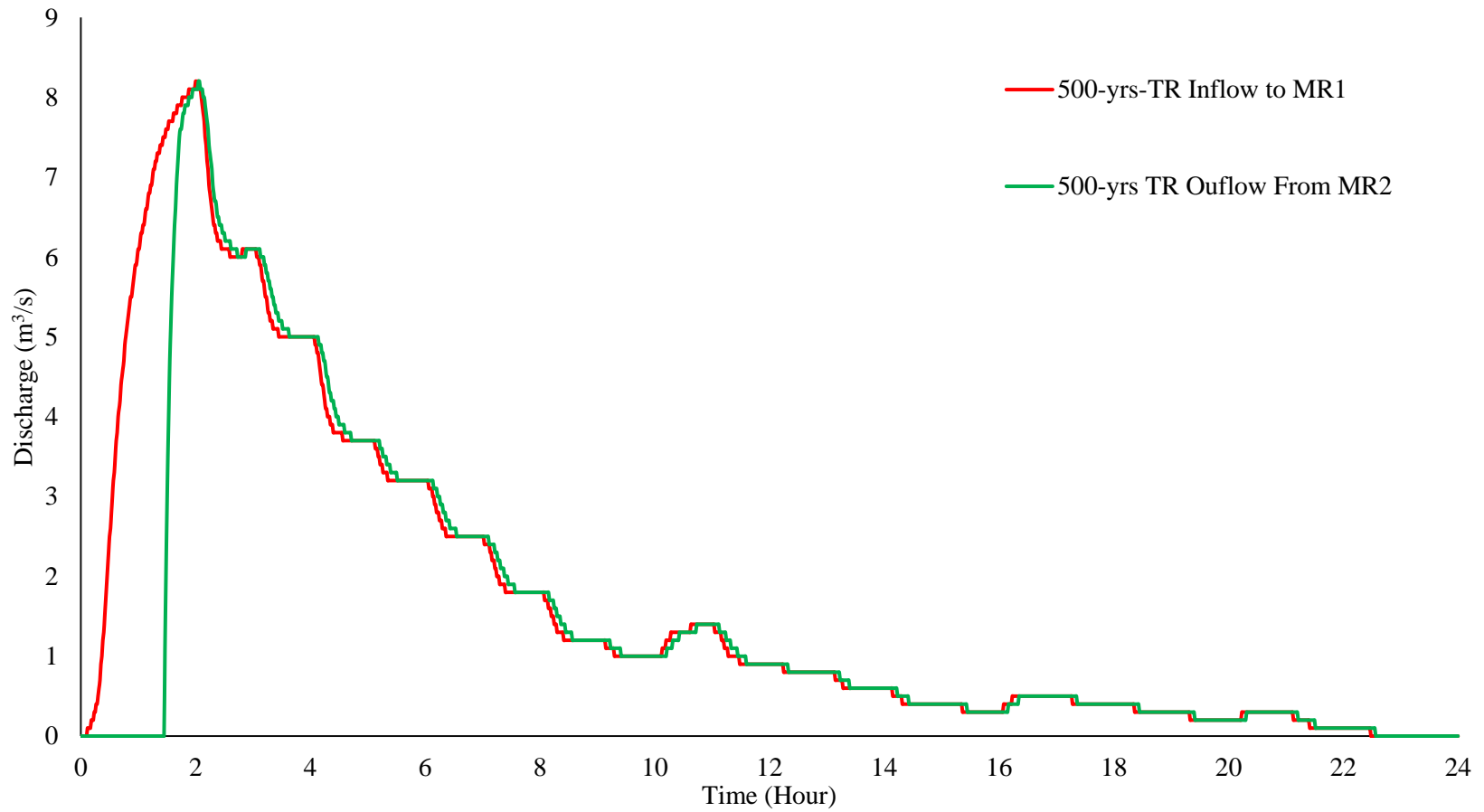


Figure 7.24 Effect of Reservoirs W/O Bottom Outlets on 500-year Flood Hydrograph of Mid Sub-basin

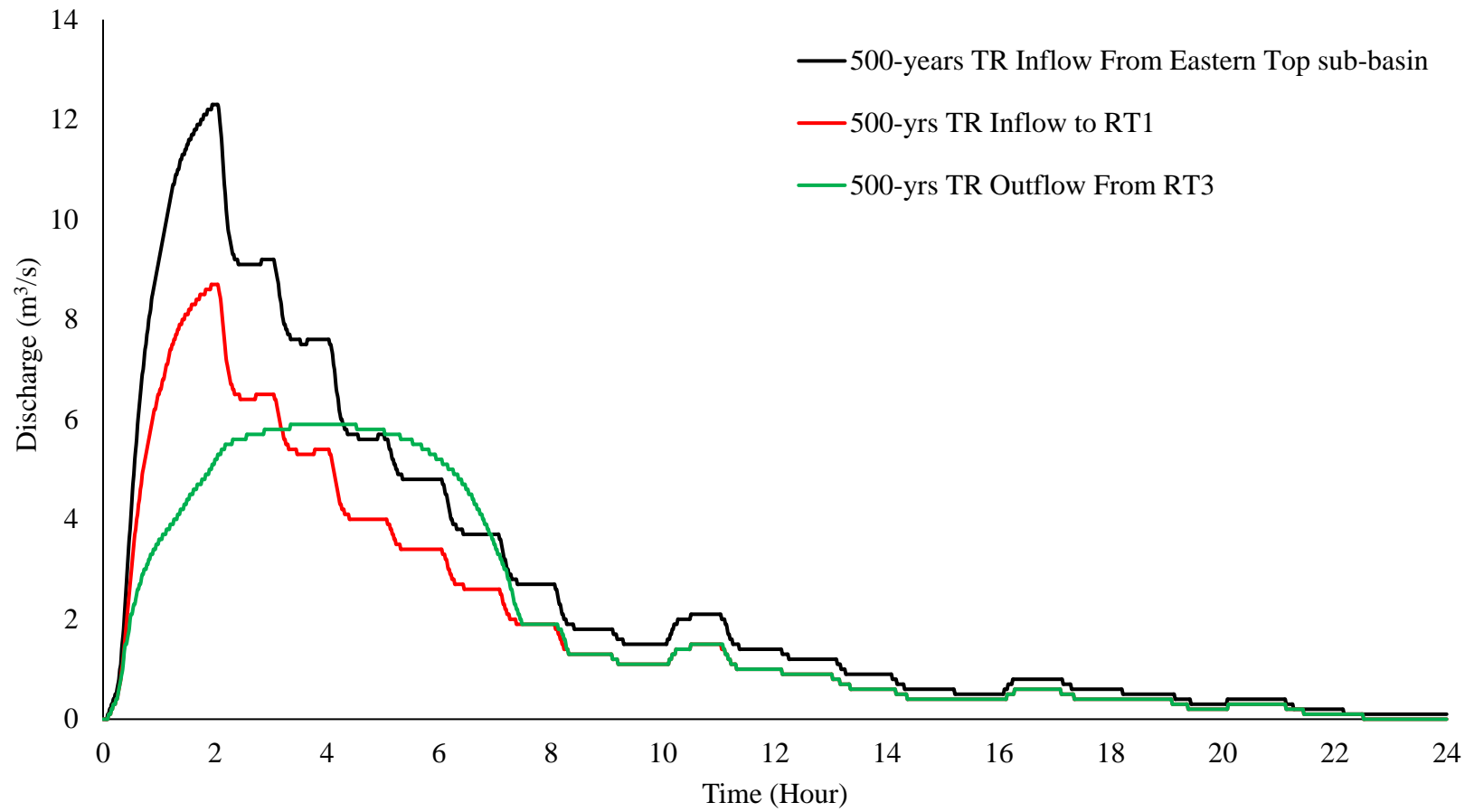


Figure 7.25 Reservoir with 1.0 m Bottom Outlet effects on 500-year Return Period Flood Hydrographs of Top Sub-basin.

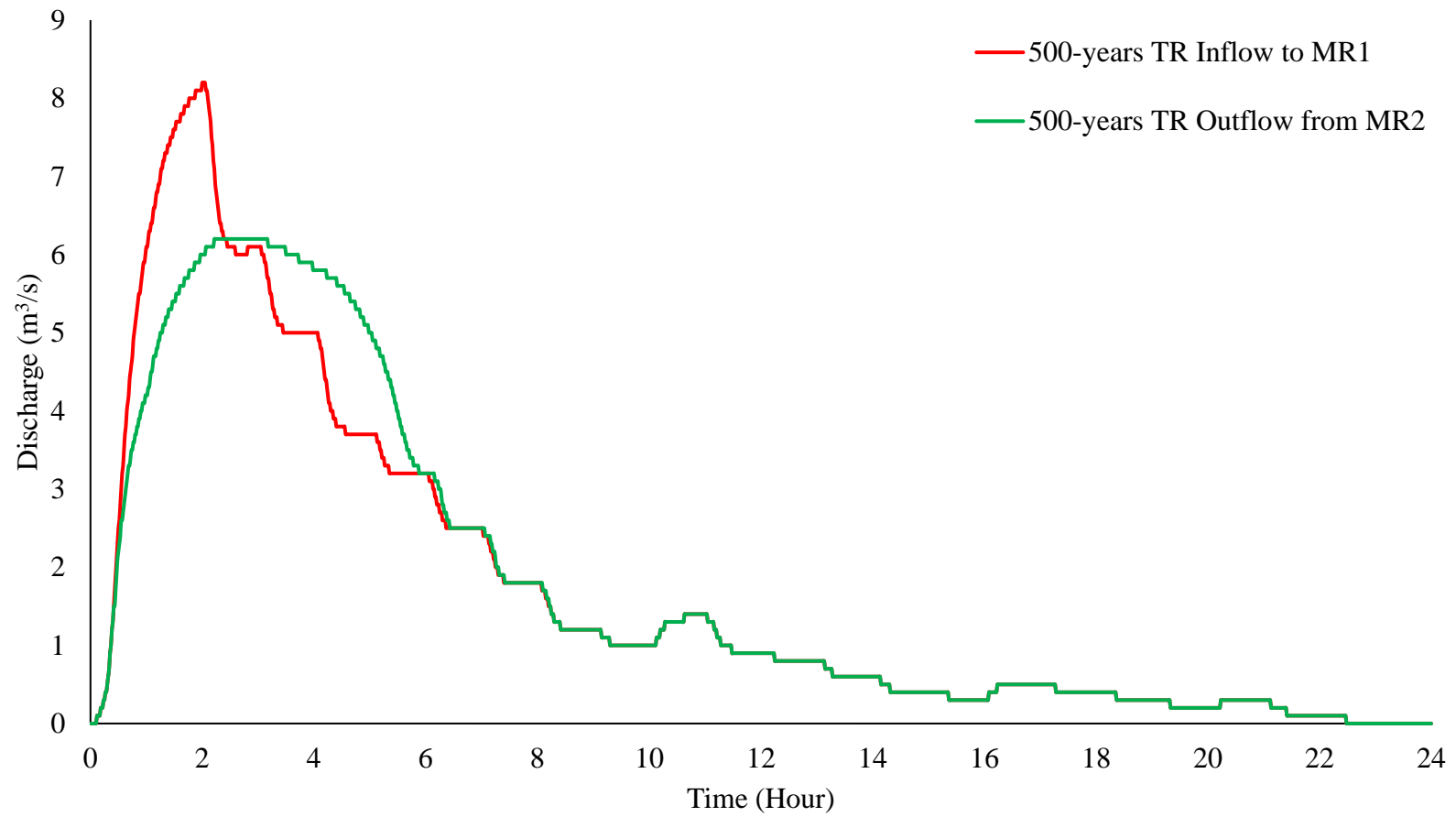


Figure 7.26 Effect of Reservoirs with 1.0 Diameter Bottom Outlets on 500-year Flood Hydrograph of Mid Sub-basin

Table 7.10 Summary of the Flood Routing Analysis of Reservoirs Without Bottom Outlets

Flood Event	Sub-basins	Type	Name	Inflow		After Routing		ETS-B Inflow (m ³ /s)	W/O/R (m ³ /s)	W/R (m ³ /s)
				Peak Time (H:m)	Peak value (m ³ /s)	Peak Time (H:m)	Peak value (m ³ /s)			
2018 - Event	Top sub-basin	Without Bottom Outlet	RT1	12:00	13.6	12:00	13.6	19.2	45.0	45.0
			RT3	12:00	13.6	12:01	13.5			
	Mid Sub-basin		MR1	12:00	12.6	12:00	12.6	-		
			MR2	12:00	12.6	12:00	12.6	-		
500-yr TR	Top sub-basin		RT1	2:00	8.7	2:00	8.7	12.3	29.2	28.1
			RT3	2:00	8.7	2:10	7.6			
	Mid Sub-basin		MR1	2:00	8.2	2:00	8.2	-		
			MR2	2:00	8.2	2:03	8.2	-		
100-yr TR	Top sub-basin	RT1	2:00	6.6	2:00	6.6	9.4	22.2	20.4	
		RT3	2:00	6.6	3:01	5.0				
	Mid Sub-basin	MR1	2:00	6.2	2:00	6.2	-			
		MR2	2:00	6.2	2:10	6.0	-			
50-yr TR	Top sub-basin	RT1	2:00	5.7	2:00	5.7	8.1	19.1	17.2	
		RT3	2:00	5.7	3:07	4.3				
	Mid Sub-basin	MR1	2:00	5.4	2:00	5.4	-			
		MR2	2:00	5.4	2:10	4.8	-			

Table 7.11 Summary of the Flood Routing Analysis of Reservoirs With 1.0 m Diameter Bottom Outlets

Flood Event	Sub-basins	Type	Name	Inflow		After Flood Routing		ETS-B Inflow (m ³ /s)	W/O/R (m ³ /s)	W/R (m ³ /s)
				Peak Time (H:m)	Peak value (m ³ /s)	Peak Time (H:m)	Peak value (m ³ /s)			
2018 - Event	Top sub-basin	With 1.0 m Pipe Bottom Outlet	RT1	12:00	13.6	12:00	13.6	19.2	45.0	32.0
			RT3	12:00	13.6	12:25	6.3			
	Mid Sub-basin		MR1	12:00	12.6	12:00	12.6	-		
			MR2	12:00	12.6	12:00	7.8			
500-yrs TR	Top sub-basin		RT1	2:00	8.7	2:00	8.7	12.3	29.2	23.6
			RT3	2:00	8.7	4:00	5.9			
	Mid Sub-basin		MR1	2:00	8.2	2:00	8.2	-		
			MR2	2:00	8.2	3:00	6.2			
100-yrs TR	Top sub-basin	RT1	2:00	6.6	2:00	6.6	9.4	22.2	19.0	
		RT3	2:00	6.6	3:25	5				
	Mid Sub-basin	MR1	2:00	6.2	2:00	6.2	-			
		MR2	2:00	6.2	2:15	5.3				
50-yrs TR	Top sub-basin	RT1	2:00	5.7	2:00	5.7	8.1	19.1	16.8	
		RT3	2:00	5.7	3:40	4.6				
	Mid Sub-basin	MR1	2:00	5.4	2:00	5.4	-			
		MR2	2:00	5.4	2:10	4.8				

7.1.4.3 Cost Analysis of the Proposed Reservoirs

In this section, the cost analysis of the proposed reservoirs is presented to give an idea about the project's potential cost. To determine the geometric characteristic of each reservoir, a detailed analysis of the forces acting on the reservoir's structures is required. However, in this thesis, the recommended geometry is accepted to estimate the geometry of a reinforced concrete (RC) retaining wall shown in Figure 7.27 (Geotech 2022).

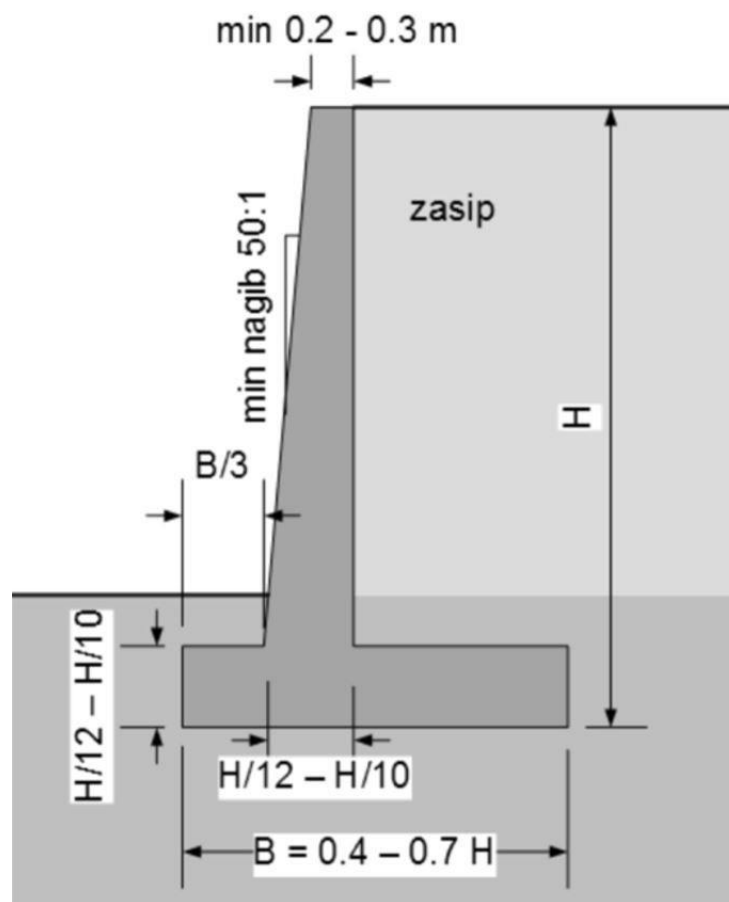


Figure 7.27 RC Retaining Wall Recommended Geometry

In order to calculate the volume of the concrete required for each reservoir, each structure is divided into several blocks of smaller sizes, as shown in Figures 7.28, and 7.29. In the design specifications, the inner side of the retaining wall is flat, whereas the outer side has a mild slope of 50:1 according to the recommended geometry shape. Following a similar approach, concrete volume calculations are carried out for all the reservoirs. The description of the reservoirs and relative workloads are presented in Table 7.12. Meanwhile, the considered unit cost of the analysis is given in Table 7.13, and the total reservoir cost, including 20% undefined cost in reservoirs (Çam 2012), is calculated in Table 7.14.

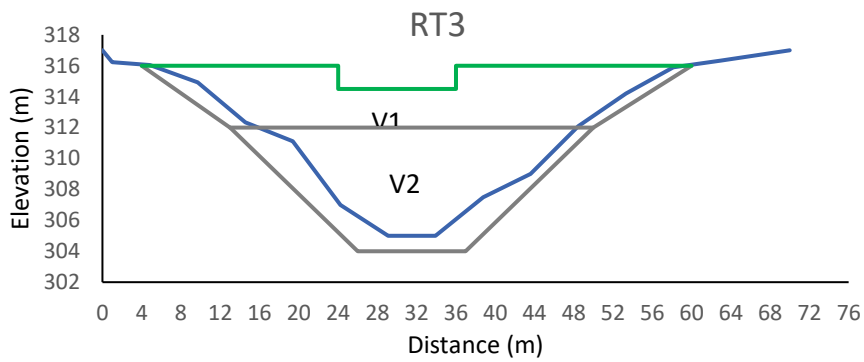


Figure 7.28 RT3 Reservoir Front View

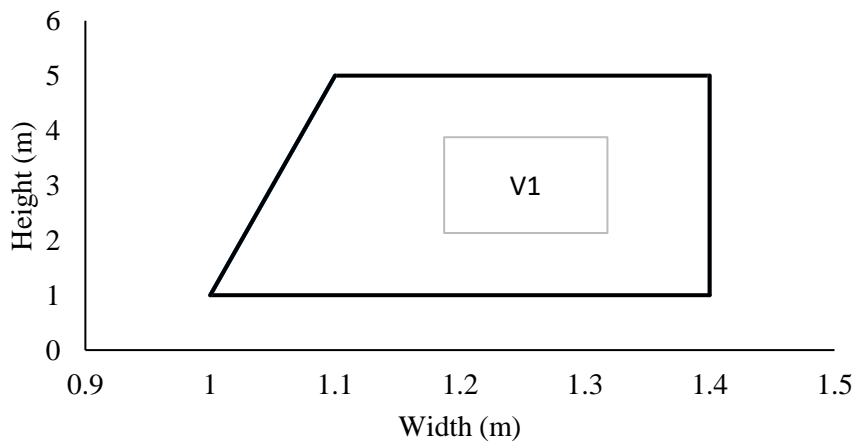


Figure 7.29 RT3 Side View of the Reservoir Structure

Table 7.12 Reservoirs Description and Work Loads

Description	RT 1	RT2	RT3	MR1	MR2
H _{net} (m)	7.0	12.0	12.0	7.0	13.0
L (m)	46.0	43.0	54.0	45.0	74.0
H (m)	9.0	15.0	15.0	9.0	16.2
B (m)	6.3	10.5	10.5	6.3	11.3
Tf (m)	0.7	1.2	1.2	0.7	1.3
Df (m)	1.3	1.8	1.8	1.3	1.9
Excavation	90.1	283.5	207.9	98.3	430.9
Volume (m ³)					
Concrete	140.3	387.3	402.0	149.7	627.4
Volume (m ³)					
Steel Volume	21.0	58.1	60.3	22.5	94.1
(Ton)					
Formworks	435.0	780.0	804.0	528.0	1287.0
(m ²)					

Table 7.13 Reservoir Unit Cost

Excavation					
Unit Cost	3.3	3.3	3.3	3.3	3.3
(\$/m ³)					
Concrete Unit					
Cost (\$/m ³)	75.0	75.0	75.0	75.0	75.0
Formworks					
(\$/m ²)	8.3	8.3	8.3	8.3	8.3
Steel Unit					
Cost (\$/ton)	1333.3	1333.3	1333.3	1333.3	1333.3

Table 7.14 Reservoir Cost Analysis

Excavation Cost (\$)	295.3	929.3	681.5	322.1	1412.5
Concrete Cost (\$)	10522.5	29043.8	30152.3	11227.5	47055.0
Formworks Cost (\$)	3625.0	6500.0	6700.0	4400.0	10725.0
Steel Cost (\$)	28060.0	77450.0	80406.0	29940.0	125480.0
Total Cost (\$)	42,502.8	113,923.0	117,939.7	45,889.6	184,672.5
Total Cost (\$)					504,927.6
Grand Total (\$) = Total Cost (\$) + 20% undefined Cost					605,913.1

In Table 7.12, H describes the height from the bottom of the foundation to the top, H_{net} represents the height from the ground surface to the top, B is the width of the foundation, L is the length of the reservoir, T_f is the thickness of the foundation, and D_f is the foundation depth. The unit costs in Table 7.13 are used in the calculation, which is adapted from the document provided by local authorities (Tok. 2022). The cost analysis results in Table 7.14 of reservoirs indicate that the construction of the reservoirs would cost around \$605,913, almost twice the required cost for channel construction. On the other hand, the effect of the reservoirs on reducing the peak discharge and arrival time during the flood is very insignificant, especially during extreme events. However, reservoirs are great tools for storing rainwater for groundwater recharge and preventing the sediments and pollutants from getting carried into the urban area and contaminating the water resources.

7.1.5 Mitigation Measure - M3: Concrete Channel and Reservoirs

In this section, the effects of the concrete channel along with the construction of reservoirs to mitigate the impacts of the flooding in Dikmen town are investigated.

7.1.5.1 Concrete Channel and Reservoirs Impact Against 2018 - Flood Event

In the first scenario, the combined effects of the concrete channel and reservoirs without a bottom outlet are assessed to reduce the potential damages imposed by the 2018 Flood event. The individual assessment and impact analysis of the concrete channel on the flood hazard reduction are examined (see Figure 7.9). The result indicated that a significant part of the flood could be carried out with the help of the channel. However, some parts of the Dikmen, especially the downstream side, were still vulnerable to flooding and damage.

The flood routing assessment of the reservoirs without the bottom outlet and the resultant flow hydrographs are shown in Figures 7.15, and 7.16. The results suggested that the impacts of the reservoirs without bottom outlets on discharges from the Top sub-basin and Mid sub-basin are insignificant, especially during the arrival of the second peak values. Therefore, the reservoirs without a bottom outlet along with the concrete channel would not decrease the potential hazard level to a safe level, and a small part of Dikmen town would still be at a high risk of flooding. However, the reservoirs with 1.0 m bottom outlets can decrease the total inflow rate from 45 m³/s to 32 m³/s, which is significant compared to the reservoirs without bottom outlets. Although the rate is still higher than the channel capacity, a significant part of the flood peak can be routed with the reservoirs, as shown in Figure 7.30.

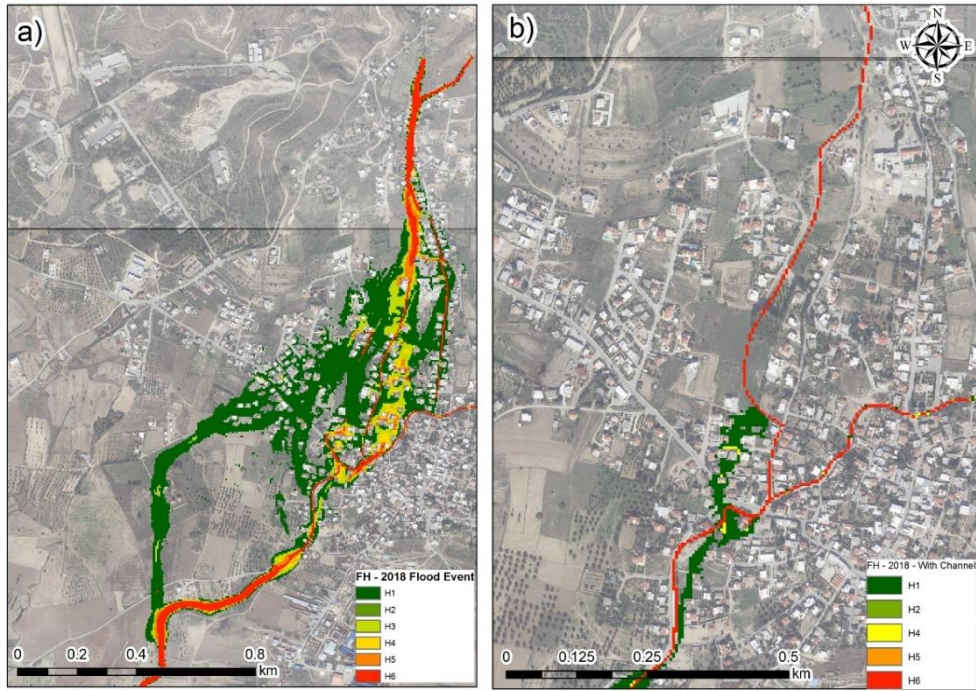


Figure 7.30 2018 - Flood Hazard Map After Channel and Reservoirs with 1.0 m Bottom Outlets

7.1.5.2 Concrete Channel and Reservoirs Impacts Against 50-, 100-, and 500-year Flood Events

The integration of the concrete channel with the reservoir without the bottom outlet showed that the discharge rate as a result of the 50- and 100-year return period are under the channel capacity. On the other hand, for the events with the 500-year return period, the flood routing analysis considering the reservoirs without bottom outlets indicates a flow with a magnitude of $28.1 \text{ m}^3/\text{s}$ contributed from the Top sub-basin and Mid sub-basin at the same time. Figure 7.31 shows the flood inundation map of the Dikmen town after integrating both reservoirs without bottom outlets and concrete channel.

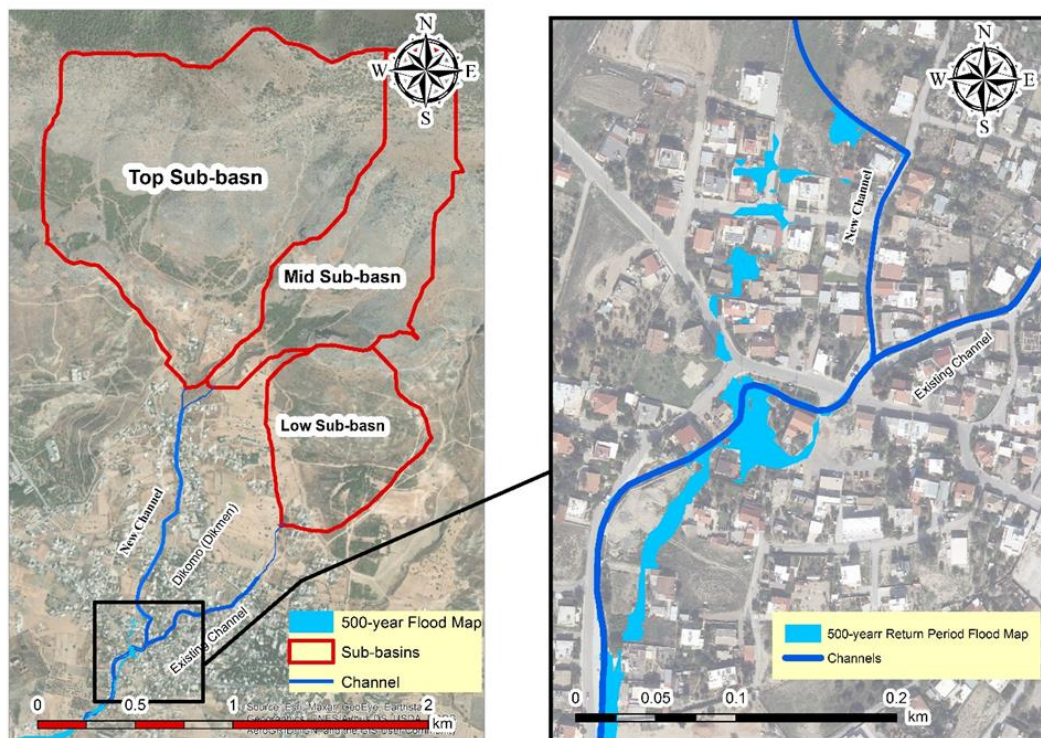


Figure 7.31 500-year Return Period Flood Map After Reservoirs and Channel Implications

On the other hand, the summary of the routing analysis shown in Table 7.11 indicates that if reservoirs are built with 1.0 diameter bottom outlets, the peak discharge of a 500-year return period would drop from 29.2 m³/s to 23.6 m³/s, which is below the channel capacity of 26 m³/s.

7.1.5.3 Cost Analysis of the Combined Mitigation Measures

This section considers the combined cost analysis of both mitigation measures, concrete channel, and reservoirs. The combined cost results of these two systems are listed in Table 7.15.

Table 7.15 Total cost of the Combined Mitigation Measures

Measure	Cost (\$)
Mitigation Measure – 1 Concrete Channel	320,853.5
Mitigation Measure – 2 Reservoirs	605,913.1
Total Cost	926,766.6

The cost comparison between all three mitigation measures indicates that the construction cost of the connecting concrete channel M1 is around \$ 320,853, which is the least among the other mitigation measures. Meanwhile, for the construction of the reservoirs M2, more than half a million dollars is required. Besides, the combination of both measures, especially M3, in the case of reservoirs with a 1.0 bottom outlet, can decrease the risk of flooding in a 500-year flood to a minimum. However, the cost of implementing the M3 can reach up to 1 million dollars.

Furthermore, the combination of two mitigation measures showed that the reservoirs would not have completely reduced the risk of flooding in a flood event with similar characteristics to the 2018 Flood event. Thus, considering the economic aspect and the feasibility of implementing mitigation measures, the best option is to consider the M1 concrete channel. However, the areas still at risk of flooding even after the

channel (see Figures 7.9, and 7.11), need to be aware of the possible risks of extreme floods that may exceed the channel capacity and start flooding the houses and roads.

7.1.6 The Effects of the Channel on the Discharge Hydrographs

The hydraulic analysis of the three mitigation measures showed that a connecting rectangular concrete channel with a minimum depth of 1.8 m and width of 4.0 m can decrease the risk associated with different flooding scenarios. Meanwhile, the economic assessment of the channel showed that it would cost the least among the other two mitigation measures. Therefore, the channel is considered the best solution for the flood mitigation efforts in Dikmen town in Northern Cyprus.

However, the design of several existing hydraulic structures, such as the Gönyeli Reservoir and the culvert that crosses the Nicosia-Kyrenia highway, are based on the current conditions of the basin. Thus, in this section, the changes in the flow hydrographs are presented considering an event with a magnitude of 2018 Flood event and a flood with a 500-year return period. The results indicate no significant changes in the peak discharges from downstream of the town for both the 2018 Flood and the flood with a 500-year return period, as shown in Figures 7.32, and 7.33, respectively.

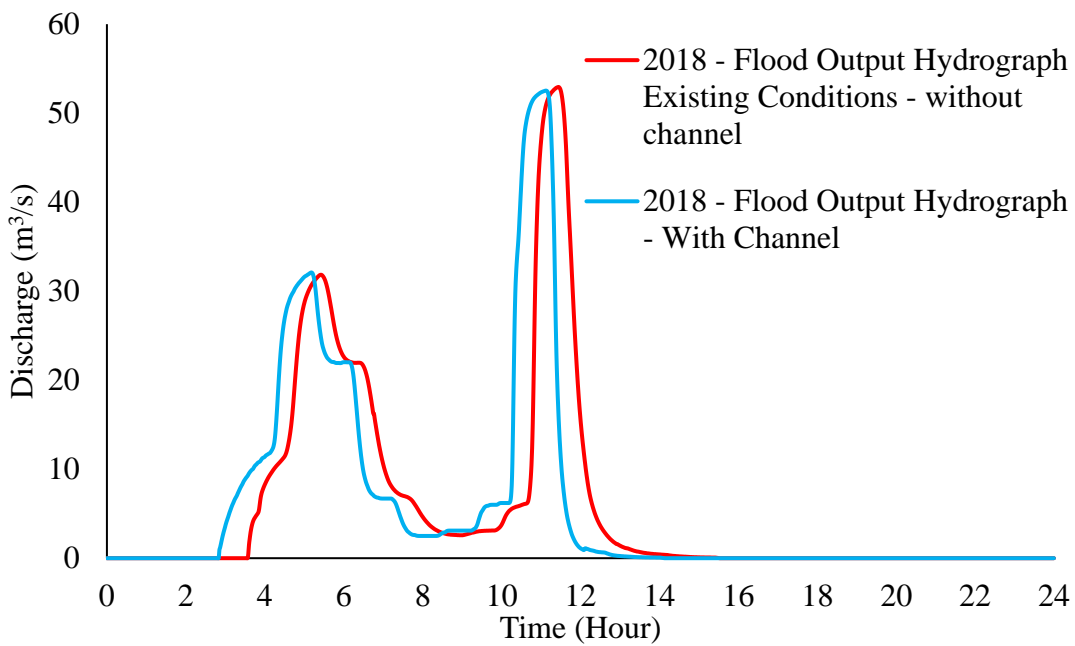


Figure 7.32 Comparison of Outputs Hydrographs Without and With channel - 2018 Flood Event

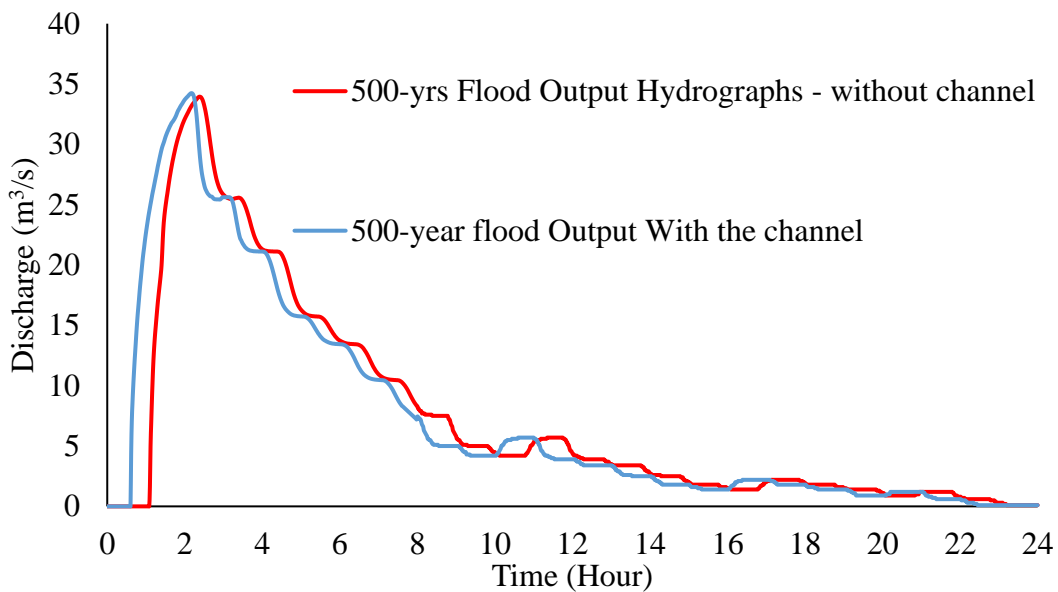


Figure 7.33 Comparison of Outputs Hydrographs Without and With channel - 500-year Flood event

7.1.7 The Sensitivity Analysis of The Channel

The implementation of the rectangular concrete channel inside the 2D hydraulic model indicated that a large amount of the inflow from the ungauged catchments could be carried downstream. In the assessment, the average daily distribution of the rainfall (see Figure 3.1) is considered to generate the outflow hydrograph. According to the average daily distribution curve, most rainfall depth occurs at the start of the rainfall events in Boğaz Station. However, in this section, peak rainfall blocks in the distribution curve are shifted toward the center to obtain a rainfall distribution pattern with the highest possible discharge from the 500-year return period event and investigate the overall impact on the concrete channel.

Figure 7.34 and Figure 7.35 indicate the average daily distribution curves of the rainfall hyetograph and the resultant discharge hydrograph from the top catchments into Dikmen town, respectively. The results show the peak discharge occurs after the 2nd hour of the rainfall and have a peak discharge value of 29 m³/s. On the other hand, in Attempt-1, the peak rainfall occurs between 4-5 hours after the rainfall starts, as shown in Figure 7.36. This would increase the peak discharge rate to 30.2 m³/s, which occurs 5 hours after the beginning of the rainfall (Figure 7.37). Similarly, Attempt-2, shown in Figure 7.38, indicates a condition in which peak rainfall happens between 8-9 hours after the event's start. The result also suggests that the peak discharge would increase further to 31.4 m³/s and occur 9 hours after rainfall, as seen in Figure 7.39.

Furthermore, Figure 7.40 shows the results of Attempt-3, in which the peak rainfall occurs with a further delay of 11-12 hours after the start of the rainfall. The obtained discharge hydrograph shown in Figure 7.41 indicates the peak discharge to be around 31.6 m³/s, which occurs 12 hours after the rainfall. Finally, in Attempt-4, the rainfall distribution is obtained with a 13-14 hours delay in the peak rainfall, as shown in Figure 7.43. According to the hydrological assessment shown in Figure 7.42, the

peak would remain at 31.6 m³/s, similar to Attempt 3. However, the peak discharge would occur 13 hours after the start of the rainfall. The summary of the peak discharge values and the delay time in the occurrence of the peak discharges are listed in Table 7.16. The result indicates that if the peak rainfall occurs between 11-14 hours after the rainfall, the study area with an amount of 31.6 m³/s experiences the highest peak discharge into the channel.

The generated hydrograph in Figure 7.42 is then entered as upstream boundary conditions to create the flood model and test the efficiency of the concrete channel against the most extreme rainfall case. The obtained results illustrate that there is a slight increase in the flood extend map of the 500-year event with Attempt-4. In general, the channel is effective enough against the increase and the changes in rainfall regime. The flood inundation and hazard maps will experience minor increases as shown in Figures 7.44 and 7.45.

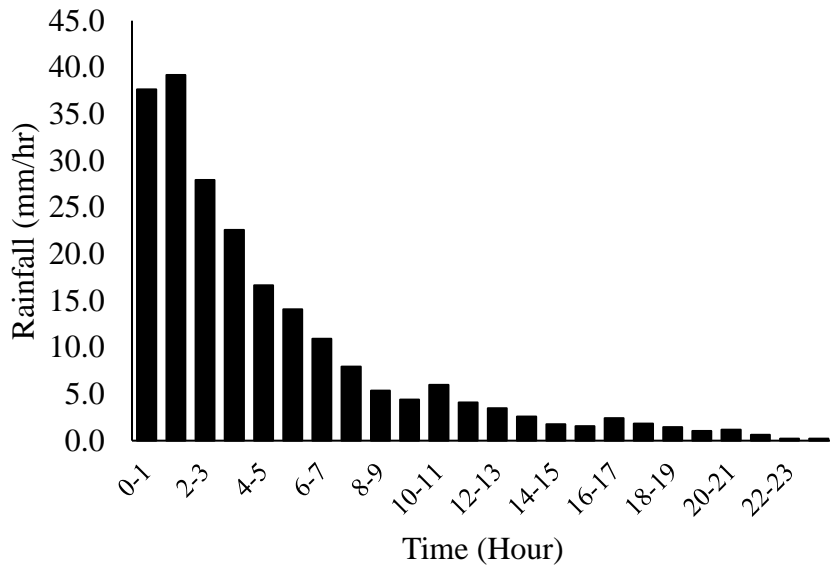


Figure 7.34 500-year Average Distribution Hyetograph

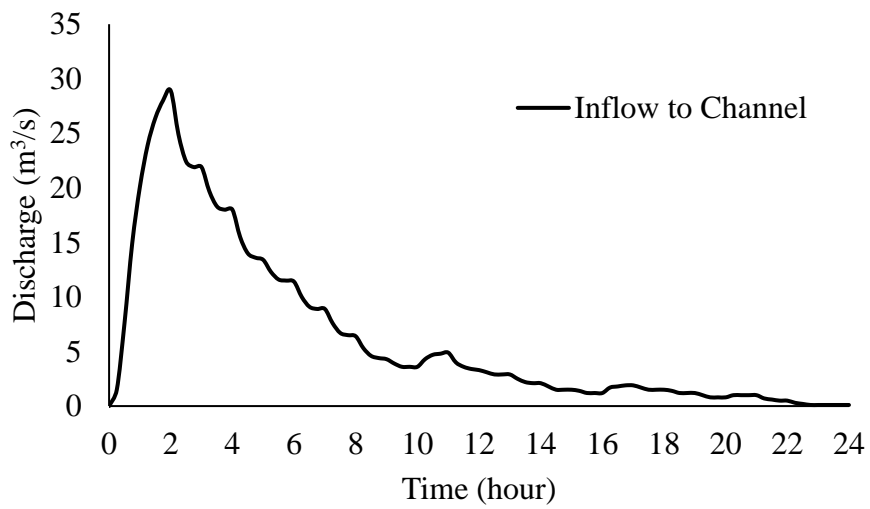


Figure 7.35 500-year Average Distribution Hydrograph

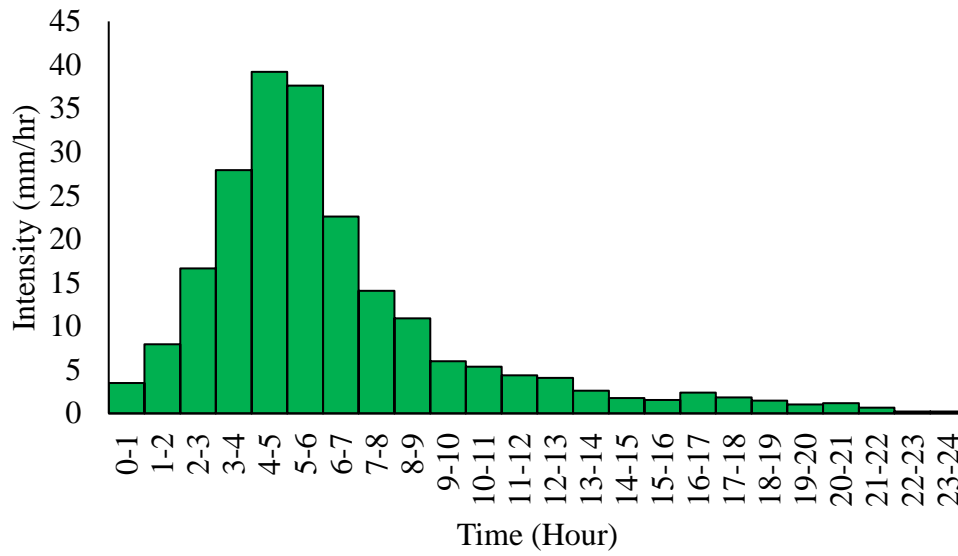


Figure 7.36 500-year Attempt-1 Distribution Hyetograph

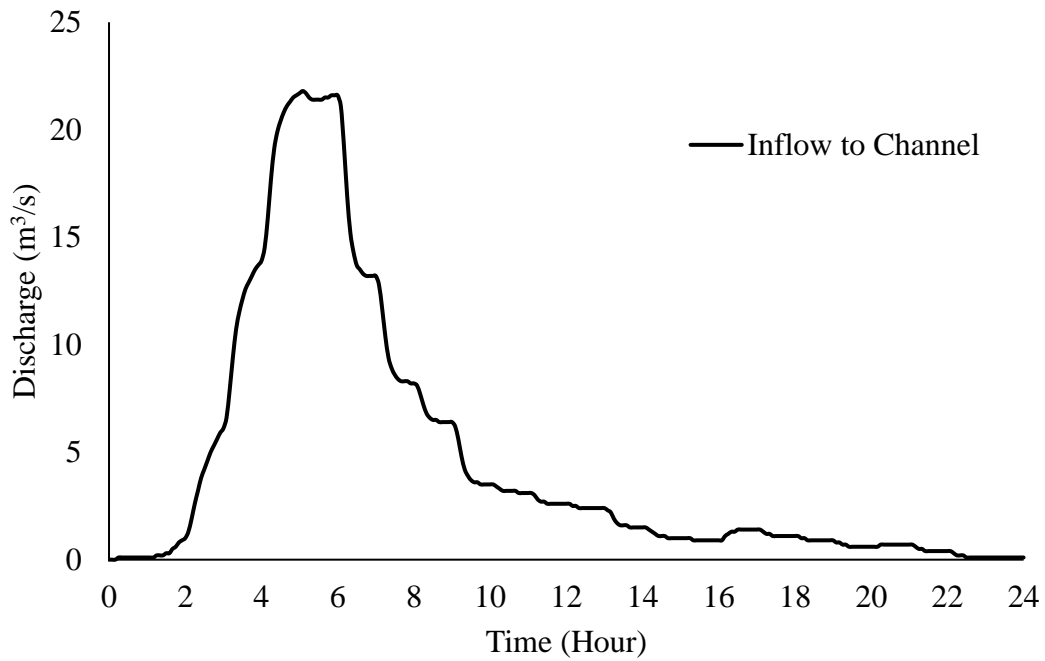


Figure 7.37 500-year Attempt-1 Distribution Hydrograph

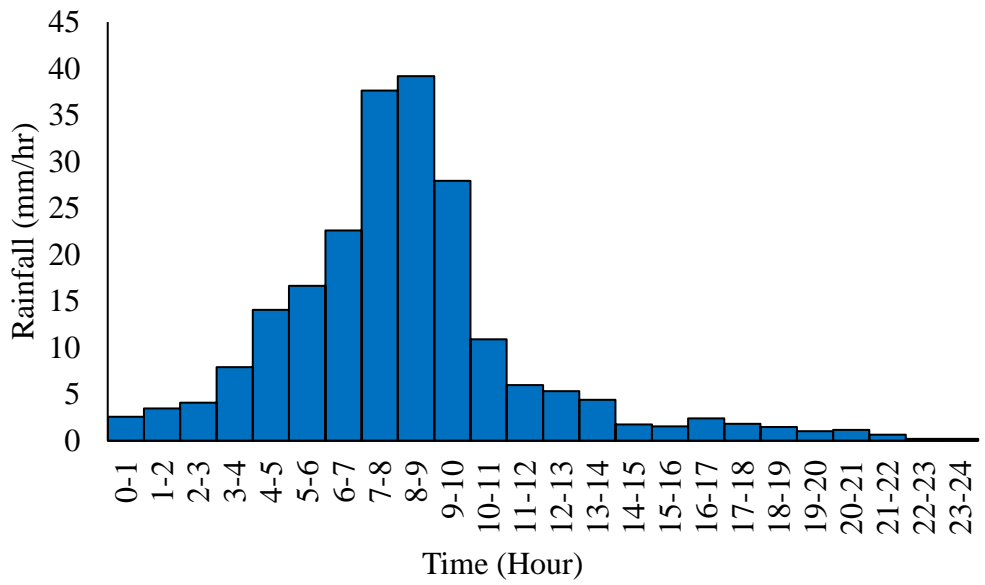


Figure 7.38 500-year Attempt-2 Distribution Hyetograph

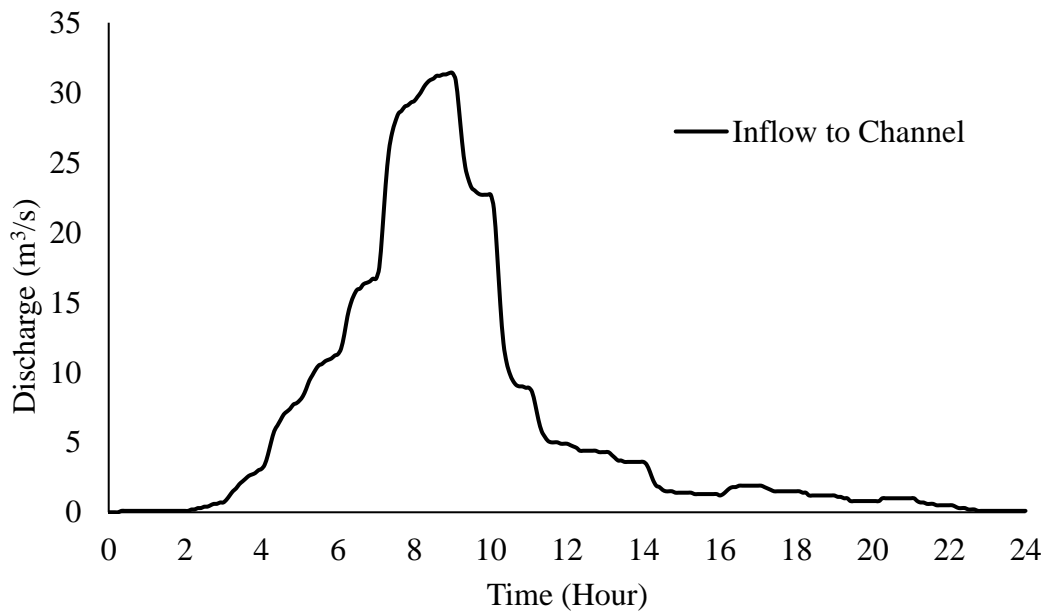


Figure 7.39 500-year Attempt-2 Distribution Hydrograph

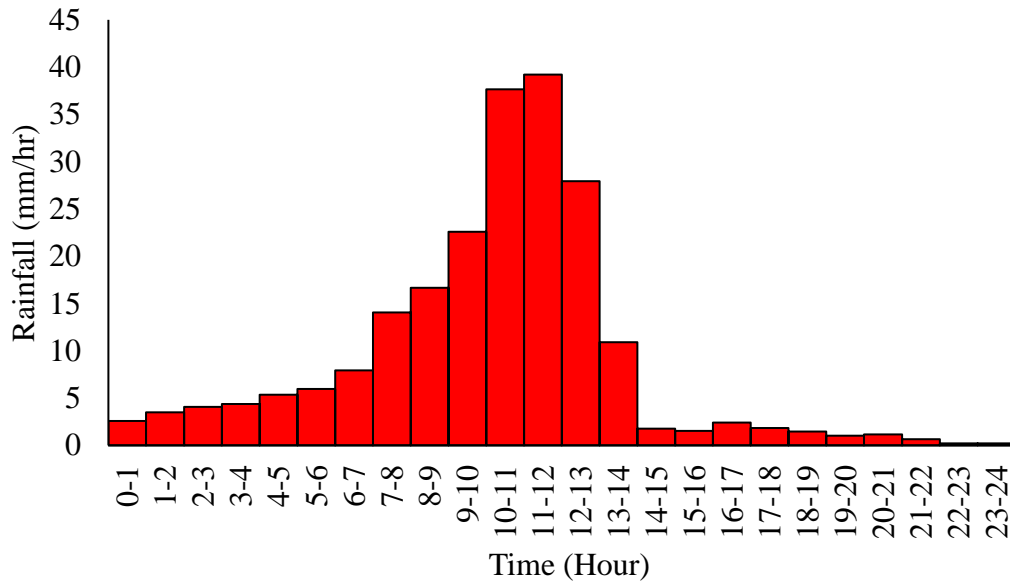


Figure 7.40 500-year Attempt-3 Distribution Hyetograph

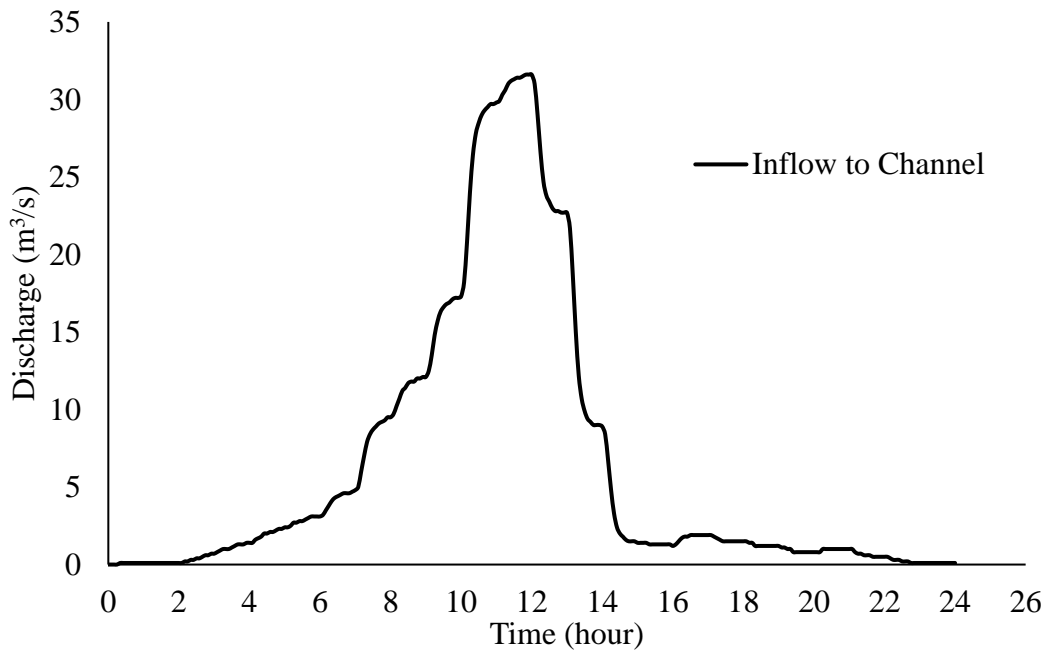


Figure 7.41 500-year Attempt-3 Distribution Hydrograph

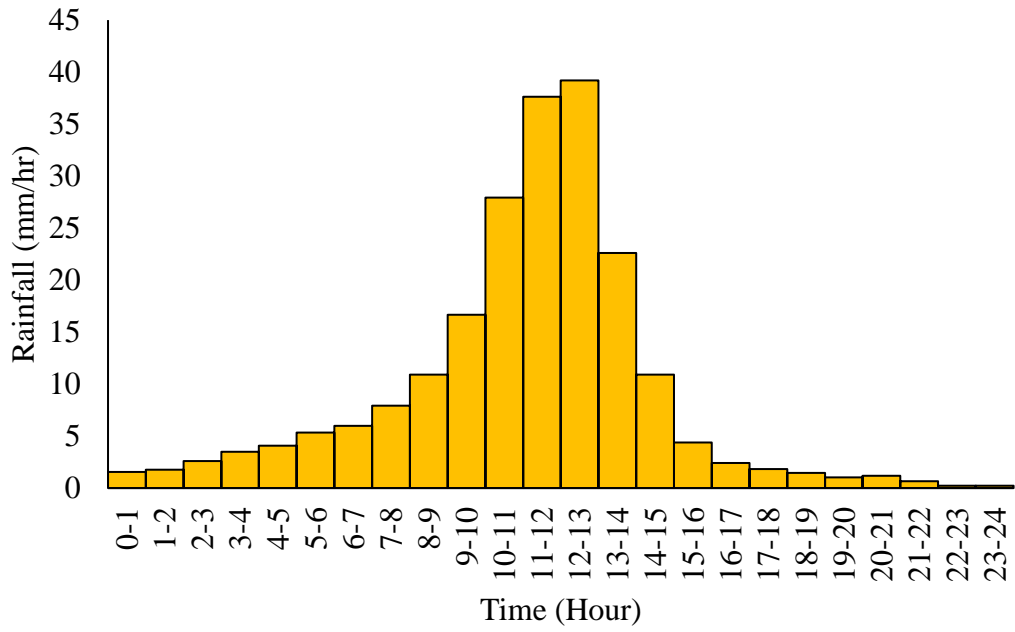


Figure 7.43 500-year Attempt-4 Distribution Hyetograph

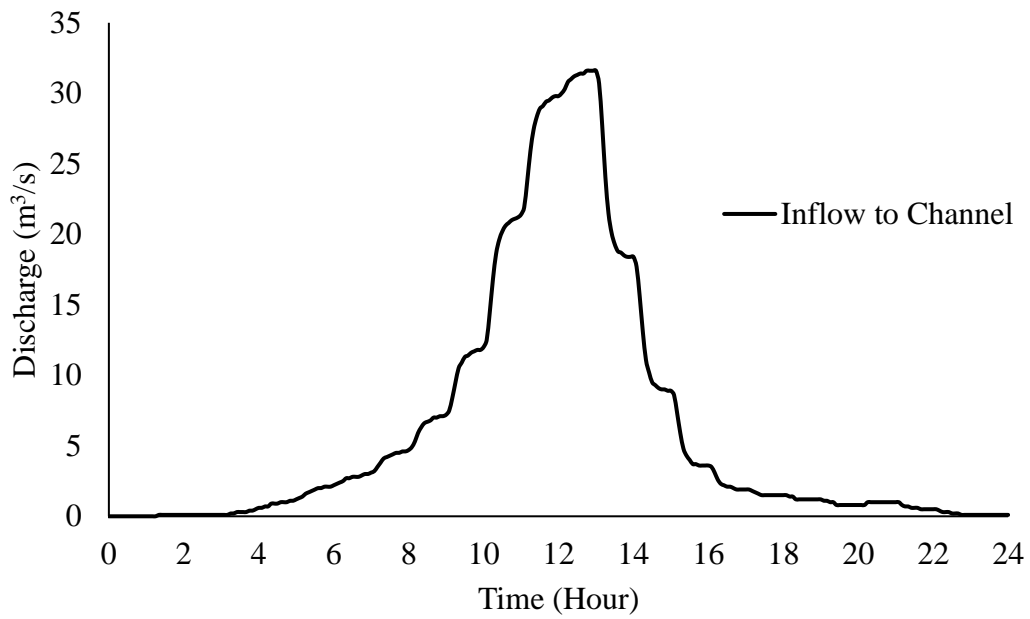







Figure 7.42 500-year Attempt-4 Distribution Hydrograph

Table 7.16 Changes in Peak Discharge

Attempts	Peak Time Occurrence (Hours From Start)	Peak Discharge (m ³ /s)	
Daily Average Distribution	1 – 2	29.0	
Attempt-1	4 – 5	30.2	
Attempt-2	8 – 9	31.4	
Attempt-3	11 – 12	31.6	
Attempt-4	13 – 14	31.6	

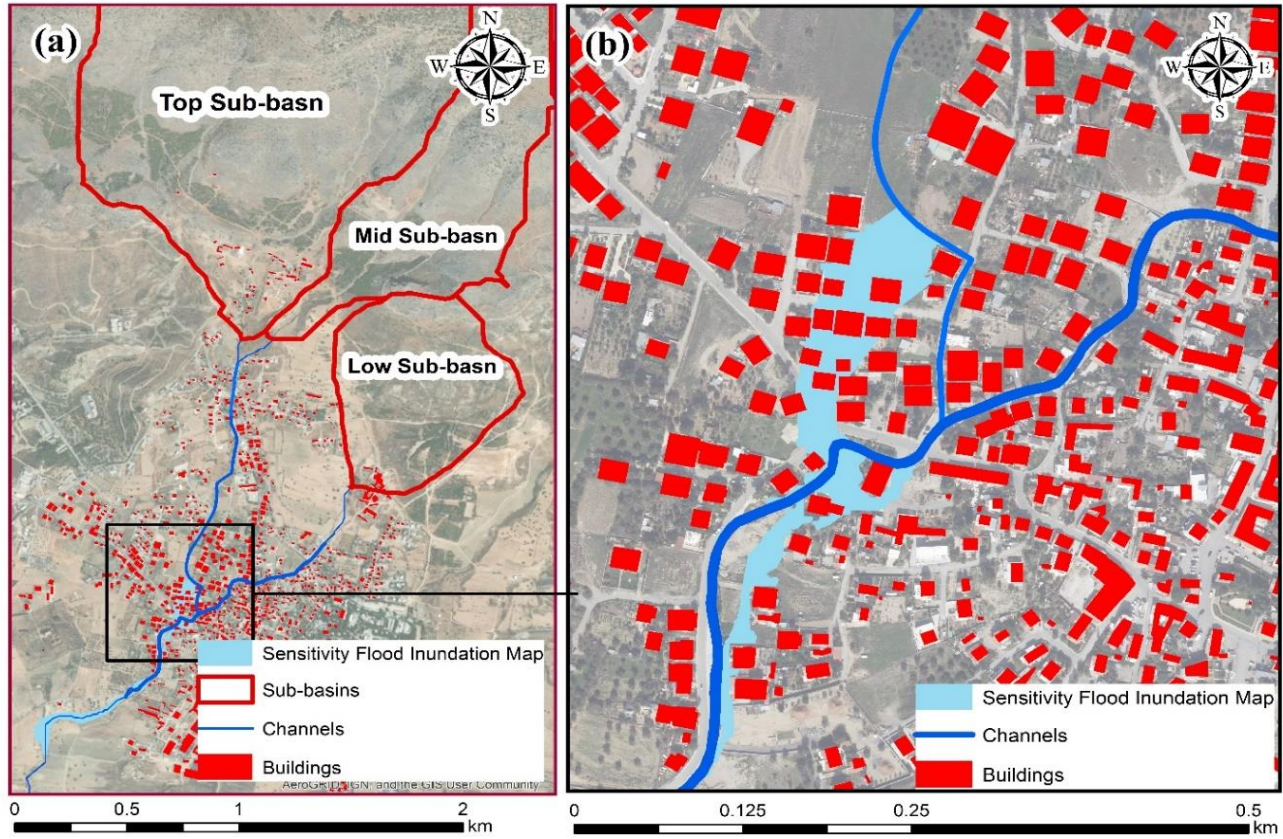


Figure 7.44 Flood Inundation Map of 500-year Attempt-4

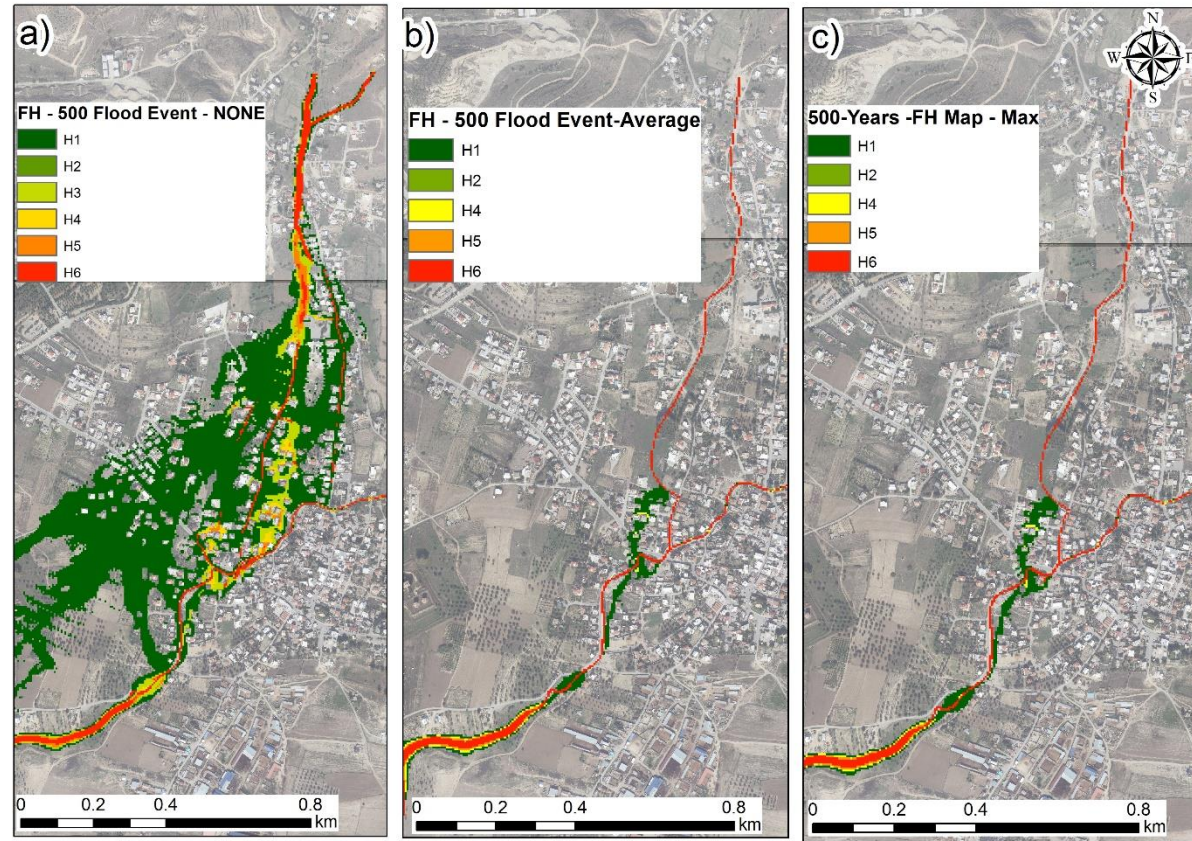


Figure 7.45 500-year Flood Event. a) Before Channel, b) After Channel – Ave, c) After Channel - Attempt-4

CHAPTER 8

SUMMARY AND CONCLUSION

8.1 Summary and Conclusion

In this project's scope, a flood management study is performed to identify the appropriate structural means of protecting Dikmen town against severe cases of flooding events. To achieve this goal, a hydrological model of the area is developed to analyze the runoff rates as a result of the rainfalls in the catchments. Furthermore, a calibrated hydraulic model is developed to determine the vulnerable areas in the study area. Additionally, appropriate structural measures are considered to check against historical events and for the events with different return periods as future scenarios.

The first part of the study involves the development of hydrological models of the three main ungauged sub-basins: Top sub-basin, Mid sub-basin, and Low sub-basin. The sub-basins are located on the hillside of the Kyrenia mountains with a high surface slope at the upstream side of the urbanized part of Dikmen town. The HEC-HMS hydrological model is developed to understand and simulate the rainfall-runoff processes for each sub-basin. The SCS unit hydrograph method generates the flow hydrographs for each sub-basin. Then, these hydrographs are used as the main inflow boundary condition in the hydraulic model.

Accurate topographic data sets are needed to represent the ground conditions such that the results of the flooding modeling project the realistic condition of the study area. The required topographic data sets of the study area were obtained in the paper-based format from the Northern Cyprus Mapping Office. Therefore, the Geographic Information System (GIS) processing tools are used for digitizing the conventional survey map into Digital Elevation Model (DEM).

Following the completion of the hydrological analysis and the pre-processing of the topographic map, the discharge hydrographs of the rainfall records are created. Initially, the 2018 Flood event flood model is developed in 2D HEC-RAS. The results of the initial flood model indicated a 78% match, with 0.042 relative error between the observed flood extend map and generated flood inundation map. However, the hydraulic model is calibrated by adjusting the local roughness coefficient's values to increase the match ratio further and decrease the relative error rate. Therefore, the goodness-of-fit ratio has risen to 84%, and the relative error (RE) between the maps has declined from 0.042 to 0.015. The results of the calibrated model illustrated that the model could simulate the 2018 Flood event with acceptable accuracy. Thus, based on the calibrated 2018 Flood event model, the flood maps of the high, medium, and low probability of occurrences are generated.

Furthermore, three mitigation measures were assessed, and their cost analyses were performed to identify the optimal solution for safely reducing the risk of future flooding in Dikmen town. The first mitigation measure, M1, included the construction of a channel that will safely convey flood water from the top sub-basins to the downstream. The second mitigation measure M2 is the construction of five detention reservoirs to act as water storage during the floods, providing water for irrigation and recharging the groundwater resources. The last flood mitigating measure M3 involved the integration of the concrete channel and detention reservoirs to decrease the flood impacts in Dikmen town.

The results indicated that the concrete channel could provide protection against 50- and 100-years return period flood events. Moreover, the cost analysis result showed that channel construction is the most economical solution that offers sufficient protection. Considering the channel's performance in reducing the flood risks associated with events with 100-year or lower return periods and lower economic costs, M1 is selected as the best solution. However, in cases of 500-year or higher return periods, the channel capacity is insufficient to reduce the risk of flooding completely. Therefore, some non-structural measures, such as flash flood awareness

programs for all the residents in the risk zones, need to be organized. Furthermore, early flood warning systems can be developed to decrease the flood risk in vulnerable areas and give adequate time for the safe evacuation of the residents.

The analysis showed promising outcomes that implementing the channel can decrease the associated risk of flooding in the Dikmen urban area. Therefore, some points need to be noted:

- The hydrological analysis of the sub-basins response to rainfall and generation of the resultant outflow hydrographs are based on the SCS UH method since stream gauge records are unavailable in the area to calibrate and validate the results.
- The obtained results are based on the topographic maps with a scale of (1:5000), with an elevation contour every 5 m height. In order to have a more accurate result, higher resolution topographic data sets are needed.
- The current model is calibrated based on the flood extend map of the 2018 Flood event, which was drawn after the event. A good correlation between the modeled and observed map is found. But, more data sets are required to validate the current model.
- Since the mean surface slope in the sub-basins and the urban area are relatively high, the arrival of the floods is expected to be rapid with high velocity. Therefore, extra reinforcement must be considered in the concrete channel construction, especially in junctions and bends.

8.2 Recommendation For Future Studies

- In the development of the current model, 2D HEC-RAS is used to identify the areas at risk and determine the risk level. However, TUFLOW, SOBEK, MIKE, and other modeling software can also be used to verify the model results.
- The development of conventional 2D and 3D flood models, even for a small area, is extremely time-consuming and expensive. For that, other efficient automatic flood prediction methods, such as machine learning methods, are encouraged.

REFERENCES

- Akan OA, Houghtalen RJ (2003) Urban hydrology, hydraulics, and stormwater quality : engineering applications and computer modeling. Hoboken, N.J. : J. Wiley & Sons
- Al-Ghobari H, Dewidar A, Alataway A (2020) Estimation of surface water runoff for a semi-arid area using RS and GIS-Based SCS-CN method. *Water (Switzerland)* 12:. <https://doi.org/10.3390/w12071924>
- Alzahrani A (2019) Application of Two-Dimensional Hydraulic Modeling in Riverine Systems Using HEC-RAS. University of Dayton
- Arrighi C, Campo L (2019) Effects of digital terrain model uncertainties on high-resolution urban flood damage assessment. *J Flood Risk Manag* 12:. <https://doi.org/10.1111/jfr3.12530>
- Atasoy A (2011) Population Geography of Turkish Republic of Northern Cyprus. *Mustafa Kamal Univ J Soc Sci Inst* 8:29–62
- Baltaci H (2017) Meteorological analysis of flash floods in Artvin (NE Turkey) on 24 August 2015. *Nat Hazards Earth Syst Sci* 17:1221–1230. <https://doi.org/10.5194/nhess-17-1221-2017>
- Banholzer S, Kossin J, Donner S (2014) The impact of climate change on natural disasters. In: *Reducing Disaster: Early Warning Systems for Climate Change*. Springer Netherlands, pp 21–49
- Benabdelouahab T, Gadouali F, Boudhar A, et al (2020) Analysis and trends of rainfall amounts and extreme events in the Western Mediterranean region. *Theor Appl Climatol* 141:309–320. <https://doi.org/10.1007/s00704-020-03205-4>
- Brunner GW (2016a) Benchmarking of the HEC-RAS two-dimensional hydraulic modeling capabilities. *US Army Corps Eng Eng Cent* 1–116

- Brunner GW (2016b) HEC-RAS River Analysis System Hydraulic Reference Manual
- Çam UE (2012) Scour Countermeasure Design For Sequential Viaducts on Ankara - Pozanti Highway. Metu
- Cea L, Costabile P (2022) Flood Risk in Urban Areas: Modelling, Management and Adaptation to Climate Change. A Review. *Hydrology* 9:50. <https://doi.org/10.3390/hydrology9030050>
- Chow V Te (1959) *Open Channel Hydraulics*. McGraw-Hill Book Co, New York
- Dutta D, Herath S, Musiaka K (2006) An application of a flood risk analysis system for impact analysis of a flood control plan in a river basin. *Hydrological Process* 20:1365–1384. <https://doi.org/10.1002/hyp.6092>
- E. LINDSEY (2020) Climate Change: Atmospheric Carbon Dioxide. In: NOAA Clim. <https://www.climate.gov/news-features/understanding-climate/climate-change-atmospheric-carbon-dioxide#:~:text=Increases in atmospheric carbon dioxide,in a can of soda>. Accessed 2 Jun 2022
- EEA, JRC (2011) Corine Land Cover. <https://land.copernicus.eu/pan-european/corine-land-cover>. Accessed 1 May 2022
- ESRI (2022) Slope function. https://pro.arcgis.com/en/pro-app/latest/help/analysis/raster-functions/slope-function.htm#ESRI_SECTION1_4246944619A4469FA79DFCCB368F5CDE. Accessed 29 Jun 2022
- European Parliament C of the EU (2007) Directive 2007/60/EC of The European Parliament and of The Council of 23 October 2007 on the assessment and management of flood risks (Text with EEA relevance)
- FDOT DS (2013) Standard Precast Concrete Box Culverts. <https://www.fdot.gov/docs/default-source/roadway/ds/12/idx/00292.pdf>.

Accessed 24 Jul 2022

- Fedorov M, Badenko V, Maslikov V, Chusov A (2016) Site Selection for Flood Detention Basins with Minimum Environmental Impact. In: *Procedia Engineering*. Elsevier Ltd, pp 1629–1636
- Feng B, Zhang Y, Bourke R (2021) Urbanization impacts on flood risks based on urban growth data and coupled flood models. *Nat Hazards* 106:613–627. <https://doi.org/10.1007/s11069-020-04480-0>
- Geotech (2022) Retaining structures. In: *Geotech Website*. <https://www.geotech.hr/en/odabir-geometrije-armiranobetonskog-potpornog-zida/>. Accessed 17 Aug 2022
- Giannakis E, Serghides D, Dimitriou S, Zittis G (2020) Land transport CO₂ emissions and climate change: evidence from Cyprus. *Int J Sustain Energy* 39:634–647. <https://doi.org/10.1080/14786451.2020.1743704>
- Gül GO, Harmancıoğlu N, Gül A (2010) A combined hydrologic and hydraulic modeling approach for testing efficiency of structural flood control measures. *Nat Hazards* 54:245–260. <https://doi.org/10.1007/s11069-009-9464-2>
- Habib M, Alzubi Y, Malkawi A, Awwad M (2020) Impact of interpolation techniques on the accuracy of large-scale digital elevation model. *Open Geosci* 12:190–202. <https://doi.org/10.1515/geo-2020-0012>
- Hannah Ritchie, Roser M, Pablo Rosado (2020) CO₂ and Greenhouse Gas Emissions. In: *OurWorldInData.org*. <https://ourworldindata.org/co2-and-other-greenhouse-gas-emissions>. Accessed 3 Jun 2022
- HEC-HMS (2022) Hydrologic Modeling System HEC-HMS Users Manual
- HEC-RAS (2022) HEC-RAS River Analysis System HEC-RAS 2D User's Manual
- Hunt D, Stather W, Bowman, et al (2022) Cyprus. In: *Encycl. Br*. <https://www.britannica.com/place/Cyprus>. Accessed 10 Jun 2022

- Huxley C, Ryan P (2016) Flood Modeling: How Accurate is Your Model?
- Ibrahim-Bathis K, Ahmed SA (2016) Rainfall-runoff modelling of Doddahalla watershed—an application of HEC-HMS and SCN-CN in ungauged agricultural watershed. *Arab J Geosci* 9:1–16. <https://doi.org/10.1007/s12517-015-2228-2>
- Kaboosi K, Jelini R (2017) The efficiency of detention reservoirs for flood control on the Jafar Abad River in Golestan province (Iran). *Russ Meteorol Hydrol* 42:129–134. <https://doi.org/10.3103/S1068373917020078>
- Kibrisgazetasi (2018) Flood Disaster in Dikmen. In: *Kibr. Gazetasi*. <https://www.kibrisgazetesi.com/kibris/fotografli-dikmende-sel-felaketi-h55304.html>. Accessed 9 Jun 2022
- Kocaman S, Tavus B, Nefeslioglu HA, et al (2020) Evaluation of Floods and Landslides Triggered by a Meteorological Catastrophe (Ordu, Turkey, August 2018) Using Optical and Radar Data. *Geofluids* 2020:.. <https://doi.org/10.1155/2020/8830661>
- Kryžanowski A, Brilly M, Rusjan S, Schnabl S (2014) Review Article: Structural flood-protection measures referring to several European case studies. *Nat Hazards Earth Syst Sci* 14:135–142. <https://doi.org/10.5194/nhess-14-135-2014>
- Kumar N, Kumar M, Sherring A, et al (2020) Applicability of HEC-RAS 2D and GFMS for flood extent mapping: a case study of Sangam area, Prayagraj, India. *Model Earth Syst Environ* 6:397–405. <https://doi.org/10.1007/s40808-019-00687-8>
- Kundzewicz ZW (2002) Non-structural Flood Protection and Sustainability. *Water Int* 27:3–13. <https://doi.org/10.1080/02508060208686972>
- Lionello P, Scarascia L (2018) The relation between climate change in the Mediterranean region and global warming. *Reg Environ Chang* 18:1481–

1493. <https://doi.org/10.1007/s10113-018-1290-1>

Madhuri R, Raja YSLS, Raju KS, et al (2021) Urban flood risk analysis of buildings using HEC-RAS 2D in climate change framework. *H2Open J* 4:262–275. <https://doi.org/10.2166/H2OJ.2021.111>

Mai DT, De Smedt F (2017) A combined hydrological and hydraulic model for flood prediction in Vietnam applied to the Huong river basin as a test case study. *Water (Switzerland)* 9:. <https://doi.org/10.3390/w9110879>

Mailhot A, Duchesne S, Caya D, Talbot G (2007) Assessment of future change in intensity-duration-frequency (IDF) curves for Southern Quebec using the Canadian Regional Climate Model (CRCM). *J Hydrol* 347:197–210. <https://doi.org/10.1016/j.jhydrol.2007.09.019>

Mańko R (2018) The influence of weight coefficients in the Preissman scheme on flows in the lower Odra river network using the Hec-Ras software. *ITM Web Conf* 23:00024. <https://doi.org/10.1051/itmconf/20182300024>

Mays LW (2010) *Water Resources Engineering*, 2nd edn. John Wiley and Sons Ltd, Tempe, Arizona

Mihu-Pintilie A, Cîmpianu CI, Stoleriu CC, et al (2019) Using high-density LiDAR data and 2D streamflow hydraulic modeling to improve urban flood hazard maps: A HEC-RAS multi-scenario approach. *Water (Switzerland)* 11:. <https://doi.org/10.3390/w11091832>

Mishra SK, Singh VP (2003) SCS-CN Method. In: Mishra SK, Singh VP (eds) *Soil Conservation Service Curve Number (SCS-CN) Methodology*. Springer Netherlands, Dordrecht, pp 84–146

NRCS Staff (2009) Part 630 Hydrology National Engineering Handbook Chapter 07 Hydrologic Soil Groups. In: *National Engineering Handbook*

NRCS Staff (2007) Part 630 Hydrology National Engineering Handbook Chapter

16 Hydrographs. Engineering

- Ongdas N, Akiyanova F, Karakulov Y, et al (2020) Application of hec-ras (2d) for flood hazard maps generation for yesil (ishim) river in Kazakhstan. *Water (Switzerland)* 12:1–20. <https://doi.org/10.3390/w12102672>
- Peng A, Liu F (2019) Flooding simulation due to Hurricane Florence in North Carolina with HEC RAS
- Ponce VM, Hawkins RH (1996) Runoff Curve Number: Has It Reached Maturity? *J Hydrol Eng* 1:11–19. [https://doi.org/10.1061/\(asce\)1084-0699\(1996\)1:1\(11\)](https://doi.org/10.1061/(asce)1084-0699(1996)1:1(11))
- Rangari VA, Umamahesh N V., Bhatt CM (2019) Assessment of inundation risk in urban floods using HEC RAS 2D. *Model Earth Syst Environ* 5:1839–1851. <https://doi.org/10.1007/s40808-019-00641-8>
- S̃pitalar M, Gourley JJ, Lutoff C, et al (2014) Analysis of flash flood parameters and human impacts in the US from 2006 to 2012. *J Hydrol* 519:863–870. <https://doi.org/10.1016/j.jhydrol.2014.07.004>
- Şahin E (2013) A STUDY ON FLOOD MANAGEMENT PRACTICES FOR GÜZELYURT. METU Thesis 49–56
- Şahin E, Akıntuğ B, Yanmaz M (2013) Modeling of Morphou (Güzelyurt) Flood and. 24:6447–6462
- Satheeshkumar S, Venkateswaran S, Kannan R (2017) Rainfall–runoff estimation using SCS–CN and GIS approach in the Pappiredipatti watershed of the Vaniyar sub basin, South India. *Model Earth Syst Environ* 3:. <https://doi.org/10.1007/s40808-017-0301-4>
- Serdar Özcan (2019) Taşkın Yönetim Planı İle İlgili Çalışmalar. <https://www.tarimorman.gov.tr/SYGM/Belgeler/HİE-Taşkın-Son/Taşkın Yönetim Planları SYGM.pdf>. Accessed 8 Jun 2022
- Smith G, Cox R (2019) *The Australian Rainfall and Runoff: A Guide to Flood*

- Estimation. Commonwealth of Australia (Geoscience Australia)
- Smith GP, Davey EK, Cox R (2014) Flood Hazard
- Srinivasan V, Thompson S, Madhyastha K, et al (2015) Why is the Arkavathy River drying? A multiple-hypothesis approach in a data-scarce region. *Hydrol Earth Syst Sci* 19:1905–1917. <https://doi.org/10.5194/hess-19-1905-2015>
- Tabari H (2020) Climate change impact on flood and extreme precipitation increases with water availability. *Sci Rep* 10:. <https://doi.org/10.1038/s41598-020-70816-2>
- Tok Y (2022) Yapım işleri birim fiyatları (07.06.2022. KKTC
- Ugochukwu SC, Nwobu EA, Udechukwu-Ukohah EI, et al (2020) Regression Models for Predicting Quantities and Estimates of Steel Reinforcements in Concrete Beams of Frame Buildings. *J Sci Res Reports* 60–74. <https://doi.org/10.9734/jsrr/2020/v26i730285>
- WMO (2021) 1267_Atlas_of_Mortality_en
- Xiao B, Wang QH, Fan J, et al (2011) Application of the SCS-CN model to runoff estimation in a small watershed with high spatial heterogeneity
- Yan K, Di Baldassarre G, Solomatine DP, Schumann GJP (2015) A review of low-cost space-borne data for flood modelling: topography, flood extent and water level. *Hydrol Process* 29:3368–3387. <https://doi.org/10.1002/hyp.10449>
- Yanmaz AM (2018) Applied Water Resources Engineering, 5th Editio. METU Press, Ankara
- Zaifoğlu H (2018) Implementation of a Flood Management System for Nicosia. Middle East Technical University
- Zaifoglu H, Akintug B, Yanmaz AM (2018) Regional Frequency Analysis of Precipitation Using Time Series Clustering Approaches. *J Hydrol Eng*

23:05018007. [https://doi.org/10.1061/\(asce\)he.1943-5584.0001659](https://doi.org/10.1061/(asce)he.1943-5584.0001659)

Zaifoglu H, Yanmaz AM, Akintug B (2019) Developing flood mitigation measures for the northern part of Nicosia. *Nat Hazards* 98:535–557.
<https://doi.org/10.1007/s11069-019-03713-1>

Zittis G, Bruggeman A, Camera C (2020) 21st century projections of extreme precipitation indicators for cyprus. *Atmosphere (Basel)* 11:.
<https://doi.org/10.3390/atmos11040343>